UNIVERSITY
OF TRENTO - Italy
DEPARTMENT OF INDUSTRIAL ENGINEERING

XXIV cycle

Doctoral School in Materials Science and Engineering

Waterborne Paint System Based on CeO_2 and Polyaniline Nanoparticles for Anticorrosion Protection of Steel

Luiz Gustavo Ecco

Tutors:
Prof. Flavio Deflorian
Dr. Michele Fedel

WATERBORNE PAINT SYSTEM BASED ON CeO_2 AND POLYANILINE NANOPARTICLES FOR ANTICORROSION PROTECTION OF STEEL

Luiz Gustavo Ecco
E-mail: luizgustavo.ecco@ing.unitn.it

Approved by:

Prof. Flavio Deflorian, Advisor
Department of Industrial Engineering
University of Trento, Italy

Dr. Michele Fedel,
Department of Industrial Engineering
University of Trento, Italy

Ph.D. Commission:

Prof. Flavio Deflorian,
Department of Industrial Engineering
University of Trento, Italy

Prof. Peter Leisner,
School of Engineering
University of Jonkoping, Sweden.

Dr. Stefano Pandini,
Department of Mechanical and Industrial Engineering
University of Brescia, Italy.

University of Trento,
Department of Department of Industrial Engineering

October 2014

University of Trento - Department of Industrial Engineering

Doctoral Thesis

Luiz Gustavo Ecco - 2014
Published in Trento (Italy) – by University of Trento

ISBN: - - - - - - - - -

Preface

This thesis reports the research activity carried out over the last 3 years in the Laboratory of Industrial Corrosion Control at the University of Trento. The subject is related to corrosion control through an organic coating paint system for steel substrates. In other words, it coveres the investigation of anticorrosive pigments as viable alternatives to replace the use of hazardous and toxic substances commonly present into an organic coating paint system and in addition to this, to reduce emissions of volatile organic compounds (VOC), the organic coating paint system itself has been designed to be solvent-free.

Much of the work over the development of a water based full paint system containing the environmentally friendly nanoparticles was based on electrochemical techniques. Therefore, the contents within the next pages are divided into three main parts: i) a background about the use of electrochemical techniques for corrosion and corrosion control through organic coatings; ii) the electrochemical investigations of the environmentally friendly anticorrosive pigments; iii) the incorporation into one water based organic coating system.

Also, great effort has been spent to understand the mechanisms of the coatings degradation as well as the mechanisms of anticorrosion protection given by the pigments. In this way, the results of interest have been delivered to scientific community via a number of publications in different journals[1] as well as congresses participations.

Lastly, the activities in this thesis were supported by the SteelCoat project. SteelCoat was a consortium cooperation project within the EU Seventh Frame Programme (FP7), involving several companies and universities.

---

[1] *L.G. Ecco*, J. Li, M. Fedel, F. Deflorian, J. Pan - EIS and in situ AFM study of barrier property and stability of waterborne and solventborne clear coats, Progress in Organic Coatings, 77 (2014) 600-608

M. Fedel, A. Ahniyaz, *L.G. Ecco*, F. Deflorian - Electrochemical investigation of the inhibition effect of CeO2 nanoparticles on the corrosion of mild steel – Electrochimica Acta, 131 (2014) 71-78.

L.G Ecco, M. Fedel, A. Ahniyaz, F. Deflorian - Influence of polyaniline and cerium oxide nanoparticles on the corrosion protection properties of alkyd coating - In Press Corrected Proof - Progress in Organic Coatings DOI: 10.1016/j.porgcoat.2014.04.002

F. Deflorian, S. Rossi, *L. G. Ecco*, M. Fedel - Study of the effect of corrosion inhibitors on powder coatings applied on steel – In Press Corrected Proof - Progress in Organic Coatings DOI: 10.1016/j.porgcoat.2014.03.014

Contents

1 – Preliminary Remarks

Steel is a general term to describe a metallic alloy essentially formulated with iron and carbon. Numerous compositions, diverse elements as well as various thermal treatments are possible and, consequently, diverse classes of Steels are known. Mild steel defines the simplest composition in which Fe is alloyed with carbon at low concentrations. Mild steel has relatively high mechanical properties, however, when a bare steel surface is exposed to a reactive environment, the surface of the steel is expected to corrode.

Corrosion of metals has several definitions, however, it mainly signifies the degradation or deterioration of the metal with consequent loss of properties and reduction of the service life. In addition, the economic impact attributed to corrosion of metallic structures is a major issue among modern societies. It has been shown that the cost of corrosion was estimated to be around 3.1% of the gross national product (GNP), in most of industrialized nations, the corrosion cost is estimated to be 4 – 5% of the GNP [1].

1.1 Alternatives to anticorrosive hazardous compounds

Generally, metals are painted because of decoration as well as to protection purposes. The use of organic coatings paint system allows both of the purposes to be reached simultaneously. Traditionally, from an anticorrosive protection point of view, for metals in general, it is well recognized the effectiveness of chromium containing organic coatings and chromium conversion treatments.

In principle, the great efficiency of Chromium VI is attributed to high oxidizing potential of Cr^{6+} ion. Once in conjunction water and dissolved oxygen, a thin layer - in the order of few decades of nanometer - of complex mixture of chromium compounds is formed as a consequence of Cr^{6+} reduction. The chromate conversion coatings allows a good adhesion of steel with the coating systems, enhancing the anticorrosive performances of the surfaces [2].

On the other hand, the same oxidation potential which confers anticorrosive inhibition efficiency to the chromium containing paints are attributed to high indexes of toxicity and carcinogenic issues. As an example, Cr^{6+} has been listed by the World Health Organisation (WHO) and by the U.S. Environmental Protection Agency (EPA) as a carcinogen compound [3, 4]. Consequently, in the last decades, a number of directives about the use of Cr^{6+} based conversion treatments emerged and addressing scientists and

professionals in the field of paints towards the search of substitutes to chromates compounds and, therefore, considering environment aspects. Among new strategies for replace to chromium (VI), one can mention the use of intrinsic conductive polymers, specially Polyaniline (PAni), and rare earth compounds like cerium oxide nanoparticles. Both have been identified as promising inhibitors candidates [5, 6], in addition they are considered environmentally acceptable due to their non-toxic behaviour and a little content concentration inside coating resin is necessary.

1.1.1 Overview on the use of PAni

In the middle of 80's, the reports of DeBerry have propelled the use of Polyaniline (PAni) as a promising anticorrosive candidate for steel protection [7]. At first, several researches have demonstrated the corrosion protection effectiveness of an uniform film obtained via electrodeposition of PAni onto steel [8, 9]. Consequently, a number of mechanisms were suggested with the purpose of explaining the protection given by the PAni film. Amongst these, it is most believed that the electrodeposited PAni ennobles the surface of steel and promotes the formation of a thin but dense passive oxide layer on the surface [10]. On the other hand, once PAni is synthesized via the chemical oxidative polymerization, particles are obtained. When the particles are added into an organic coating, the distribution at the interface is considered a critical parameter in order to obtain satisfactory anticorrosive properties [11].

Pioneer use of coatings containing polyaniline particles is attributed to Wessling et al [12, 13]. According to the authors, the presence of polyaniline particles into paints has led to the formation of Fe_2O_3 film above a very thin Fe_3O_4 layer over the iron surface, as demonstrated through SEM and XPS, thus, an ennoblement of the metal surface is proposed.

Similar mechanisms have been proposed by Sathiyanarayanan et al [14, 15]. The anticorrosive properties of steel coated with epoxy containing the doped PAni under saline and acid media were investigated. In both studies it has been demonstrated that PAni is able to protect the surface of the metal by shifting the open circuit potential in the direction of more noble values.

Adhikari et al [5], prepared PAni particles via chemical oxidative polymerization in presence of methane sulfonic acid (MeSA) before addition into poly (vinyl acetate) coating. It was found via open circuit potential (OCP) observations and EIS investigations that the

presence of PAni-MeSA formed a protective oxide layer at the steel surface. Besides, supported by an increase of the charge transfer resistance (R_{ct}) observation, the reduction reaction of the conductive polyaniline after exposure to oxygen, has started the formation of the passive layer.

1.1.2 Overview on the use of CeO_2

Cerium oxide nanoparticles have been used in many industrial applications [16], such as catalysts [17, 18], semiconductor polishing agents and full additives, and they have been studied for many other applications such as electrode [19], electrolytes [20], anti-oxidant [21], UV absorbers [22, 23], as well as functional pigments [24]. Recently, there is an increased interest in potential application of cerium oxide for corrosion protection of metals [25, 26]. Considering cerium oxide, apart from few works that have demonstrated the effectiveness of those, until now the corrosion inhibition mechanism has not been completely comprehended.

R. Sharmila *et al.* demonstrated that cerium oxide shows good performance as a corrosion inhibitor for steel in HCl and H_2SO_4 solution mediums [27]. The evaluation of inhibition properties of cerium oxide nanoparticles submitted to a cerium nitrate treatment was studied by M.F. Montemor et al. [28]. CeO_2 nanoparticles and Ce^{3+} ions were added as filler on silane films on galvanized steel. It was evidenced that CeO_2 nanoparticles promote the stabilization of a passive film on galvanized steel.

Fedel et al. [29] studied the potential effectiveness of a mixture of CeO_2 and SiO_2 nanoparticles in an urethane coating coating, top coated with a polyester/epoxy blend for the protection of galvanized steel. Superior salt spray chamber performance was observed for systems containing the SiO_2/CeO_2 pigments, in which a good protection with a little delamination was observed.

1.2 Solventborne and waterborne organic coatings

The anticorrosive protection capability attributed to an organic coating paint system is related to its barrier features, in other words, to water and oxygen ions transport throughout the paint layer. Therefore, corrosion control of metal through organic coatings is one amongst the most extend methods available [30, 31].

In addition to the use of hazardous compounds, in the early 90's, the appearance of few strict environmental protection regulations motivated the development of solvent free

coatings in order to reduce the emissions of volatile organic compounds (VOC). Likewise, the paint industry alongside corrosion scientists was encouraged to become more environmentally adapted. Consequently, a number of new coating technologies have been developed, for instance, the solvent-free powder coating, the water based organic coatings, etc [32, 33]. Among them, waterborne organic coatings appeared as environmentally friendly alternative to the traditional solvent-based coatings, since water is used as vehicle of the organic coating to disperse the pigments.

Furthermore, organic coatings using water as the dispersive medium have gained increased attention due to their economic viability in combination with anticorrosion performance relatively comparable to solvent-borne [34-36]. On the other hand, most of the disadvantages attributed to waterborne coatings are associated with the use of water as a solvent. Due to their chemical reactivity with water, waterborne coatings have lower chemical resistances and shorter shelf lives. Moreover, flash rusting is the rapid onset corrosion formed by the reaction of iron in the presence of air and water that can affect the adhesion of the coating [37-39].

1.3 Electrochemical Impedance Spectroscopy

Among the many definitions of corrosion, it can be defined as an electrochemical process. Ever since corrosion reactions are processes where chemical reactions take place and produce electrical current. In view of that, much effort in science was dedicated to the study of corrosion by means of electrochemical methods.

From a production and engineering point of view, the continuous development of long shelf lives organic coatings systems requires fast methodologies to evaluate their anticorrosive properties and to classify them as possible long term durability products or not. Industry is aware about well-known accelerated tests, which assess the paints anticorrosive properties under higher levels than in natural conditions of temperatures, humidity, salts and UV light exposures. On the other side, from a scientific approach, such tests do not provide deep information about the mechanisms of protection given by the newest developed paint system.

In this way, Electrochemical Impedance Spectroscopy (EIS) has been extensively used for the investigation of organic coatings for several reasons: to understand the mechanism an organic coating protects metals, to predict lifetime of the coating, to detect changes in the

coating performance after time of exposure, etc [31, 40-42]. EIS measurements are normally performed on an exposed sample area of the order of few square centimetres, and coating thicknesses of tens of micrometres. In addition, the information obtained is representative of the entire volume of the coating [31, 43].

1.3.1 Basics fundamentals of EIS

Although the fundamentals of EIS are well explored, and it can be found elsewhere [31, 34, 40-42, 44], it is worth to dedicate part of the chapter on some topics which along this thesis will be brought into the discussion of results.

The ability of a circuit element to resist the flow of electrical current (I) when a potential (V) is applied is defined as electrical impedance (Z) (Equation 1). The definition of Z comes from a sinusoidal voltage perturbation at certain amplitude, therefore alternate current (AC), and is dependent of frequency of the wave.

$$Z = \frac{V}{I} \qquad \text{Eq.1}$$

Electrochemical impedance is usually measured by applying an AC potential to an electrochemical cell and then measuring the current through it. The term spectroscopy arises when the electrochemical system is submitted to a sinusoidal voltage at a certain range of frequencies. The applied voltage is expressed as a function of time, and can be written as in the Equation 2;

$$V = Vo.\sin(\omega t) \qquad \text{Eq.2}$$

In Eq. 2 where V stands for the potential at time t, V_0 is the amplitude of the signal, and ω stand for the frequency. The values of the potential can be represented into complex planer, usually written as:

$$\Delta U = \Delta Ure + i\Delta Uim \qquad \text{Eq.3}$$

Then, eq. 3 leads to the complex form of impedance, described as follows in Equation 4:

$$Z = \frac{\Delta U}{\Delta I} = Zre + iZim \qquad \text{Eq.4}$$

However, impedance is most represented by its modulus (|Z|) and the phase angle shit (φ), represented in Equation 5 and 6, respectively.

$$|Z| = \sqrt{(Zre)\text{^}2 + (Zim)\text{^}2} \qquad \text{Eq.5}$$

$$Tg(\varphi) = \frac{Zim}{Zre} \qquad \text{Eq.6}$$

As a result, the impedance data is usually deliberated with respect to these two ways of representation:

- Bode Impedance (log of |Z|) and Bode phase angle (φ) versus the log of frequency;
- Nyquest spectrum, $-Z_{im}$ as function of Z_{re}.

In addition to the qualitative results, by modelling the EIS spectra with a proper equivalent circuit based upon an appropriate combination of simple electrical elements, *e.g.* capacitors and resistor. This technique provides quantitative data on electrical parameters of the coatings and also, about their evolution versus time of exposure to a corrosive solution, so-called electrolyte. [44-47]. The modeling assessment represents both, the processes occurring on the coating layer itself as well as on the coating-metal interface.

In most of its applications, EIS measurements are conducted on organic coatings under intact conditions in presence the electrolyte. In some cases, the coating layer might behave as a dielectric and can be represented by an ideal capacitor. One can expect that the impedance spectra would exhibit a quasi-capacitive behaviour with only one time constant associated to the coating layer and therefore, the electrical circuit which would better fit these spectra is shown in Figure 1a.

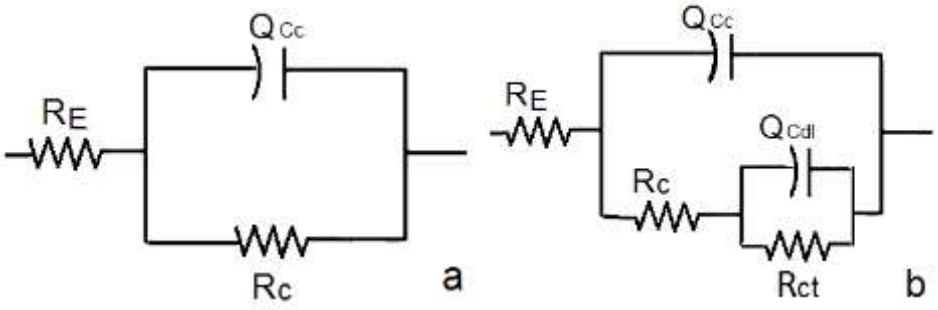

Figure 1 - Examples of equivalent Electrical circuit used for modeling the EIS spectra; (a) Re(QCcRc) and (b) Re(QCc(Rc(QdlRct)))

The quantitative approach allows the assessment of electrical parameters which define the coating layer and, all the electrical elements must be related to specific physical phenomena. From Figure 1a:

i. Coating capacitance (C_c or Q_{Cc}): the coating capacitance is defined according to Equation 1;

$$Cc = \frac{\varepsilon 0.\varepsilon r.A}{d} \qquad (1)$$

ii. Coating resistance (R_c): Rc has been generally interpreted as the pore resistance due to electrolyte penetration through microscopic pores, or in areas where more rapid solution uptake occurs due to inadequate cross-linking of the polymer [11,21]. Thus, the magnitude of Rc is indicative for the state of degradation of the coating. Rc can also increase with time, probably as a result of pore or defect blockage by corrosion product build-up. Incorporation of conductive pigments (*e.g.* zinc) also enhances the electric conductivity of the coating, resulting in a lower coating resistance;

From Equation 1, the ε_0 is the vacuum permittivity or the permittivity of the free space, ε_r is the relative permittivity or coating dielectric constant, *A* the coating surface area under investigation and *d* its thickness. It is frequently found in the literature a further treatment of Eq. 7 which assesses the content of water into the organic coating layer. One can expect water is absorbed by the coating while exposed to the electrolyte. The absorption of water changes the ε_r, consequently, the coating capacitance. In the middle of 50's, Brasher and Kingsbury proposed an equation to calculate the water content of an organic coating from capacitance measurements on that coating on a metal substrate. Nowadays, the so-called Brasher-Kingsbury formula is yet used to evaluate the absorption of water by an organic coating layer and is shown in Equation 2 [48].

$$\Phi = \frac{\log(\frac{C}{C0})}{\log(\varepsilon 0)} \quad (2)$$

On the whole, the dielectric constant of the typical polymers used in the formulation of an organic coating system range between 3 – 8, approximately [49], and that of water being at 78.5 at 25°C. The estimation of water absorption comes from the evolution of the dielectric constant, which tends to increase as function of time of exposure.

As long the coating remains exposed to the electrolyte, it can be expected that oxygen and hydroxyl ions will move along the coating layer towards the metal substrate. Once the metal surface is reached, corrosion reactions initiate at the metal-coating interface and corrosion products are formed underneath the paint. Thus, the electrical circuit shown in Figure 1b described the interfacial phenomena. This circuit consists of the double layer capacitance and an electrical element describing the electrochemical reactions at the metal/electrolyte interface. Therefore:

i. Double layer capacitance (C_{dl} or Q_{dl}): the double-layer capacitance which is proportional to the active metallic area in contact with the electrolyte;

ii. Charge transfer resistance (R_{ct}), the charge-transfer resistance inversely proportional to the active metallic area.

In case of detachment of the coating from the metal, an electrochemical double layer is established at the interface. This layer can be modelled with a double layer capacitor C_{dl} and charge transfer resistance R_{ct} in parallel. The double layer capacitance C_{dl} originates from the difficulty of charge carriers (electrons and ions) to cross the interface, resulting in a separation of charge. Charge transfers can only occur through electrochemical reactions. The resistance of this charge transfer is represented by resistor R_{ct} and it is related to the rate of the anodic and cathodic reactions. The elements C_{dl} and R_{ct} are often considered as a measure for the area over which the coating has detached. Besides, it has been stated that C_{dl} measures an electroactive area of the delaminated area. This implies that C_{dl} also depends on the electrochemical state of the surface (*i.e.* active or passive). For the same reason, the assumption that R_{ct} is solely proportional to the delaminated area is too crude. In many cases, C_{dl} is also replaced by a CPE to account for non-ideal behavior of the double layer.

Considering that electrochemical impedance spectroscopy is, at the same time complete and complex technique, it is frequently cited that EIS might be handled with caution. In contrast to its contribution, drawbacks on the use of electrochemical techniques are likewise found in literature. For instance, EIS is limited in the evaluation of delamination of the coating in presence of defects. Or else, misinterpretation on the use of equivalent circuit models to modeling and quantify the electrical parameters attributed to the coating layer might happen from an erroneous impedance data fitting.

Additionally, among the discussed matters on the use of EIS for coated metals studies, the evaluation of water content into organic coatings has been several times subject of investigation. For instance, in the Brasher-Kingsbury formula, few restrictions are attributed to the water content evaluation:

- Water is homogeneously absorbed by the organic coating layer;
- No change in the coating dimension, *e.g* swelling occurs;
- No interaction between water and the organic coating occurs.

It is also mentioned that the increase in the coating capacitance cannot be attributed to other effects unless because of water absorption.

1.4 Motivation and Objectives

Preliminary observations attracted attention to the use of cerium oxide and polyaniline nanoparticles as promising anticorrosive pigments for steel. As an example, mild steel was immersed into sodium sulphate solution containing equal concentration of PAni and ceria nanoparticles and the OCP has been monitored, as demonstrated in Figure 2. The evolution of OCP showed more noble potentials when ceria and PAni, at same concentrations, were added together into sodium sulphate solution.

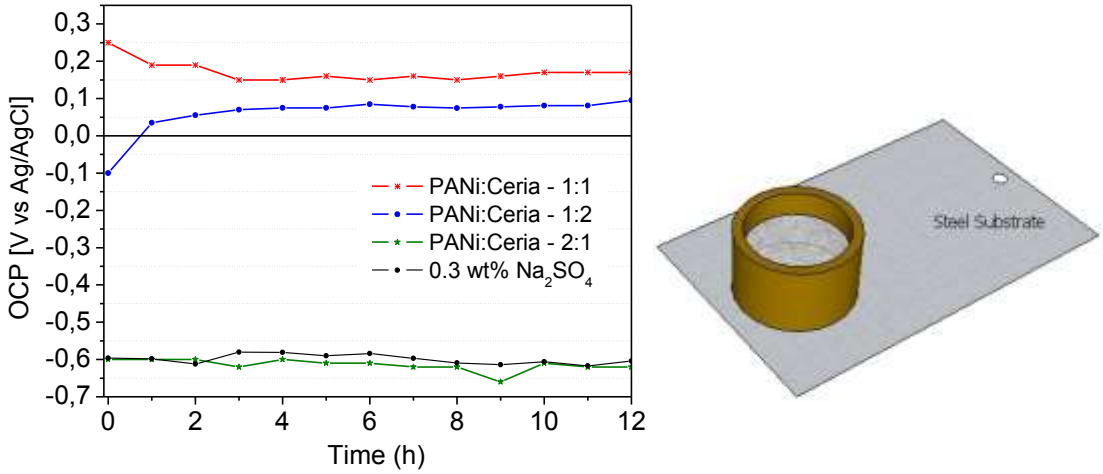

Figure 2 - OCP versus time of ceria and PAni containing solutions (left) and scheme of the cell used during OCP monitoring (right).

Considering the above, the development of a water based paint system with long durability for corrosion protection of steel stands as the overall objective of this project. Moreover, the corrosion protection of this novel environmentally friendly anticorrosion organic coating will be achieved by combining polyaniline and cerium oxide nanoparticles, defined as green or environmentally acceptable materials. In order to achieve the overall objective, few prior steps have been followed and they can be described as minor objectives:

- A comprehension of the mechanisms of protection against corrosion of Polyaniline and Ceria nanoparticles onto steel accomplished by electrochemical techniques;
- Selection of a proper water-based polymeric binder to formulate the full organic paint system accomplished by electrochemical and accelerated techniques;
- A comprehension of the mechanisms of protection against corrosion given by PAni and Ceria nanoparticles when present into the water based organic coating, accomplished by electrochemical and accelerated techniques.

2 Cerium Oxide nanoparticles

Part of this chapter has been published in:

- M. Fedel, A. Ahniyaz, L.G. Ecco, F. Deflorian - Electrochemical investigation of the inhibition effect of CeO2 nanoparticles on the corrosion of mild steel – Electrochimica Acta, 131 (2014) 71-78.

- L.G Ecco, M. Fedel, A. Ahniyaz, F. Deflorian - Influence of polyaniline and cerium oxide nanoparticles on the corrosion protection properties of alkyd coating - In Press Corrected Proof - Progress in Organic Coatings DOI: 10.1016/j.porgcoat.2014.04.002

Taking into consideration the preliminary observations mentioned above, the more environmental acceptable alternatives to promote corrosion protection of steel studied in this thesis are: *cerium oxide and polyaniline nanoparticles*. Therefore this chapter is dedicated to the cerium oxide nanoparticles. Initially, a state-of-art on the use of cerium oxide nanoparticles for corrosion protection purposes was considered, followed by the methodology of study and, finally, the obtained results are reported.

It is important to highlight that most of the work on the characterization of the ceria nanoparticles has been done by electrochemical techniques. Ahead in the Chapter 4, the influence of ceria nanoparticles into a waterborne organic coating system were investigated. In other words, diverse water based containing ceria nanoparticles dispersions were firstly studied in order to comprehend their anticorrosive performances when inside of a waterborne organic paint system for protection of steel.

2.1 Introduction to CeO_2

On the periodic table, cerium (Ce) is found on the rare earth metal, group IIIB, atomic number 58 and atomic mass 140.12. It is mainly found in nature on the form of two minerals, monazite and bastnaesite. Cerium oxide, or cerium dioxide, presents the fluorite structure, Therefore, the Ce ions have a formal charge of 4+ and oxygen ions have a formal charge of 2-. CeO_2 is one of the most reactive rare earth metal oxides which possess wide band gap energy and high refractive index in the visible region [50].

Some applications of cerium dioxide are well-known: it is used in making lamp mantles; also as polisher agent in the glass industry and owing to its optical properties, it is usually used in UV absorbing applications.

2.1.1 Nanometer sized CeO_2

As mentioned, CeO_2 is the stable stoichiometric form of bulk cerium oxide and shows all of the cerium in the Ce(IV) state. On the other side, it is often found in literature that CeO_2 particles, when reduced into nanoscale, show physical and chemical properties which differs from the bulk materials. However, up to days, literature data on the structure and properties of nanoceria often contradict each other and thus, most of the properties of nanometer sized CeO_2 yet remain vague. Hence, an overview on the physic-chemical novel properties of nanoceria is given.

The large ratio of number of atoms in the surface, in other words the increased role of the surface for nanoceria, compared to the bulk lead to the nonstoichiometric structure and, consequently give new properties for cerium oxide nanoparticles [51, 52].

At nanoscale, cerium oxide is attributed two different structures of the oxidation state of ceria: i) Ce^{4+} state from the CeO_2 oxide form and ii) Ce^{3+} state form the Ce_2O_3 [53, 54]. Ceria nanoparticles have a core-shell type of structure with cerium (IV) oxide in the core and Cerium (III) on the shell mostly. In this way, the proper nanocrystalline formula of cerium oxide should be written as $CeO_{2-x,}$ where *x* ranges between 0 to 0.2. Due to the low value of oxidation-reduction potential of the Ce^{4+}/Ce^{3+} pair (1.61 eV) cerium dioxide is able to attach and release oxygen rather easily, as shown below:

$$2CeO_2 \leftrightarrow Ce_2O_3 + ½\ O_2 \qquad \text{Eq. 5}$$

Owing to this, nanoceria particles are given a number of possible high-technological applications; automotive exhaust catalyst [55], UV absorbers [50, 51], fuel additives [56], etc.

As an example, nanoceria switches between Ce^{3+} and Ce^{4+} states (as proposed in Eq. 5), whereupon this switch is believed to raise the dynamic oxygen storage and release capability (OSC) of Cerium oxide close to the ideal stoichiometric conditions, allowing the application of nanoceria as catalytic converter [57]. Similarly attributed to the Ce3+/Ce4+ ratio, it has been published the ability of nanoceria to deactivate hydroxide radicals, hydrogen peroxide and nitroxyl radicals [58].

Another study investigated the ability of Ce(III) to promote a redshift on the UV-visible absorption spectrum. The 300 nm absorption peak corresponded to the Ce(IV) band gap whereas the 400 nm absorption peak was attributed Ce(III). It was suggested that the

presence of Ce(III) ions in the crystal lattice created a trap state of 3 eV above the CeO_2, as shown in the Figure 3 [59].

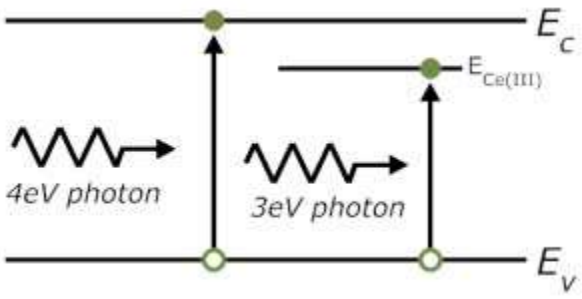

Figure 3 - Scheme of trap state generated by the presence of Ce(III). Adapted from [59]

2.1.2 CeO_2 for corrosion protection

Regarding the search for new ecological alternatives in order to replace the hazardous Cr(VI) for metal protection against corrosion, lanthanides compounds, also identified as rare earth metals, are among the substances that have been hardly investigated by scientists in the last years. Lanthanides have low toxicity and their inhalation or ingestion has not been considered harmful [60]. Generally, lanthanides ions can form insoluble hydroxides, which enable them to be used as cathodic inhibitors. Besides this, cerium oxide/ hydroxide formation is the main reason for the corrosion protection property of cerium compounds.

Therefore, preceding the use of cerium oxide, cerium salts have been investigated for corrosion protection purposes. Pioneering studies employing lanthanides salts for corrosion protection were done by Hinton, Arnott and co-workers [61, 62]. They have found that the lanthanides salts, in particular the chlorides, such as Cerium trichloride ($CeCl_3$), Praseodymium trichloride ($PrCl_3$) and Neodymium trichloride ($NdCl_3$) showed protective effect against corrosion of aluminum alloys, reducing the corrosion rate by three orders of magnitude. It was suggested the action of the lanthanides salts as cathodic inhibitors**,** by forming an oxide film on the metal surface, particularly at cathodic sites in the alloy microstructure. In another study, however, it was reported that cerium particles were found in accumulated regions instead, described as ‘’dispersed islands’’ along the aluminum surface [63]. Nevertheless, the described mechanisms have matched each other; at the first stages of the corrosion process, hydroxyl ions (OH^-) are generated over the cathodic sites due to the oxygen reduction. After that, OH^- groups react with the cerium ions present in the solution and therefore, the cerium islands have arisen. The cerium

islands decreased the cathodic current and, consequently, reduced the overall corrosion rate. Thus, this proposal was supported from results obtained by Davenport, Isaacs and co-workers [64]. In summary, lanthanides salts, particularly $CeCl_3$, have been shown to be promising cathodic inhibitors against uniform and localized corrosion of a large variety of aluminum alloys.

Following these observations over aluminum alloys, the possibility of cerium ions were likewise investigated over steel and its classes. A synergistic interaction was observed by X. Li et al. between cerium ions and sodium oleate (SO) mixtures on the corrosion of cold rolled steel acidic media [65]. Ce^{+4} showed weak inhibition efficiency by itself, and SO was described as moderate. Their mixture, however, showed inhibition efficiency higher than the sum. According to the authors, interactions between the components are facilitate due to chemical structure of both, oxygen atoms with lone-pair electrons from SO and vacant orbits (4f, 5d and 6s) from Cerium, and the Ce^{4+}-SO compound is formed onto the steel surface and drop the corrosion extent.

The above overview discusses the inhibition effect given by cerium ions from cerium salts. However, the oxide form of CeO_2 particles, most specially the ceria particles in the nanometric size range, are is likewise matter of discussion and up to present days, there are three proposals regarded the protection or inhibition action from ceria nanoparticles on steel: **i)** the release of Cerium ions; **ii)** the effect of CeO_2 as complexing agent **iii)** the oxidation reduction capability of CeO_2/Ce_2O_3.

i) Release of cerium ions

The idea of oxide nanoparticles can absorb inhibitor ions and, when in contact with moisture, slowly release them was proposed by Zheludkevich et al. [66]. In their study, zirconia nanoparticles were firstly synthesized followed by cerium nitrate addition, for Ce^{3+} absorption. EIS analysis demonstrated that the films prepared with cerium doped zirconia nanoparticles conferred higher corrosion than the undoped after 250h of immersion on neutral media, and this fact is attributed to the formation of an oxide layer between the metal and the film. Moreover, the oxide layer resistance versus time of immersion for films with cerium doped zirconia nanoparticles showed a slight decrease on the downward direction, as an indicative of a slower releasing of cerium ions. Films without the cerium treatment showed a rapid decrease.

The evaluation of inhibition properties of cerium oxide nanoparticles submitted to a cerium nitrate treatment was studied by M.F. Montemor and M.G.S Ferreira [28]. CeO_2 nanoparticles and CeO_2 + Ce ions were added as filler on silane films on galvanized steel. Scanning vibrating electrode technique (SVET) was made on scratched samples and CeO_2 filled films exhibited low current densities until the 72th hour. After that, delamination of the films and an increase on the current densities were observed. The presence of cerium ions on the CeO_2 + Ce filled films, however, promoted a better adhesion and inhibition, owing to insignificant delamination and slight anodic activity longer than 72 hours. Moreover, d.c. polarization curves were performed and both filled films, CeO_2 and CeO_2 + Ce, shifted the corrosion potential to the noble direction. Authors reported that the CeO_2 nanoparticles created a more protective and stable film over the metal.

A comprehension of the mechanism of protection involves the electrolyte applied in the electrochemical tests, 5_x10^{-3} M of NaCl solution. It is well know that Zn^{2+} ($Zn + 2e^- \rightarrow Zn^{2+}$) can react with chloride ions and form a great insoluble compound, $Zn_5(OH)_8Cl_2$ which leads for passivation [67]. However, excess of Cl^- ions can penetrate on the passive film, nucleate and grow some corrosion spots. CeO_2 shows a high stability, in a wide range, and possess the ability to easily absorb other species, for instance, chlorides. In doing so, CeO_2 nanoparticles promote the stabilization of the passive film. In addition, the presence of cerium ions, enhance this mechanisms and justified the better performance showed by the CeO_2 + Ce filled films.

On the overview above the oxide nanoparticles, zirconia or ceria, have gone through any treatment or doping process in order to enhance their properties. Thus, the mentioned release of ions is due to these further treatments which the nanoparticles have been exposed to. On the other hand, in the case of CeO_2, one is mentioned about the physic-chemical changes which the nanoparticles undergo when reduced into the nanoscale.

Therefore, the proposal on the release of ions from an oxide nanoparticle into a solution is covered. These concepts are originally based on the thermodynamics of Gibbs. For example, the solubility of spherical solid particles and the size dependence into large liquid solution has been proposed by Ostwald (1900), further adapted by Freundlich (1909). The Ostwald-Freundlich expression is shown in Equation 6.

$$\frac{RT\rho}{M} ln \frac{S1}{S2} = 2\gamma \left(\frac{1}{r1} - \frac{1}{r2}\right) \quad \text{Eq.6}$$

In Eq.6 the tags can be read as follows: *R* is the gas constant, *T* stands for the absolute temperature, M is the molecular weight of the solid in the solution, *γ* is the interfacial tension between the solid and liquid phases, *ρ* is the density of the solid, S1 and S2 are the solubility whereas *r1* and *r2* are the radius of the particles size. According to the Eq. 6, the smaller the particles size, higher their solubility into a large solution. That is to say, the solubility of particles increases with decreasing the particles size, attributed to higher specific surface area of the particles.

Such concept can be extrapolated for the applications of nanoparticles as anticorrosive additives when added into an organic coating paint system. For instance, an investigation about the use of CeO_2 and SiO_2 particles added as an additive in a urethane primer was done by Fedel et al. [29]. After 500 hours of exposure, superior salt spray chamber performance was observed for systems containing the SiO_2/CeO_2 and SiO_2 pigments, in which a good protection with a little delamination was promoted. Furthermore, EIS evidenced a possible synergistic effect when CeO_2 was added together with SiO_2. Two hypotheses were suggested to explain the role of Cerium; (a) (OH-) ions produced at the cathode reacted with Cerium ions released by Cerium oxide particles, the product of this reaction precipitated on the cathodic sites and reduced the cathodic current; (b) Cerium oxides formed complexes compounds with greater corrosion stability.

The two hypothesis observed above: (a) comes to an agreement with reports given by [63, 64] whereas the hypothesis (b) is better detailed by Aramaki [68], who described the formation of a passive film, composed by $Zn(OH)_2$, $ZnSi_2O_5$ and some cerium silicates (Ce^{3+} -SiO_5^{2-}). After oxidation of Zn into Zn^{+2} at the anodic region, ions Zn^{2+} reacted with hydroxyl ions produced at the cathodic process and $Si_2O_5^-$, forming a passive film on the surface. In addition, $Si_2O_5^-$ ions reacted with Ce^{+3} and formed a $Ce_2(Si_2O_5)$ compound.

ii) the effect of CeO2 as complexing agent

Complexes agent

It is most believed that the general mechanism of protection provided by cerium ions is controlled by a local pH increase causing the precipitation of cerium hydroxides, oxides or mixture of both on the metal surface, specifically at the cathodic sites and this is believed to diminish the cathodic current. Perhaps a good foundation to clarify the formation of cerium compounds could be given by the Pourbaix diagram, also known as potential – pH

(E-pH) diagram [Poubaix's atlas, 1974], is a theoretical tool used to identify or indicate the conditions under which passive films might be formed.

Two main variables, pH (chemical) and potential (electrochemical) play a role on the formation of cerium compounds. By means of the corrosion reactions, the local pH at the cathodic sites increases as the corrosion is occurring and the generation of OH^- delivers the precipitate of the desired cerium compounds. Certain reactions that would raise the pH are:

a) $2H^+ + 2e^- \rightarrow H_2$
b) $2H_2O + 2e^- \rightarrow H_2 + 2OH^-$
c) $H_2O_2 + 2e^- \rightarrow 2OH^-$

The above reactions will stimulate the followings:

d) $Ce^{3+} + 3OH^- \rightarrow Ce(OH)_3$
e) $2Ce^{3+} + 2OH^- + H_2O_2 \rightarrow 2Ce(OH)_2^{2+}$
f) $Ce(OH)_2^{2+} + 2OH^- \rightarrow Ce(OH)_4$

An updated version of the Cerium - H_2O Pourbaix diagram was proposed by Hayes et al. [69] and it is shown in Figure 4. Besides, in order to observe phase transformation of cerium in aqueous solution and to better understand the pH range in which the precipitation of cerium compounds occur, an experimental precipitation study was also done as shown in Figure 5.

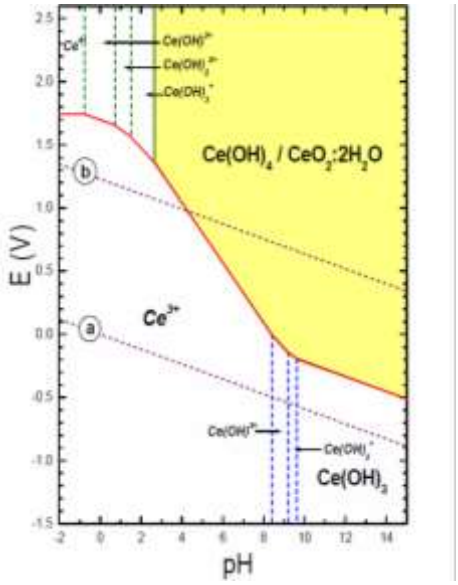

Figure 4 - Revised Pourbaix diagram for Ce-H2O System [38]

Some features from the revised diagram: a) the pH required for precipitation to cerium oxide Ce^{4+} ions is in the range of 4.5; b) the possibility of the Ce^{3+} to CeO_2 reaction could occur over a broad range of operating conditions of pH and potential; c) the region of stability of CeO_2 is large.

Through the titration experimental analysis of Ce(III) species authors have observed: a) the controlled addition of OH^- ions remained stable and centered at pH 6 and the stoichiometry of 3:1, hydroxide to cerium, was reached. After that the pH rose dramatically and the precipitation of $Ce(OH)_{3(precip)}$ from the $Ce(OH)_{3(Aq)}$ occurred when the pH was higher than 10. See the above Equation d). Due to the presence of O_2, some Ce(IV) compounds were found to be formed according to the following reaction:

g) $4Ce(OH)^{2+} + O_2 + 2H_2O \rightarrow 4Ce(OH)_2{}^{2+}$

The titration analysis was also done for the Ce(IV) solution and the authors found that the Ce(IV) at the pH 1.45 is a mixture of $Ce(OH)^{3+}$ and $Ce(OH)_2{}^{2+}$ in same amounts. The hydrolysis of $Ce(OH)_2{}^{2+}$ into $Ce(OH)^{3+}$, is followed by the precipitation of $Ce(OH)_4$.

h) $Ce(OH)_2{}^{2+} + OH^- \rightarrow Ce(OH)^{3+}$

i) $Ce(OH)^{3+} + OH^- \rightarrow Ce(OH)_4$

Owing to the presence of oxygen the authors noticed the existence of a yellow precipitate attributed to the formation hydrated cerium oxides, such as $CeO_2.H_2O$.

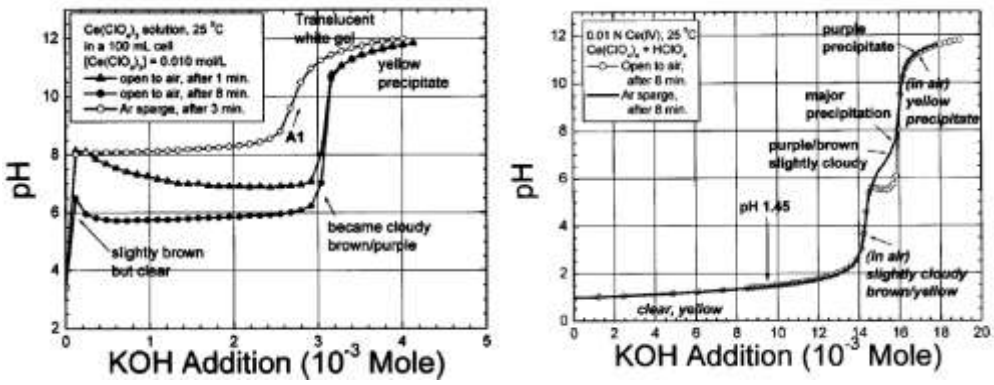

Figure 5 - Titration curve for Ce(III) ions (left) and Ce(IV) ions (right) [38]

A complementary overview of the precipitation of a cerium hydroxide film on the cathodic areas due to the precipitation of cerium(III) ions into a protective layer of $Ce(OH)_3$ is given by M.A. Arenas and J.J. de Damborenea. In their study, galvanized steel panels were immersed in a NaCl solution containing several concentrations of $CeCl_3$ salts. Polarization

curves showed a displacement on the cathodic branches toward lower currents, which is justified by the presence of the inhibitor Ce^{3+} ions on the electrolyte.

The complementary discussion how Ce^{3+} ions form cerium compounds and these precipitate over the metal surface was relevant:

Trivalent rare earth ions will precipitate as follow:

j) $M^{3+} + 3H_2O \rightarrow M(OH)_3 + 3H^+$,

for cerium(III) ions:

k) $Ce^{+3} + 3H_2O \rightarrow Ce(OH)_3 + 3H^+$,

and the pH for the hydroxide formation could be estimated through:

l) $\log[M^{3+}]_{sat} = x - 3pH$, where x is the a constant of 22.15.

From formula l), the founded pH range for precipitation of Ce is around 8.3. Besides, the local pH at the cathodic sites, where the O_2 reduction takes place, was estimated and they have found to be near 10.5. Thus, the formation of cerium(III) hydroxides is thermodynamically favored since the pH at the cathodic sites is higher than the critical pH for the precipitation. Authors likewise enhanced that the solubility of Ce hydroxides is lower than that of Zn. Owing the that, $Ce(OH)_3$ will precipitate with less difficulty than $Zn(OH)_2$.

iii) Redox reactions

Recalling the changes in the oxidation states of ceria nanoparticles discussed in section 2.1.1, nanoceria can exhibit both Ce^{3+} and Ce^{4+} oxidation states, and intermediate oxidation states with composition alternating between Ce_2O_3 and CeO_2 can be formed. Thus, nanoceria hold the capacity to release and attach oxygen with certain facility and the cerium oxides nanoparticles (CeO_{2-x}) are attributed to have disordered arrangement of oxygen vacancies.

In one study, a CeO_2-Ce_2O_3 coating, 1.0 µm thick, was cathodically deposited over 404 stainless steel. By means of potentiodynamic curves, it was detected that the values of the corrosion potential (E_{corr}) were shifted towards the positive direction, from -890 mV up to +160 mV [6]. The shifting of E_{corr} is attributed to the occurrence of another cathodic process in addition to the reaction of hydrogen evolution.

$$CeO_2 + 2H^+ \rightarrow Ce(OH)_2^{2+}$$

$$2Ce(OH)_2^{2+} + 2e^- \rightarrow Ce_2O_3 + H_2O + 2H^+$$

Another investigation have shown the electrochemical properties of mild steel were modified when the metal specimens were immersed into water based dispersions containing of cerium oxides nanoparticles. By means of EIS, ceria water based solutions promoted an ennoblement of steel surface alongside significant changes in the impedance response. It has been suggested, the capability of nanoceria to shift the oxidation state from $Ce^{4+} \leftrightarrow Ce^{3+}$ as a function of oxidative/reduction conditions [89].

2.1.3 The use of nanoceria for corrosion protection of steel

Following that, corrosion scientists turned their attention to the catalytic activities of the nanoceria. Nowadays, few publications can be found reporting their use in anticorrosive protection of metals. However, limited literature review is presented regarded mechanisms of protection given be nanoceria.

The evaluation of inhibition properties of Cerium oxide nanoparticles submitted to a Cerium nitrate treatment was studied somewhere [28]. CeO_2 nanoparticles and CeO_2 + Ce ions were added as filler on silane films onto galvanized steel. The presence of Cerium ions on the CeO_2 + Ce filled films, promoted a better adhesion and inhibition of corrosion reactions. Moreover, from d.c. polarization curves it was verified that CeO_2 and CeO_2 + Ce, shifted the corrosion potential to the noble direction. Authors reported that the CeO_2 nanoparticles created a more protective and stable film over the metal.

Zheludkevich et al. proposed that CeO_2 nanoparticles can absorb inhibitor ions and, when in contact with moisture, release them [66]. In their study, zirconia nanoparticles were firstly synthesized followed by Ce^{3+} treatment. EIS analysis demonstrated that the Cerium doped films conferred higher corrosion than the undoped and this fact was attributed to the formation of an oxide layer between the metal and the film. Moreover, resistance of the oxide layer versus time of immersion decreased slowly, as an indicative of a slower releasing of Cerium ions. On the other hand, films without the Cerium treatment rapidly decreased.

2.1.4 Toxicity of nanoceria

Many of the studies dealing with human or mammal toxicity have found negative effects from nanoceria to some extent. Nevertheless, all of these studies carried tests where nanoceria was either directly introduced into the organism or the exposure was to temperatures lower than could be expected in the environment. As an example, it has been observed negative cytotoxicity effects in hepatic cells after 24 hours of exposure [70]. Another study verified that nanoceria induced fibrotic lung injury in rats, suggesting it may cause potential health effects [71]. In addition, it has been found that systematically introduced ceria nanoparticles were retained in different rat organs causing negative effects [72].

Beside, few reports have concluded that nanoceria is relatively less toxic than other metal nanoparticles [73-75]. Moreover, one can find studies which have drawn results suggesting that human toxicity from ceria nanoparticles is not expected to be significant. However, another study suggested that genotoxic effects occurred at very low doses of nanoceria (7 nm) [76]. Another investigation reported that nanoceria is relatively nontoxic to mouse cells [77], while a second study from the same association and concluded that painted surfaces containing nanoparticles do not represent a risk for human health.

2.1.5 Methods of synthesis of CeO_2

The processes to obtain ceria nanoparticles can be classified into three main methods: i) solid phase, ii) liquid phase and iii) gas phase methods. Liquid phase methods hold the advantages of low cost of synthesis in lab scale, and they respect environmentally directives [78]. In the last decade, several researches synthesized nanoceria through different liquid phase methods, such as, microwave assisted synthesis [79, 80], reverse micelle emulsion [52], homogenous precipitation method [50], wet-chemical method, etc.

Amongst, the homogeneous precipitation route appears as an environmentally acceptable approach, since water can be used as one component in the medium reaction. It is attributed relatively low costs of synthesis associated with easiness of scale-up. Homogeneous precipitation method has been mostly used for synthesis of diverse metal oxide compounds in the nanoscale, for instance Fe_2O_3, TiO_2 , Al_2O_3 [81, 82]. In the case of

CeO_2 nanoparticles, homogeneous precipitation method is reported to obtain nanoceria [50, 83].

As an example, the influence of several kinds of alcohol and diverse volume concentration of water in the reaction medium on the ceria nanoparticles synthesis has been studied somewhere [83]. Basically, it was verified, the lower volume concentration of alcohol in the reaction medium, the higher was the nanoceria particles size and the higher was the dielectric constant of nanoceria. Furthermore, authors have shown that the kind of alcohol volume concentration in the reaction medium did not play a role on the crystalline structure. The same X-ray diffraction patterns were found either when the reaction medium was prepared with pure water.

2.2 Methodology

2.2.1 – Materials

Ceria nanoparticles investigated in this thesis were obtained via two methods of synthesis: i) supercritical flow method and ii) homogeneous precipitation.

Via supercritical flow method

The ceria nanoparticles obtained via the supercritical flow method were synthesized and supplied by Aarhus University (Aarhus, Denmark).

The stabilized CeO_2 has been synthesized by wet-chemical precipitation. An aqueous solution was prepared of $CeCl_3$ heptahydrate and citric acid. Aqueous ammonium hydroxide was added dropwise until complete precipitation and the mixture heated to 90 °C for 24 hours under reflux. It was then cooled, ethanol was added to force a precipitation of the nanoparticles. The suspension could then be centrifuged and the particles were washed repeatedly. This eventually produced a "cake" of surface-modified CeO_2 nanoparticles. Afterwards, the particles were re-dispersed in water by simple stirring and pH adjusted to just above neutral.

Via homogeneous precipitation method

The ceria nanoparticle obtained via the homogeneous precipitation method were synthesized and supplied by SP Chemistry, Materials and Surfaces (Stockholm, Sweden).

The ceria nanoparticles were produced by the precipitation of cerium $Ce(NO_3)_3.6H_2O$ with NH_4OH in the presence of H_2O_2 and acetic acid at elevated temperature. First, 30g of $Ce(NO_3)_3 \cdot 6H_2O$ and 2.6 g of acetic acid were dissolved in 2000 ml preheated water at 80°C; 28% ammonia was slowly added drop-wise to the above solution until pH reached 9 and then heated another 1 hour under stirring with Ultra Turrax at 10000 rpm. Then, reaction was cooled down by turning off the heat source. The resultant precipitate was collected by centrifugation at 4000 rpm for 20 minutes. To remove all the free-ions, such as acetate, nitrate ions in the nanoparticle dispersions, nanoparticles were extensively washed with double distilled water and re-dispersed in distilled water.

For both the methods, later the synthesis of the cerium oxide nanoparticles, the precipitated was stabilized into water-based slurry at the level of 10.0 wt. % of CeO_2. Following the synthesis of the ceria nanoparticles diverse surface modifiers and/or modification processes were used. Examples of water based solutions containing stabilized ceria are shown in Figure 6.

Figure 6 - Picture of a three different stabilized water based solution containing 10.0 wt. % of cerium oxide nanoparticles

Finally, the pH of the dispersions after stabilization was monitored. Therefore, the variety of each ceria nanoparticles water based solution was classified according to the final pH of each, as shown in Table 1.

Table 1 - Water based dispersion of ceria nanoparticles at concentration level of 10.0 wt. % obtained by SF and HP methods; pH values after stabilization

Method of synthesis	Label	pH after stabilization
Supercritical Flow	Ce.SF-3	3
	Ce.SF-5	5
	Ce.SF-8	8
	Ce.SF-10	10
Homogeneous Precipitation	Ce.HP-3	3
	Ce.HP-8	8

The electrochemical studies which are described ahead in this chapter have been conducted over the ceria water based solution at diverse levels of pH, as shown in Table 1, but also at diverse ceria nanoparticles weight concentrations, as shown in Table 3. Whenever the dissolution of the ceria solutions was required, it has been done as follows:

I. at first, two different salt solutions were prepared; sulphate solution (Na_2SO_4) to and chloride (NaCl). The salts were added into distilled water and whenever pH changes were necessary, it was adjusted with 0.1 M of H_2SO_4 or 0.1 M of NH_3OH.

Exclusively for these, the term blank is used to describe the two salt solutions. Table 2 summarizes the main features of the blank solutions.

Table 2 - Blank solutions: labels and pH values

Salt solution	Label	pH
0.3 wt. % Na_2SO_4	Blank.S.3	3
	Blank.S.5	5
	Blank.S.8	8
	Blank.S.10	10
0.1M of NaCl	Blank.C.3	3
	Blank.C.5	5
	Blank.C.8	8
	Blank.C.10	10

In the case of sulphate solution, for a trustable measurement the low content of Na_2SO_4 intended to raise electrical conductivity of the solution to avoid the IR drop or Ohmic loss – during the measurement, the drop of the potential across the electrochemical cell through

passage of current due to the internal resistance of the cell itself – and thus, to guarantee the quality of data acquisition. On the other hand, the NaCl solution has been prepared to simulate an aggressive aqueous media to steel.

II. to obtain ceria water based dispersions at the concentration of 0.5, 1.0 and 5.0 wt. %, the original ceria water based dispersion (Fig 6) were dissolved into these two salt solutions. Table 3 shows the labels and main features of these ceria water based solutions at lower concentration levels.

Table 3 - Ceria concentration and pH values after stabilization for ceria containing nanoparticles water-based dispersions. Blank reference solutions with balanced pH to 8.

Original Dispersion	Label	CeO_2 (wt. %)
Ce.SF-8	Ce.SF-0.5/8	0.5
	Ce.SF-1.0/8	1.0
	Ce.SF-5.0/8	5.0
Ce.HP-8	Ce.HP-0.5/8	0.5
	Ce.HP-1.0/8	1.0
	Ce.HP-5.0/8	5.0

The labels in Table 3 can be read according to:

- Ce, stands for Ceria nanoparticles;
- SF and HP, represent the Supercritical Flow and Homogeneous Precipitation methods, respectively;
- 0.5/8 – concentration level of 0.5 wt. % ceria and 8 is the final pH value.

These two parameters, pH and wt. % concentration, of the ceria nanoparticles water based dispersion were intensively investigated prior to the addition of the ceria nanoparticles into an organic coating. In other words, before the incorporation of the nanoparticles into an organic coating paint system, an optimal balance between the stabilization of the ceria nanoparticles into the binder alongside anticorrosive performance was investigated. At this point, it should be mentioned: i) the pH is important variable when the ceria nanoparticles are incorporated into a waterborne organic coating system; ii) therefore, the diverse pH values obtained were tested for an optimized distribution of ceria nanoparticles into the waterborne coating systems.

2.2.2 – Characterization

The cerium oxide nanoparticles water based solutions were studied by means diverse techniques as described below.

X-Ray diffraction - XRD

For the X-ray diffraction (XRD) analyses, a RIGAKU DMAX3 diffractometer was used. A Cu target, wavelength of λ = 1.54056 Å, a graphite monochromator and a Bragg-Brentano configuration have been used. The angular range 2θ between 20-100° was scanned, with a sampling step of 0.05° in 2θ and 3 seconds counting time. The experimental data was analyzed with the software Material Analysis Using Diffraction (MAUD) based on the Rietveld method [12]. The method enables the evaluation of crystallite dimensions from a Line Profile Analysis (LPA) approach based on the Warren-Averbach theory [13]. The required crystallographic data for the expected phases were taken from the Inorganic Crystal Structure Database (ICSD). The X-ray diffraction scans were performed at room temperature.

Dynamic light scattering - DLS

Dynamic light scattering study was carried out using a Zetasizer (Nano ZS, 2003, Malvern Instruments, UK). Zeta potential of cerium oxide nanoparticle was measured using Zetasizer in 10 mM NaCl solution at pH 6.

Transmission Electron Microscopy - TEM

Transmission Electron Microscopy (TEM) images and Selected Area Electron Diffraction (SAED) patterns were obtained using a JEOL JEM-3010 microscope operating at 300 kV (Cs = 0.6 mm, Point resolution 0.17 nm). Images were recorded with a CCD camera (MultiScan model 794, Gatan, 1024 x 1024 µm). TEM images were obtained from the very diluted and pH adjusted (to pH 6) dispersion of cerium oxide nanoparticles which was sonicated for additional 30 min during the TEM sample preparation. In order to avoid the aggregation of ceria nanoparticle during the drying process, hydrophobic carbon-coated TEM grid modified with 0,5% SDS (sodium dodecyl sulfonic acid) was used. Due to the hydrophilic nature of the modified TEM grid surface, drying and induced evaporation, aggregation of cerium oxide nanoparticles was avoided.

Electrochemical studies

The electrochemical properties of the cerium oxide nanoparticles were studied by means of Potentiodynamic polarization curves and Electrochemical Impedance Spectroscopy (EIS). The electrochemical measurements were conducted with an electrochemical cell, as schematized in Figure 7.

Figure 7 - Electrochemical cell used for the studies of CeO2 nanoparticles

The cell shown in Figure 7 has mainly three components: i) cold rolled steel metallic substrate, as the working electrode, supplied from Q-Panel. The arithmetic roughness (Ra) of the Q-Panels was controlled prior to the electrochemical cell set-up and it was found to be near 0.15 μm; ii) Ag/AgCl (+205 mV vs SHE) was selected as the reference electrode and platinum ring was used as the electrical conductive counter electrode; iii) the ceria water based solutions depicted in Tables 1 and 3 as the electrolytes.

Potentiodynamic polarization curves

The potentiodynamic polarization curves were collected at two different moments, anodic and the cathodic branches have been acquired separately. In the case of the anodic branch, the delta potential has been set to + 1.2 V with respect to the open circuit potential (OCP) whereas the – 1.2 V *vs.* OCP for the cathodic curve. The scan rate was set to 0.166 mV/s. All the potentiodynamic polarization measurements have been conducted at room temperature.

Electrochemical Impedance Spectroscopy – EIS

EIS measurements were performed at the free corrosion potential using an Autolab 302N Potentiostat/Frequency Response Analyzer. The selected signal amplitude was 5 mV, 10^{5} – 10^{-2} Hz frequency range and approximately 0.6 cm^{2} testing area was employed. Once again, the Ag/AgCl reference electrode (+205 mV vs SHE) and platinum ring counter electrode were employed while the working electrode was the cold rolled steel panel. The

impedance data were analyzed with the software ZSimpWin 3.22. All the EIS measurements have been conducted at room temperature.

The OCP between ceria solutions with respect to steel was monitored with the use of two electrodes arrangement using an AMEL Ammeter/Electrometer (Model: 668/RM). The potential of the mild steel as working electrode with respect to the Ag/AgCl (+205 mV vs SHE) reference electrode was monitored during immersion time. All OCP the measurements have been conducted at room temperature.

2.3 Results and Discussion

The studies of the ceria nanoparticles started with the electrochemical measurements of the stabilized water based solutions at the concentration level of 10.0 wt. %. Moreover, for a distinguished presentation of the results, this section is divided into two parts: first, the ceria nanoparticles obtained via supercritical flow method is presented, followed by those obtained via homogeneous precipitation.

2.3.1 Physic-chemical investigation of the ceria nanoparticles

Figure 8 shows the XRD pattern for the ceria nanoparticles obtained via supercritical flow method. The broadening of the peaks may suggest that the particles were relatively small in dimension. Moreover, one should be noticed that an overlap between the peaks might have occurred due to the broadening. From Figure 8, the peaks were attributed to (111), (200), (220) and (311) diffraction planes, therefore representative of the cubic fluorite structure for cerium oxide without any other crystalline phase. Similar observations were seen elsewhere [87,88].

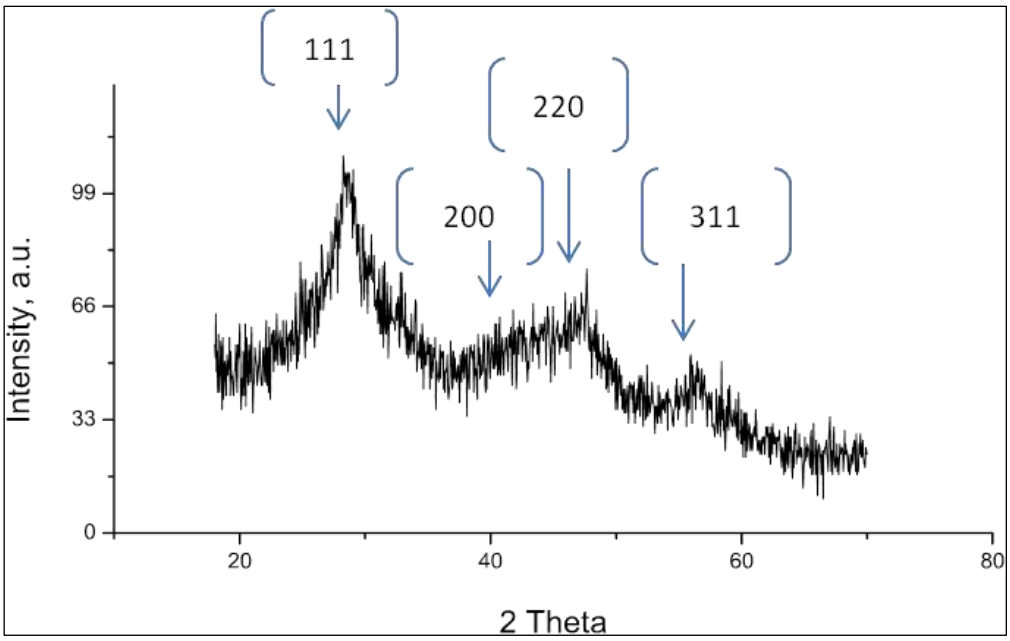

Figure 8 - XRD spectra (left) and TEM (right) for the ceria SF nanoparticles

The particles size estimated according to the Debye-Sherrer equation and was found approximately near 5.0 nanometers. Such value represents the mean size of the nanocrystalline domains. It is important to highlight that the ceria nanoparticles are comprised of these nanocrystalline domains of 5 nm in diameter approximately and similar observation can be found elsewhere. The mean nanocrystalline size is verified by means of high resolution TEM, as shown in Figure 9. The particle size was valued to be near 5 nanometers and, therefore, in accordance with XRD and the Debye-Sherrer equation.

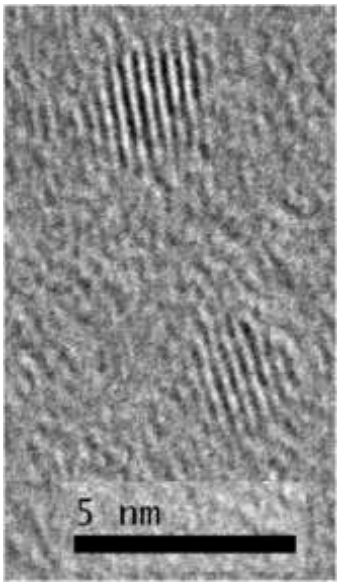

Figure 9 - TEM for the ceria SF nanoparticles

Likewise to the ceria nanoparticles obtained via supercritical flow method, following the process of synthesis *via homogeneous precipitation method*, the cerium oxide nanoparticles were stabilized into water based solutions. Figure 10 shows the TEM image and correspondent selected area diffraction pattern (SAED) of Ce.HP ceria solution prepared for these techniques.

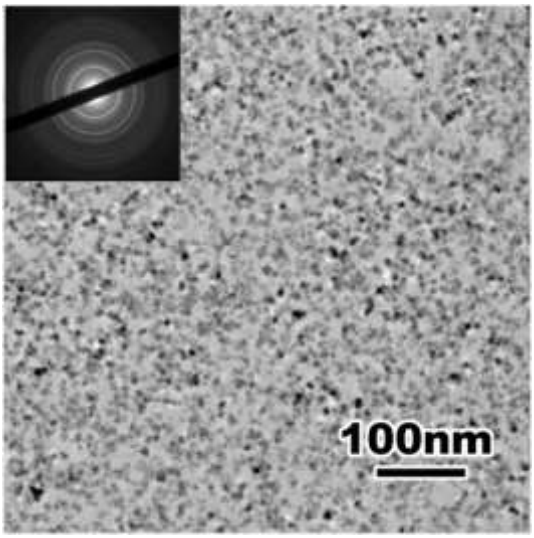

Figure 10 - TEM image of Ce.HP nanoparticles and correspondent SAED pattern

According to TEM image, it has been verified the primary particle sized distribution between 5 – 20 nm. From SAED, the ring electron diffraction pattern was attributed to randomly distributed crystals of the nanoparticles. Moreover, the particle sized distribution has been confirmed by means of XRD. The estimation according to the Debye-Sherrer equation has found a crystallite size approximately around 7.0 nm. Once again, this estimation represents the mean size of the nanocrystalline domains and the peaks were attributed to (111), (200), (220) and (311) diffraction planes, therefore representative of the cubic fluorite structure for cerium oxide without any other crystalline phase. Figure 11 depicts the XRD pattern for the ceria nanoparticles obtained via homogeneous precipitation method.

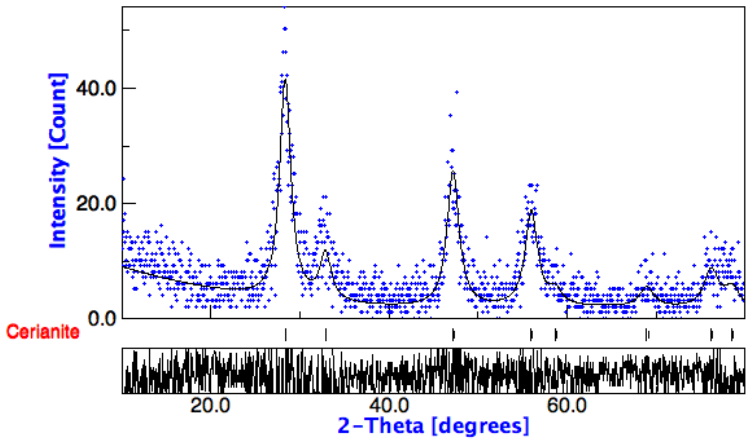

Figure 11 - XRD pattern of ceria nanoparticles obtained via homogeneous precipitation method

2.3.2 Electrochemical investigation of the ceria nanoparticles

The anodic and cathodic polarization curves of steel substrate immersed into the ceria water based solution Ce.SF-5 are shown in Figure 12. All the potential values were referred to the +205 mV vs SHE.

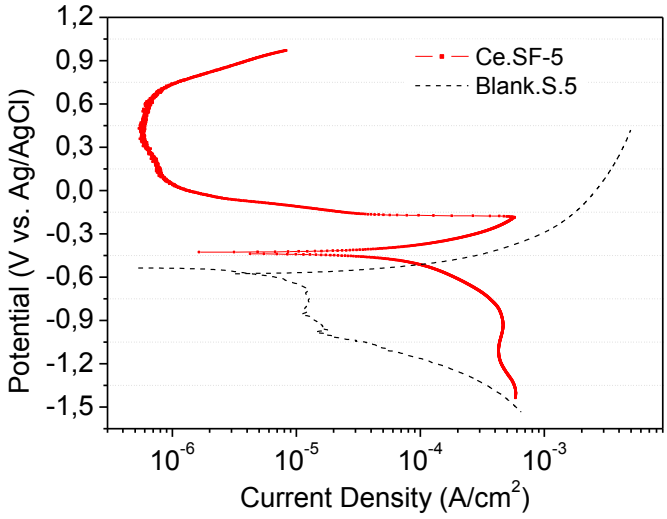

Figure 12 - Potentiodynamic polarization curves of mild steel exposed to Ceria10.pH5 solution and to the blank at pH 5

Recalling the label *Ce.SF-5,* it represents the cerium oxide nanoparticles obtained via Supercritical Flow method at the concentration level of 10.0 wt. % and pH equal to 5. A comparison is done between Ce.SF-5 and, the salt solution labeled as *Blank.S.5*.

For Blank.S.5, the free corrosion potential (E_{corr}) or open circuit potential (OCP) was verified near -0.6 V, this value goes in accordance to literautre. In the cathodic direction, in other words, when potential was reduced to more negative values, from -0.6 to -1.0 V, the current density was found constant near 10^{-5} A/cm^2. On the other side, when potential is

raised, one can see that the current density was quickly raised from 10^{-5} to 10^{-3} A/cm^2 from -0.6 V to -0.3 V approximately, indicating relatively high corrosion rates.

In the case of Ce.SF-5 solution, OCP was verified near – 0.5 V. When potential was raised from the OCP towards the anodic direction, one can see significant changes in the anodic polarization curve. At potentials near - 0.1 V a reduction of about 3 orders of magnitude of anodic current density, from 10^{-3} to 10^{-6} A/cm^2, is verified. After, while potential was increased until 0.6 V, the current density remained constant at 10^{-6} A/cm^2. Finally, higher than 0.6 V the current density started to increase again.

In particular, the shape of the anodic branch is well representative of the anodic polarization curve of a passive-active metal. Regardless the similarities, the maximum current density (i_{max}) was found near 10^{-3} A/cm^2. The repeatability of these results was verified another two times and considered reasonable.

The presence of 10 wt. % of ceria nanoparticle into the sulphate solution promoted a reduction of three orders of magnitude of anodic current with respect to the blank sulphate solution. Owing to a further investigation about the electrochemical activity of the Ce.SF-5 water-based solution, diverse panels of mild steel were immersed into this solution. Following, every 24 hours passed, two panels were taken off the ceria solution, rinsed with distilled water, dried with compressed air and finally, potentiodynamic polarization curves have been acquired in presence of Blank.S.5 electrolyte. Figure 13 depicts the evolution of the mild steel polarization diagrams of steel panels not immersed into the ceria solution (0 h), as well after 24 and 288 hours of immersion.

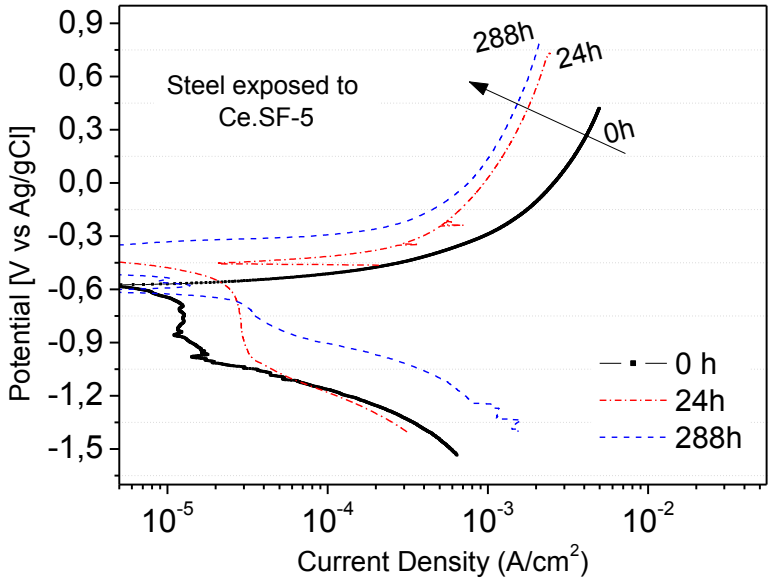

Figure 13 – Evolution of polarization curves of mild steel immersed in Na_2SO_4 solution after 24 and 288 hours of exposure

After these periods of immersion into Ceria-pH5 water-based solution, few differences are seen on the polarization diagrams of mild steel. For instance there was a slight shift towards lower current density in the anodic branch, after 24 hours, highlighted with the arrow. Apart from this, after 288 hours, a slight ennoblement effect is noticed, OCP has been increased from – 0.6 to – 0.3 V. Therefore, the active-passive transition effect of steel immersed into Ce.SF-5 solution has been necessarily given while steel was immersed into Ce.SF-5.

Cerium oxide nanoparticles were stabilized into diverse water based solutions with the use of various surfactants/stabilizers. Therefore, the pH was among the parameters influenced by the different stabilization routes. Figure 14 shows the potentiodynamic polarization curves of mild steel immersed into the ceria water based solution Ce.SF-8 and, for this ceria solution, pH was found near to 8 after the stabilization process.

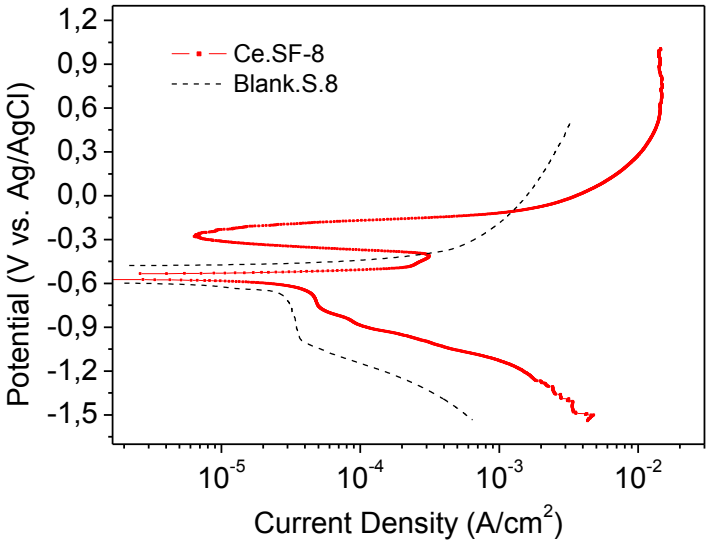

Figure 14 - Potentiodynamic polarization curves of mild steel exposed to Ce.SF-8 solution and to the blank at pH 8.

The label Blank.S.8 denotes the 0.3 wt. % of Na_2SO_4 with pH adjusted to 8. For the Blank.S.8 solution OCP was verified near -0.6 V. When potential was increased towards more noble values, from -0.6 V to -0.3 V approximately, the current density was quickly raised from 10^{-5} to 10^{-3} A/cm^2 indicating relatively high corrosion rates. On the contrary, when potential was reduced to more negative values, from -0.6 to -1.0 V, the current density was found constant near 10^{-5} A/cm^2 due to hydrogen evolution. In general, both anodic and cathodic curves were slightly shifted to lower current densities when compared with the Blank.S.5.

As regarded to mild steel exposed to the Ce.SF-8 water based solutions, the OCP between mild steel and the ceria solution was verified between -0.5 ~ -0.6 V. The correspondence of the anodic shape of Ce.SF-8 with an active-passive of passive metals is yet seen for Ce.SF-8, however much less evident than Ce.SF-5. The i_{max} was observed near and 10^{-3} A/cm^2.

When the stabilization process of the ceria nanoparticles led to water based solution with final pH value near to 3, the potentiodynamic polarization curves of steel immersed into this solution have shown diverse behavior. Figure 15 displays the comparison of Ce.SF-3 and Blank.S.3 curves.

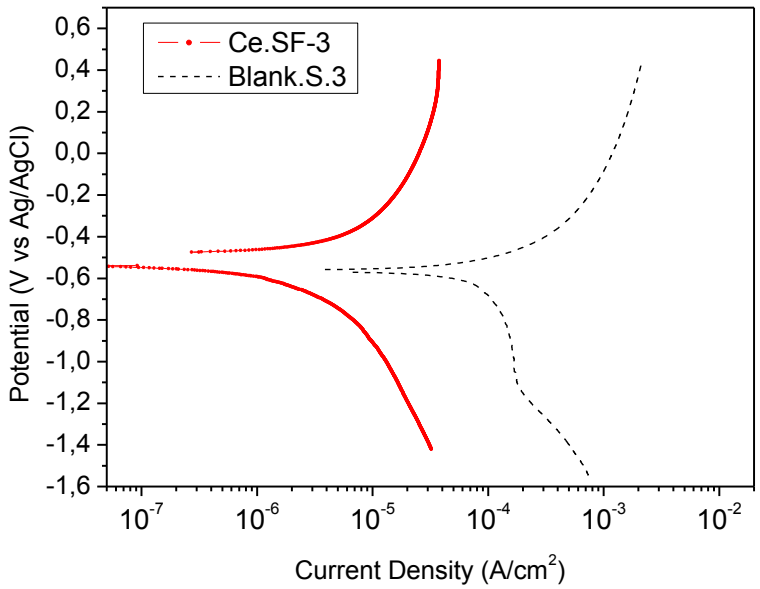

Figure 15 - Potentiodynamic polarization curves of mild steel exposed to Ce.SF-3 solution and Blank.S.3

The OCP values of both solutions were found very similar, around – 0.6 V. In the case of mild steel immersed into the Ce.SF-3 water based solution, although the shape of curves did not show active-passive transition effect, one can notice a two orders of magnitude shift towards lower current densities on both branches, anodic and cathodic.

In the anodic polarization, the potential is changed in the direction of positive values, thus the working electrode, in this case mild steel, becomes the anode and electrons are withdrawn from it. Therefore, the displacement in the direction of lower current densities, from 10^{-3} to 10^{-5} A/cm^2, observed in the anodic branch of Ce.SF-3 when compared to Blank.S.3 solution, suggests that the rates of withdrawing electrons has been reduced of about two orders of magnitude. Analogue to that, in the cathodic polarization the working electrode becomes the cathode and electrons are deposited onto its surface. Hence, the reduction of cathodic rates, suggested lower rates of electron being deposited onto the surface of steel. Figure 16 shows the potentiodynamic polarization curves of mild steel immersed into Ce.SF-10 and into the Blank.S.10 solution.

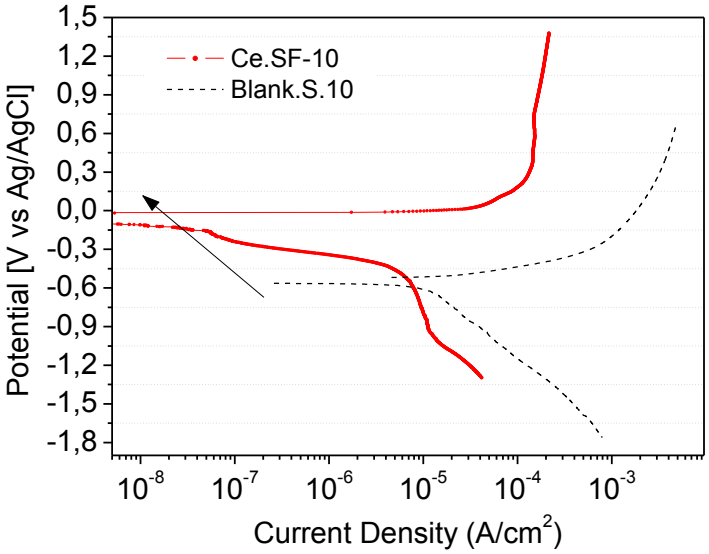

Figure 16 - Potentiodynamic polarization curves of mild steel exposed to Ce.SF-10 solution and to the blank at pH 10

Two significant effects are distinguished when polarization curves of mild steel were collect in presence of Ce.SF-10 water based dispersion: i) OCP value was found approximately 0.5 V more noble than Blank.S.10; ii) the curves were shifted nearly two orders of magnitude towards lower current densities, moreover, the current densities reached a steady state from 0.25 V at a current density of 10^{-4} A/cm^2 for the anodic branch.

Owing to more detailed investigation of Ce.SF-.10, panels of steel were immersed into this ceria solution for over 12 days. Every 24 hours, one panel had been taken out of the solution and anodic polarization curve was carried out in presence of Blank.S.10. Figure 17 shows the evolution of the anodic polarization curve of steel before immersion and after 24, 120 and 312 hours. In addition, the surfaces topography of the steel not immersed and after 312 hours is shown.

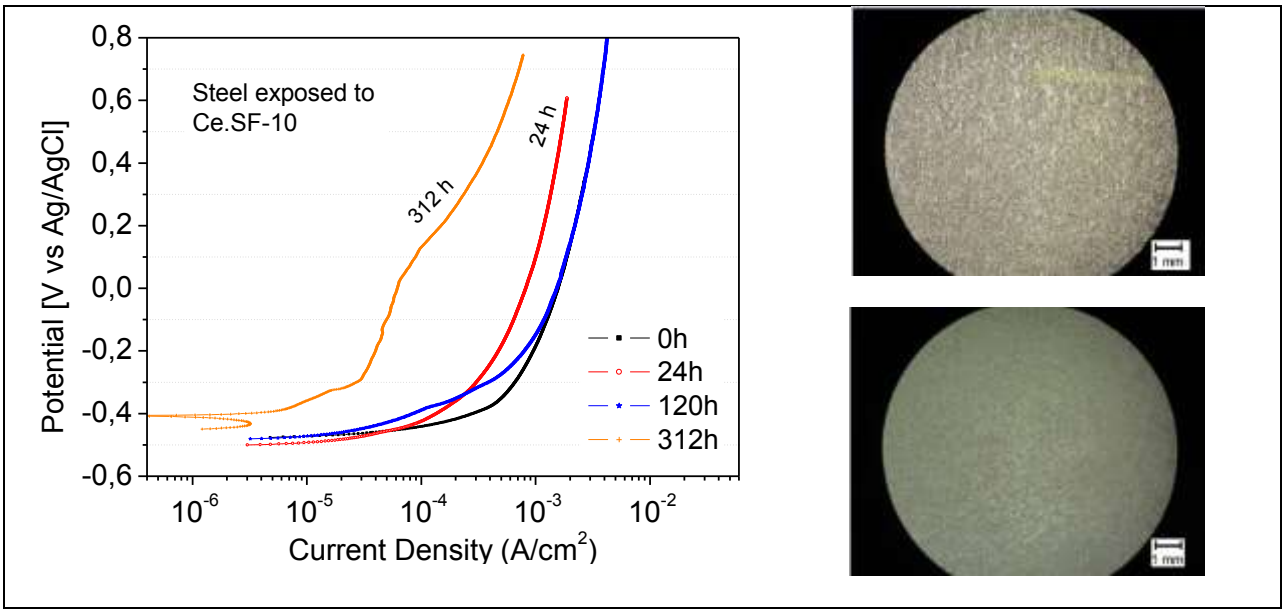

Figure 17 - Anodic polarization curves of steel in sulphate solution after 0, 24, 120 and 312 hours of immersion into Ceria10-pH10 solution. Surface of steel before (top-right) and after 312 hours of immersion into Ce.SF-10 (bottom-right).

The anodic curve at time = 0h represented the steel panel which was not immersed into solution. Thus, the OCP was found near -0.5 V and there was a rapid increase in the current densities when potential was risen from -0.5 to -0.4 V indicating that corrosion of steel occurred at high rates. After 24 hours, one can see a slight shift of anodic curve towards lower current densities, however, after 120 hours the anodic polarization curve was very similar to the 0 h.

On the other hand, the anodic curve of steel collected after 13 days of immersion showed few differences from the previous curves: i) the OCP was slightly increased to -0.4 V; ii) the whole diagram has been shifted towards lower current densities and a reduction of one order of magnitude was appreciated. In this case, the ennoblement effect of 0.2 V of magnitude alongside with the reduction in the anodic current densities suggested that the long period of immersion promoted changes onto the surface of steel.

From the microscopic images, one can see that after 312 hours into the ceria containing solution the aspects of steel surface were modified. The steel surface presented a grayish appearance. Such assumption remains limited to the visual aspect, since after the acquisition of the images, the steel sample was used for the acquisition of anodic polarization curve and nothing can be mentioned about the chemical composition of the surface. However, one should consider the Ce.SF-10 was a water-based solution, with dissolved ions such as OH^- and O_2 which is considered a reactive medium for steel. Even though the long immersion period, after the steel had been taken out from ceria solution no

corrosion products were seen along the surface. It is likely that, while in contact with Ce.SF-10 solution corrosion reactions did not occur.

After stabilization, the pH values of Ce.HP-8 water solutions was monitored and ranged with significant stability for over 1 year around 8. The polarization curves of mild steel substrates recorded in presence of Ce.HP-8 is shown in Figure 18.

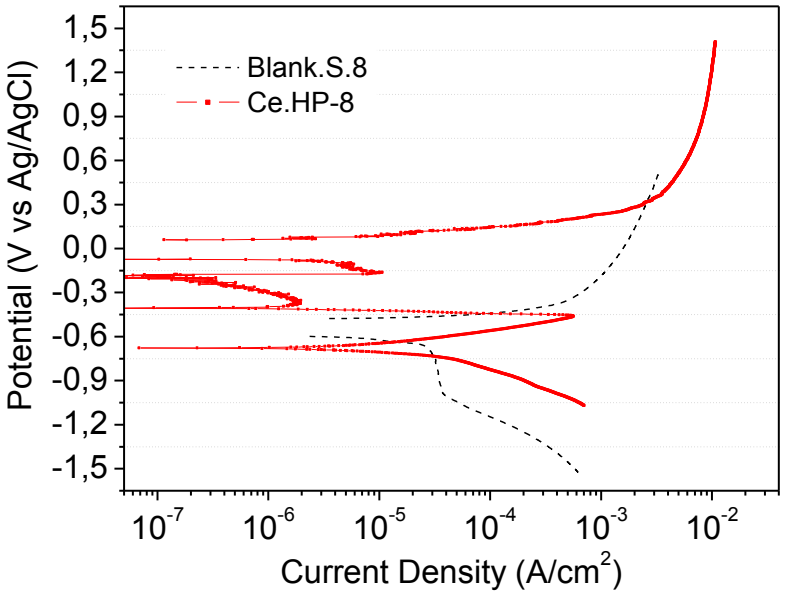

Figure 18 - Potentiodynamic polarization curves of mild steel immersed into Ce.HP-8.

The discussion about the potentiodynamic diagram of Blank.S.8 electrolyte is accessible above. Although the polarization curves of mild steel specimens immersed into both Ce.HP-10.8 water based solutions are imprecise, for instance, the identification of the OCP values was not clear, it can be appreciated signs of electrochemical activity. For example, in the anodic polarization, when potential values ranged approximately between -0.5 and 0.1 V, there was a shift of anodic current densities towards lower densities. The 'unclear' behavior of Ce.HP-8, and consequently, same interpretation was found for repeated measurements. Repeatability of Ce.HP-8 was considered consistent.

Owing to a more detailed investigation of the water based ceria solutions, the open circuit potential between mild steel, Ce.HP.8 and Ce.SF.8 has been monitored over time of exposure. Figure 19 shows the evolution of OCP of two steel specimen immersed into Ce.HP-8 as well as Ce.SF-8 water based solutions during the course of 72 hours.

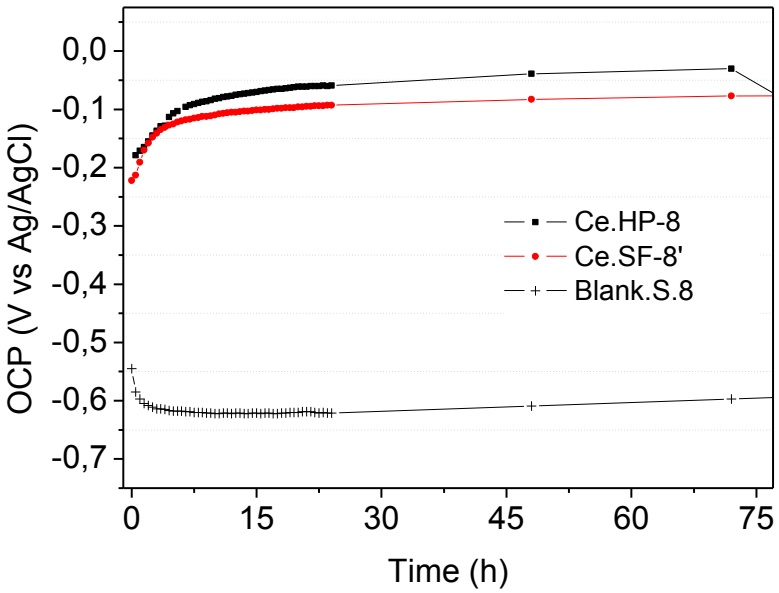

Figure 19 - Evolution of open circuit potential of mild steel immersed into Blank.S.8 and ceria solutions obtained from SF and HP methods.

The OCP of steel immersed into the Blank.8 solution dropped from -0.55 to -0.60 V in the first hours of exposure and remained near -0.60 until the end of the monitoring. This observation is in accordance with the free corrosion potential value of mild steel into sulphate solution [29]. When steel was immersed into both ceria containing solutions, the OCP evolved differently to the Blank.S.8 and can be described as follows:

In the case of steel immersed into Ce.HP-8 a higher initial OCP value, near -0.15 V, was verified for the two specimens. Later, for one of the specimens the ennoblement effect lasted about 20 hours, when a reduction to -0.7 occurred whereas, for the second sample a slight increase of about 0.1 V of magnitude towards more noble potentials occurred. After 72 hours, the OCP was verified near – 0.05 V for the steel immersed into the Ce.HP-10.8 solution.

Very similar was the evolution of one specimen of steel immersed into Ce.SF-8 water based solution. Initially, OCP was found near – 0.15 V and it evolved in the direction of more noble potential values. At the end, potential values near -0.05 V have been noticed. In view of the monitoring of OCP and the potentiodynamic polarization curves of steel immersed into diverse ceria water based solution, few links connections between the techniques are suggested.

In the case of Ce.SF-8, even though the reading of the OCP was not clear due to scattering in the potentiodynamic polarization diagrams, two out of two have shown tendency to more noble potential values before the measurement ran, from the monitoring

of the OCP displayed in Figure 19, both of steel specimens immersed into Ce.HP-8 solutions have shown more noble potential, 0.5 V higher than the potential read of steel immersed into Blank.S.8 solution. For the steel specimens immersed into Ce.SF-10 the free corrosion potential was detected 0.5 V higher than the salt solution and this information has been confirmed via the OCP monitoring shown in Figure 19.

The monitoring of the OCP proposed in Figure 19 reads the voltage difference assumed by a specimen when in contact with a corrosive liquid over time of immersion. In addition, the instrumentation is not in service, no external loads were applied. Particularly in Figure 19, steel was the specimen, the ceria solutions and the Na_2SO_4 salt solution the corrosive liquids. Hence, the OCP can be defined as the potential wherein both rates, anodic and cathodic hold equal magnitudes, or the rate of oxidation is equivalent to the rate of reduction. Therefore the more noble potentials observed for the steel when immersed into the ceria water based solutions suggests that the equilibrium between the anodic and cathodic rates has been displaced towards less active region.

At this moment, few elucidations should be emphasized: this project aimed to develop a waterborne paint system in which the ceria nanoparticles will be added. Furthermore, ceria nanoparticles have been designed to be incorporated into the primer layer of the paint system and, additionally, the primer itself has been designed to be a waterborne organic layer.

Up to now, the studies of the water based ceria solutions were dedicated to the ceria solutions stabilized after synthesis, at the concentration level of 10.0 wt. %. However, if one considers the nano size and the costs attributed to the ceria nanoparticles, the incorporation of the ceria into the primer layer of the paint system was designed at reduced contents. In particular, three possible weight concentrations of ceria nanoparticles were proposed: 0.5, 1.0, 2.0 and 5.0 wt. %.

Besides that, in Chapter 4 the waterborne binders considered for the development of the paint system alongside their evaluation will be presented. Simultaneously to the ceria studies, compatibility tests between the water based ceria nanoparticles dispersions and the waterborne binders have shown enhanced dispersion and stability of the ceria nanoparticles into the waterborne binder was obtained with the ceria nanoparticles from supercritical flow method with pH equal to 10 (Ce.SF-10) and with the ceria nanoparticles from homogeneous precipitation with pH equal to 8 (Ce.HP-8) ceria water based solutions.

For this reason, the original ceria solution, Ce.SF-10, was diluted into less concentrated contents of cerium oxide nanoparticles (see Table 3). After, the anodic and cathodic curves of mild steel were collected with respect of diverse concentration of cerium oxide nanoparticles containing solutions with pH balanced to 10. The polarization diagrams are presented in Figure 20.

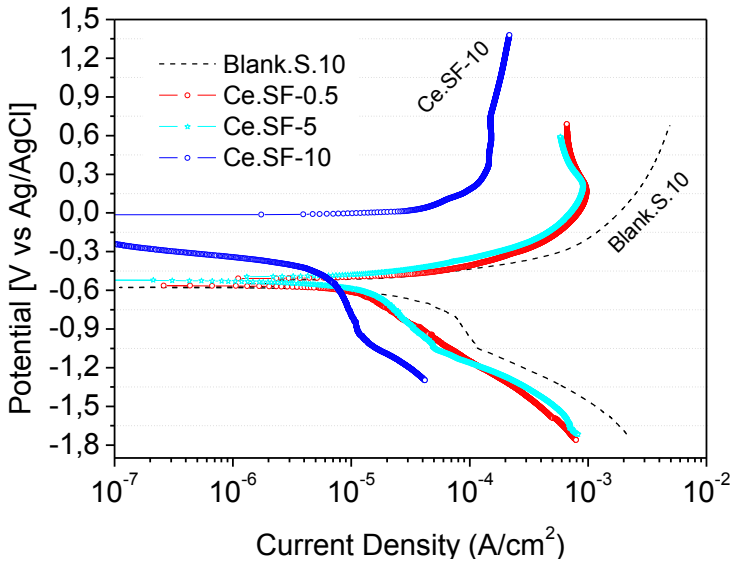

Figure 20 - Potentiodynamic polarization curves of mild steel exposed to Ce.SF-10, as well to diluted solutions: 0.5 and 5.0 wt. %

Recalling the labels in Figure 20 are with respect to the level of dissolution of Ce.SF-10. As an example, Ce.SF-0.5 denotes the water based solution containing 0.5 wt. % of ceria nanoparticles obtained via supercritical flow method with final pH near 10.

From Figure 20, no significant differences between the polarization curves of solutions with reduced contents were seen. Apart from the original Ce.SF-10 solution, which raised the OCP from -0.6 V and shifted anodic branch of the polarization curve towards lower current densities, it is likely that lower contents of ceria into the water based solution have not promoted beneficial changes in the polarization behavior.

In the case of the ceria obtained via homogeneous precipitation method, similar approach has been followed for the original solution with 10.0 wt.% and pH 8 of cerium oxide nanoparticles obtained by homogeneous precipitation method dispersed in water. Figures 21 and 22 show the potentiodynamic polarization curves of steel immersed into the Ce.HP-10 and reduced concentrations of ceria nanoparticles. For a proper comparison, the pH of the solutions was balanced to 10. It can be seen that, for concentrations lower than 5.0 wt.% of nanoparticles, the solutions seemed not to modify the electrochemical

interactions, however, higher contents of nanoparticles, 5.0 and 10.0 wt.%, have raised the OCP towards more noble values, from -0.60 to -0.10 V (vs Ag/AgCl).

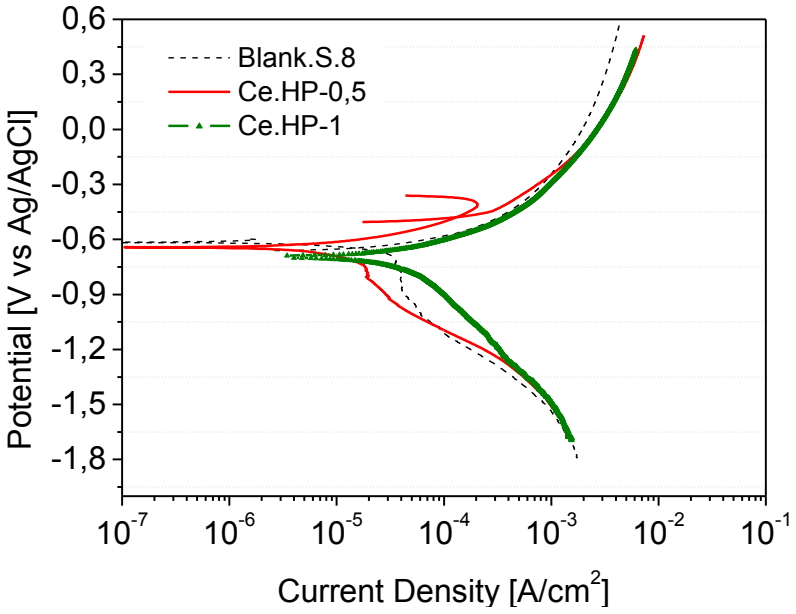

Figure 21 - Potentiodynamic polarization curves of mild steel exposed to the original Ce.HP-10, as well to diluted solutions: 0.5, 1.0

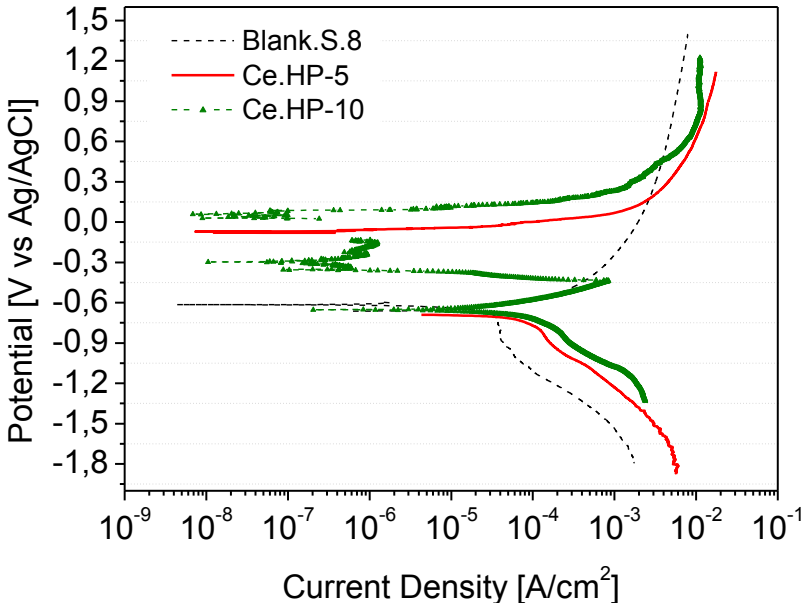

Figure 22 - Potentiodynamic polarization curves of mild steel exposed to the original Ce.HP-10, as well to 5.0 wt. %

From the Figures 21 and 22, one can see that no significant changes between the polarization curves of solutions with reduced contents were promoted by the solutions at the concentration level of 0.5 and 1.0 wt. %. when compared to the Blank.S.8. Although the shape of the polarization curves of the original Ce.HP-10 solution and the reduced concentration solution Ce.HP-5 were not clear to be interpreted, it is likely that the

presence of 5 wt. % of ceria HP into the salt solution promoted beneficial effect, since the OCP of the anodic branch of the curve was shifted in the direction of more noble values.

Considering that potentiodynamic polarization technique scans the response of the metal specimen over potentials distant from the OCP and, in the case of the measurements above the delta potential has been set approximately ± 1.2 V vs. OCP, such technique can be considered destructive for the working electrode. In particular, the measurements of the dissolved ceria solutions (0.5, 1.0 and 5. wt. %), the potentiodynamic polarization technique may have hidden any possible electrochemical activity these solutions containing lower amounts of ceria. Hence, electrochemical impedance spectroscopy has been carried out for the investigation of the dissolved ceria water based solutions.

Recalling that the ceria nanoparticles studied were designed to be incorporated into a waterborne based organic coating, simultaneously to optimization of the ceria synthesis methods, preliminary electrochemical investigation have shown the optimal ceria content into the waterborne coating was equal to 1.0 wt. %. Such investigation can be found in Chapter 4, section 4.2 and 4.3. For this reason, the Ce.SF-1 with pH 10 and Ce.HP-1 with pH balanced to 8 have been selected. Both, the Bode impedance and phase angle spectra of mild steel immersed into these ceria containing solutions from initial conditions (0 h) and their evolution after 5 and 24 hours are shown in Figures 23 - 25. For comparison, the Blank.S.8 is likewise reported. The first spectrum, labeled as t = 0h, has been acquired when the steel specimen was put into contact with the solutions.

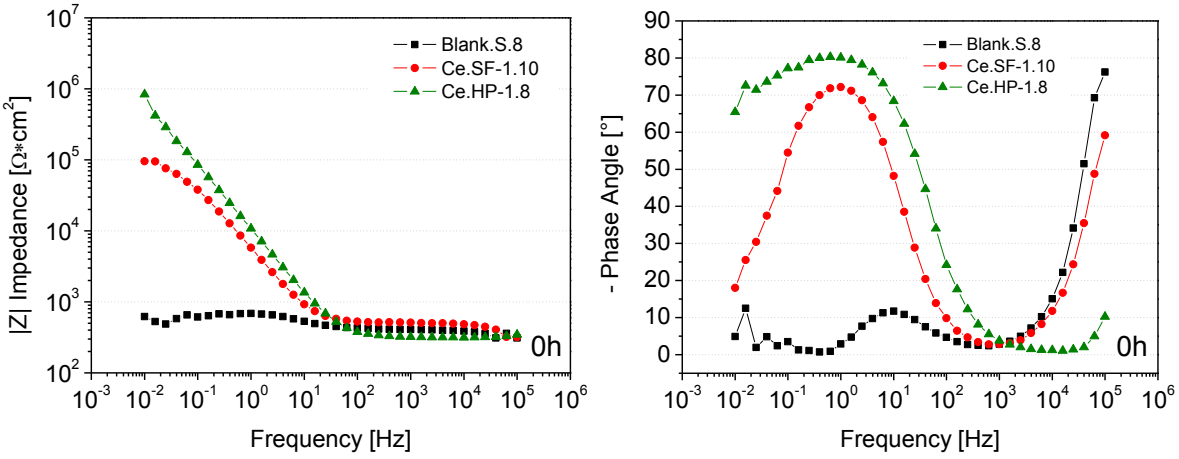

Figure 23 – Bode impedance (left) and Bode phase angle (right) spectra of Ce.SF-1.10 and Ce.HP-1.8 at the beginning 0h

In the case of mild steel immersed into Blank.S.8 solution the Bode impedance and the Bode phase angle spectra showed that corrosion may have started almost immediately. The values of the impedance were found near 10^3 Ohm.cm^2 and the phase spectrum

exhibited 10° over the entire range of frequencies. The evidences of corrosion reaction that have been initiated are seen after 5 and 24 hours, where the phase angle spectra depicted the presence of a second time constant from middle to low frequency range.

In contrast, when mild steel immersed into the sulphate solutions containing 1.0 wt. % of ceria nanoparticles, strong modifications in the EIS behavior can be noticed from the very beginning of the analysis. For instance, at t = 0h, the total impedance at low frequency range ($|Z|_{0.01Hz}$) for Ce.SF-1.10 and Ce.HP-1.8 were found 2 and 3 orders of magnitude higher than the Blank.S.8, near 10^5 and 10^6 Ohm.cm^2 respectively. Besides, their phase angle spectra were shifted towards higher angles.

The evolution of EIS behavior of mild steel immersed into Ce.SF-1.10 is described as follows: after 5 hours of exposure, the $|Z|_{0.01Hz}$ was slightly increased of about one order of magnitude, 10^6 Ohm.cm^2 accompanied by a raise in the phase angle degrees. Later, there was a reduction of $|Z|_{0.01Hz}$ to from 10^6 to 10^3 Ohm.cm^2 similarly perceived from the phase angle spectrum after 24 hours.

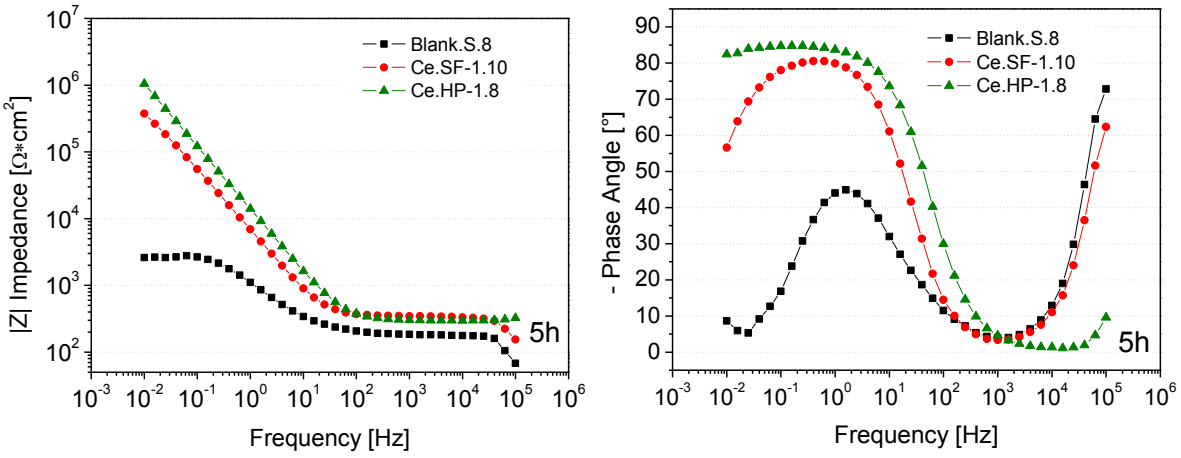

Figure 24 - Bode impedance (left) and Bode phase angle (right) spectra of Ce.SF-1.10 and Ce.HP-1.8 after 5h

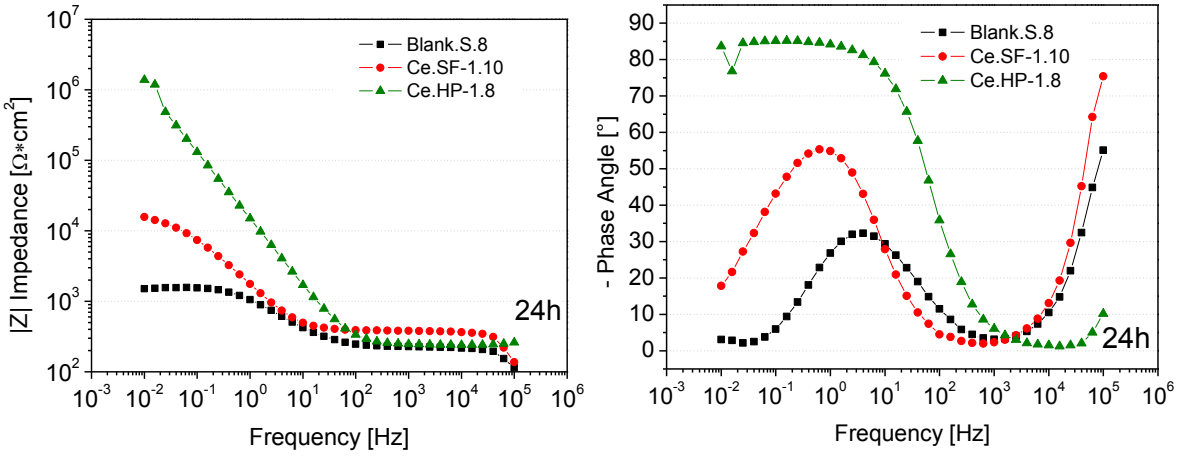

Figure 25 - Bode impedance (left) and Bode phase angle (right) spectra of Ce.SF-1.10 and Ce.HP-1.8 after 24h

In the case of mild steel immersed into Ce.SF-1.10, the EIS behavior evolved with remarkable stability. The same 10^6 Ohm.cm^2 magnitude for the $|Z|_{0.01Hz}$ was observed over the period of 24 hours. In addition to that, the $|Z|_{0.01Hz}$ remained near 10^6 Ohm.cm^2 for Ce.HP-1%.8 for over 500 hours of immersion, as shown in Figure 26.

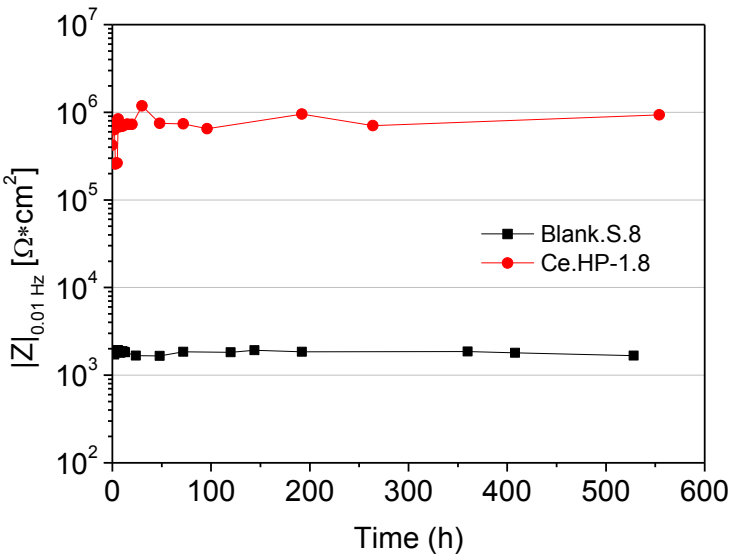

Figure 26 - Evolution of |Z|0.01 Hz of steel specimen immersed into Ce.HP-1%.8 and Blank.S.8

After the 500 hours of immersion into the Ce.HP-1%.8 solution, the steel panel was detached from the electrochemical cell and its surface was evaluated by means of scanning electron microscopy (SEM). For a proper comparison, steel surface without being immersed into ceria solution has been likewise evaluated by means of SEM as shown in Figure 27 whereas Figures 28 shows the metal surfaces exposed to the Ce.HP-1%.8 solution after 500 hours of immersion.

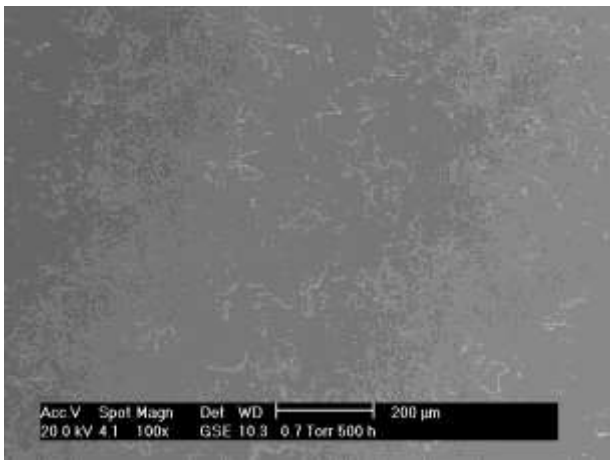

Figure 27 - SEM image of general steel surface without contact to water based ceria dispersion

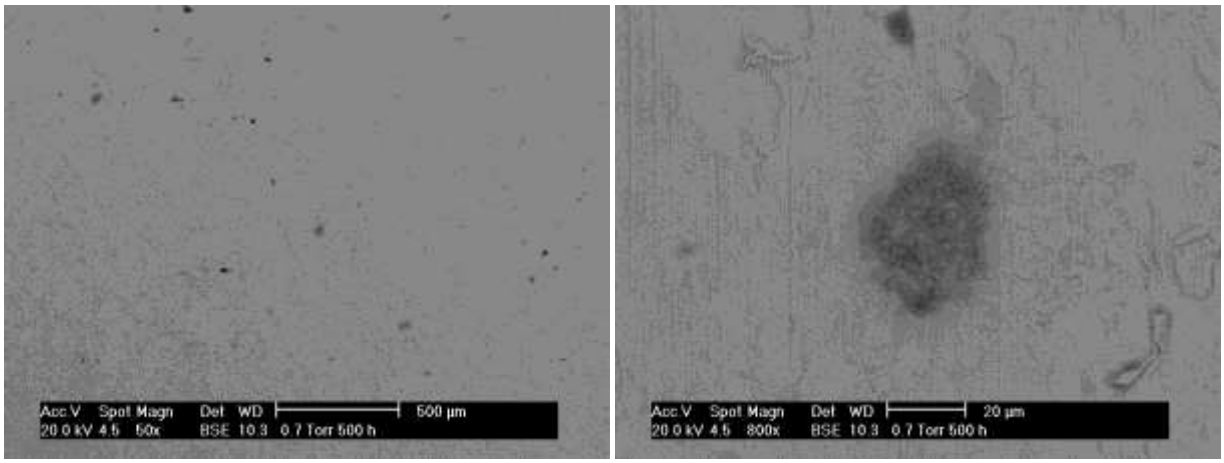

Figure 28 - SEM images of steel surface after 500 hours of immersion into Ce.HP-1%.8 ceria water based solution

From SEM images, the features of the steel surfaces without being exposed to ceria solution and the steel surface after 500 hours of contact to Ce.HP-1%.8 solution are comparable. The surface of steel exposed to the water based ceria solution presented limited corrosion products as seen from SEM images at higher magnitudes. It is likely that, a protective anticorrosion effect was given by the ceria water based solution while in contact with steel.

The corrosion protection potential of the ceria particles were further investigated in presence of sodium chloride solution. The electrochemical impedance evolution of the steel electrodes immersed in the 0.1M NaCl solutions containing 1.0, 3.0, 5.0 and 10.0 wt% of CeO_2 nanoparticles at the beginning of the immersion as well as after 5 and 400 hours is shown in in Figures 29–31. Likewise, in Figs. 28–31 the steel immersed into the blank chloride solution has been reported. At the beginning of the immersion period, one can notice the influence of ceria nanoparticles into the chloride solutions upon the impedance values of working electrode. The $|Z|_{0.01Hz}$ of steel immersed into the blank was near 10^3 Ohm.cm^2, whereas impedance spectra at time = 0h showed a strong increase of the impedance in the middle to low frequencies range for the ceria containing solutions, despite the wt.% concentration, near 10^6 Ohm.cm^2.

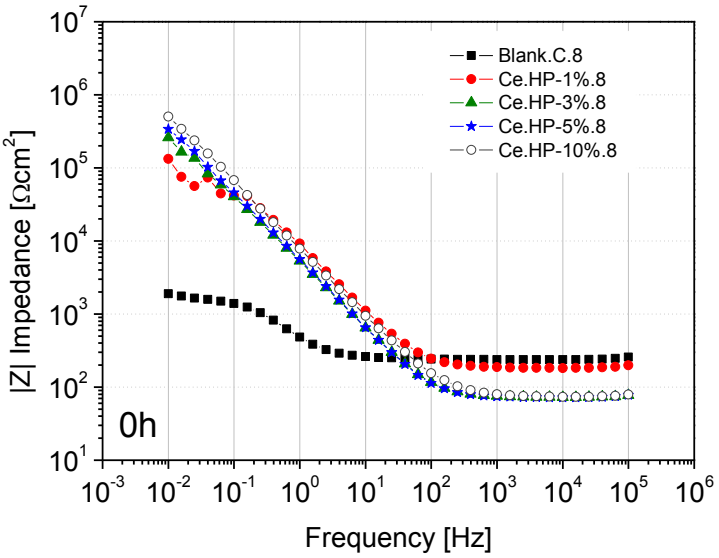

Figure 29 - Bode Impedance of steel exposed to diverse ceria concentrations at t = 0h

From Figure 30, after 5 hours of immersion, one can see that the overall impedance of steel immersed into 0.1M NaCl solutions containing 1.0 wt% of CeO_2 nanoparticles has been lowered. For instance, the $|Z|_{0.01}$ showed a reduction of about 3 orders of magnitude, from 10^6 to 10^3 Ohm.cm^2, approximately. Moreover, it is possible to appreciate a remarkable stability of the impedance spectrum of the steel immersed in the 0.1M NaCl solution containing 3, 5 and 10 wt% of CeO_2 particles. In effect, the values of total impedance at low frequency range have been found around 10^6 Ohm.cm^2 for over 400 hours of analysis.

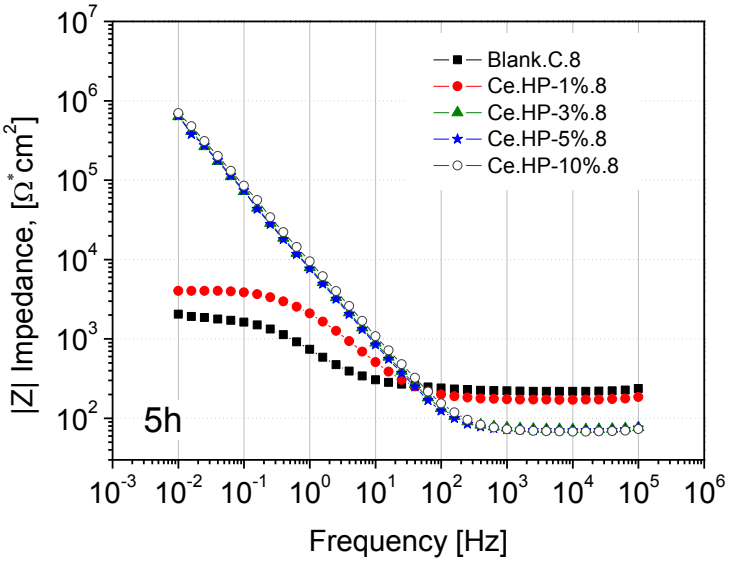

Figure 30 - Bode Impedance of steel exposed to diverse ceria concentrations at t = 5h

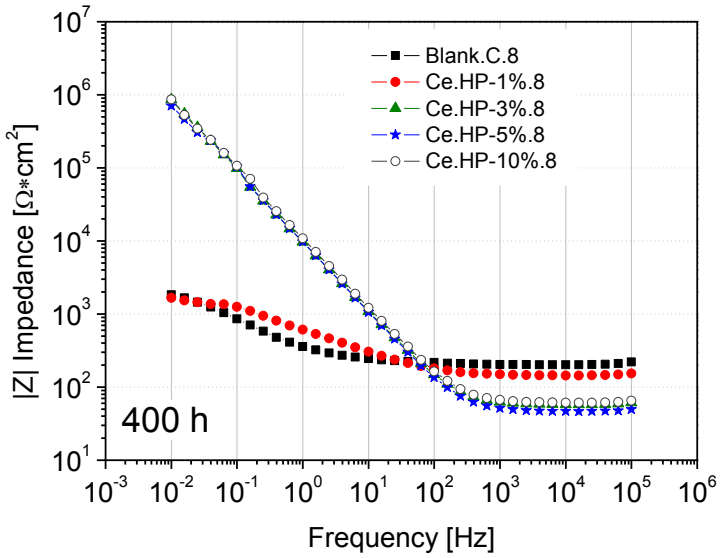

Figure 31 - Bode Impedance of steel exposed to diverse ceria concentrations at t = 0h

In view of the above, mild steel immersed in 0.1 M NaCl solution, with pH balance to 8, containing 3.0 or more wt. % of ceria nanoparticles have shown high values of the impedance alongside remarkable stability, over 400 hours of immersion. In the case of lower concentration of ceria, 1.0 wt. %, an initial, however not stable values of impedance has been seen. It is likely that the presence of a certain amount of ceria nanoparticles is needed to maintain high impedance values during immersion time. Chlorides are recognized to promote the corrosion of steel in neutral environment by forming complexes which tend to be unstable and soluble [30]. The resulting shape of the impedance spectrum seems to be in accordance with the electrochemical impedance response of a “blocking electrode” (described elsewhere in literature [31]) corresponding to an electrical circuit where no current flows when the dc limit is reached.

Going further, the impedance spectra reported above have been modelled using the electrical equivalent circuits shown in Figure 32. The electrical circuit illustrated in Figure 32 (a) consists of a $R_{el}Q$ system and, in this case, R_{el} stands for the electrolyte resistance whereas Q is likely to be related to the contribution of the passive oxide on the surface of steel. In Figure 32 (b) the $R_{el}(Q_{dl}R_{ct})$ sytems is described where, the $(Q_{dl}R_{ct})$ represents the time constant attributed to the faradic process occurring on the electrode surface [32]. The Q_{dl} is a constant phase element (CPE) related to the double layer capacitance of the steel surface, while R_{ct} represents the charge transfer resistance of the faradic process.

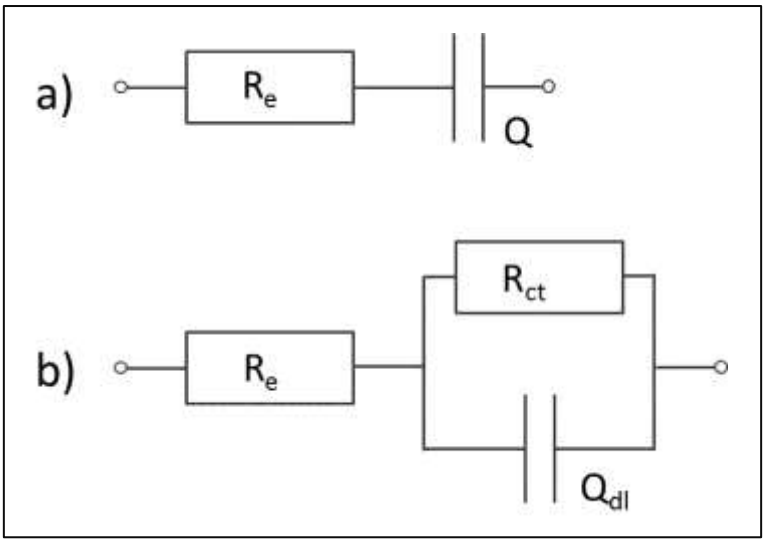

Figure 32 – Electrical circuits used for modelling the EIS data: (a) ReQ and (b) Re(QdlRct).

The EIS spectra of the steel electrode immersed in the 0.1M NaCl solutions containing 1.0 wt. % of CeO_2 particles were fitted using the circuit reported in Figure 32 (b), since one time constant was clearly visible throughout immersion time. For the steel immersed in the 0,1M NaCl solutions containing 3.0, 5.0 and 10.0 wt% of CeO_2, were fitted using the circuit depicted in Figure 32 (b) until an "active behavior " was observed and using the circuit depicted in Figure 32 (a) when a sort of "blocking electrode" impedance response was recognized. Figure 32 shows the evolution of the capacitance of the Y_0 value related to the CPE ($|Z|_{CPE} = 1/(Y_0 \cdot (j\omega)^n)$).

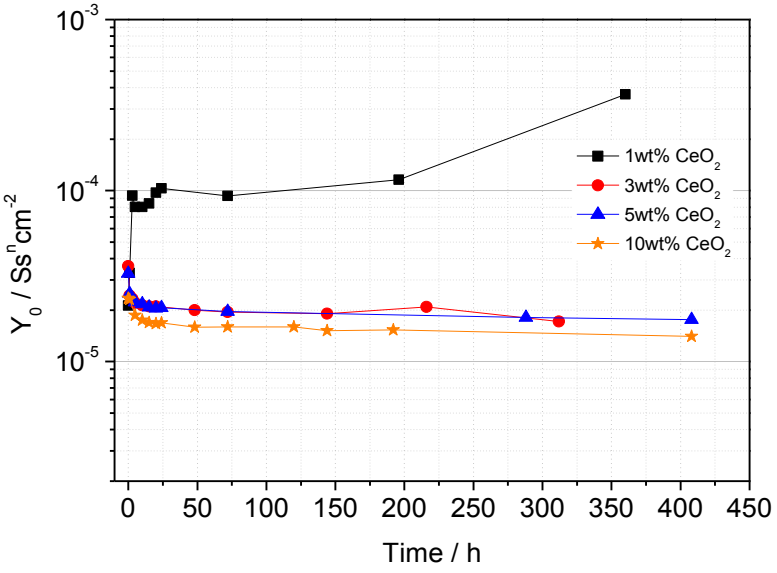

Figure 33 - Evolution of the Y_0 value (a) and exponent versus immersion time [Electrochimica Acta 131 (2014) 71–78]

From Figure 33, a continuous increase of Y_0 is seen in the case of chloride solution containing 1.0 wt. % of ceria, whereas in the case of the steel electrodes immersed in the

solution containing 3.0 wt. %, or higher than, the values of Y_0 remained considerably stable between 10^{-4} and 10^{-5} $S \cdot s^n \cdot cm^{-2}$. The evolution of the charge transfer resistance, R_{ct}, of the ceria containing solutions at the concentration levels of 1.0, 3.0, 5.0 and 10.0 wt. % over the course of 25 hours is shown in Figure 34.

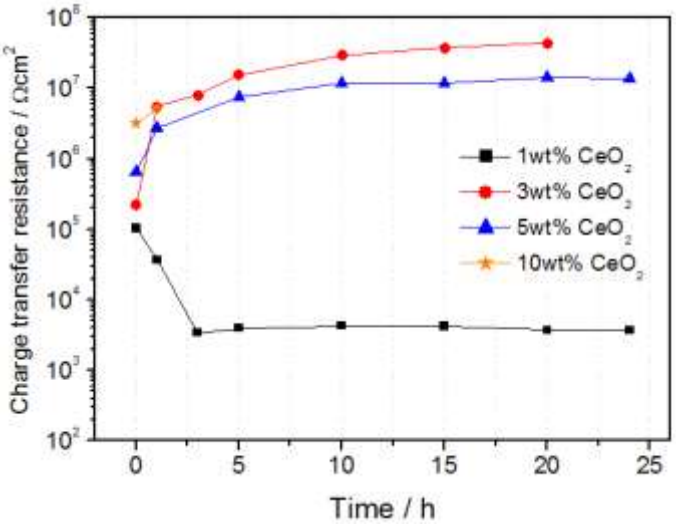

Figure 34 - Rct evolution of steel immersed into ceria solutions

The charge transfer resistance of the solution containing 1.0 wt% of CeO_2 dropped from 10^5 down to 10^3 Ohm.cm^2 after 3 hours of immersion. In the case of higher concentration levels, such as for 3.0 and 5.0 wt. %. the R_{ct} was verified to increase from 10^5 to 10^7 Ohm.cm^2 in the course of 20 hours. After, the acquisition of the R_{ct} was no longer possible. The solution containing 10.0 wt.% of CeO_2 nanoparticles behaved like an "active electrode" only in the very first hours of immersion. Thus, the acquisition of the R_{ct} was valid until the 3rd hour and the $R_{el}Q$ circuit was used to fit the experimental data from the 3rd hour onwards.

In view of the experimental results of ceria solutions, considerable observations have been verified, for instance, the ennoblement of the corrosion potential, and the stable as well as relatively high value of the $|Z|_{0.015Hz}$ around 10^6 Ohm.cm^2 versus immersion time.

Although not clearly demonstrated by the electrochemical techniques, these observations might be was associated to the formation of passive or conversion layer on the surface of the steel electrode. This hypothesis could explain the strong reductions of the corrosion rate of the metal substrate in the ceria nanoparticles containing electrolytes as the ennoblement of the corrosion potential. It is likely that the presence of the particles inhibits the corrosion processes, probably by forming or inducing the formation of a passive or

conversion layer on steel. The reason for this particular behavior is still under investigation, but it is alleged to be related to the capability to shift the oxidation state from $Ce^{4+} \leftrightarrow Ce^{3+}$ as a function of oxidative/reduction conditions.

2.4 – Conclusion on cerium oxide nanoparticles

Essentially, the investigation of the electrochemical activity of cerium oxide containing water based solution has been presented in this Chapter. In principle, two different routes of synthesis have been used to obtain the ceria nanoparticles, the supercritical flow and the homogeneous precipitation methods.

By means of Transmission Electron Microscopy and diffraction pattern alongside X-ray Diffraction and the estimation according the Debye-Sherrer equation, the nano size range of the ceria particles has been evidenced. Regardless the method of synthesis, the final crystalline size was found between 5 – 10 nanometers with consistent repeatability in the data.

Through the polarization curves conducted for steel specimens immersed into the into the cerium oxide containing water based solution, the electrochemical activity was found diverse depending on the route of synthesis. In the case of cerium oxide containing water based solution, obtained via the supercritical flow method, a reduction of about 3 orders of magnitude on the anodic currents of steel immersed into the ceria solution at the concentration level of 10 wt. % has been verified compared to the steel specimen immersed into sulphate solution. In addition to that, through the monitoring of the open circuit potential an ennoblement of the potential of mild steel has been observed over the period of 72 hours, free corrosion potential was detected 0.5 V higher than the salt solution.

Similarly, from monitoring of the open circuit potential, the water based solutions containing the ceria nanoparticles obtained via the homogeneous precipitation methods have shown an ennoblement of 0.5 V of magnitude when the steel specimens immersed into the ceria solution at the concentration level of 10 wt. %. In addition to that, the surface of steel specimens immersed into cerium oxide containing water based solution for approximately 13 days have shown minimal presence of corrosion products, consequently, while immersed into the ceria solutions, corrosion reactions have been delayed.

Later, the development of the waterborne paint system containing ceria nanoparticles has found that the concentration level of 1.0 wt. % of ceria nanoparticles was optimal for the formulation of the paint systems. In this way, electrochemical impedance spectroscopy technique has been used on the investigation of the cerium oxide containing water based solution at the concentration level of 1.0 wt. %. The EIS investigation of the steel specimens immersed into the cerium oxide water based solutions revealed that the presence of the particles into sulphate and chloride solutions have raised the impedance in the low frequency range. Simultaneously, the steel electrodes immersed in the cerium oxides containing solutions showed a switch from an “active electrode” behavior to a “blocking electrode” behavior. Moreover, another further investigation performed in chloride solutions revealed 3.0 wt. % of these particles inside the solution was needed to guarantee a long term stability of the steel electrodes surface in such a way that the corrosion processes are delayed. The hypothesis that the shift of the corrosion potential as well as the switch of the impedance response of the steel electrodes immersed in the solutions was associated to the formation of a sort of passive or conversion layer on the surface of the metal electrode. This hypothesis would explain the strong reductions of the corrosion rate of the metal substrate in the ceria nanoparticles containing electrolytes as the ennoblement of the corrosion potential. This, however, would request further and deeper investigations in order to clarify and prove the statements.

3 Polyaniline nanoparticles

Late in the 70's, the discovery that Polyacetylene (PAc) could transport electrical charge along its chains by Heeger, Shirakawa and MacDiarmid, for which they awarded the Nobel Prize in Chemistry [1-3], gave scientists a new class of materials to be explored. Denominated, nowadays, as Intrinsic Conductive Polymers (ICP), these materials can combine the electronic and optical properties of a semiconductors and metals with the mechanical properties and ease of processing associated with polymers. Subsequently to PAc a list of ICPs has come out, for instance Polypyrrole (PPy), Polythiophene (PT) and the most explored among the ICP's Polyaniline (PAni).

3.1 Introduction to PAni

Polyaniline (PAni) is defined as an intrinsic conductive polymer, conjugated polymer containing π-electron which undergoes both electronic and protonic doping reaction. Polyaniline can exist in several fundamental forms mutually differentiated by the degree of oxidation or protonation. However, not all the possible PANI states are able to conduct electrical charges, the emeraldine base (EB) form of polyaniline is a partially oxidized form of PAni and requires protonation to become highly conductive, as shown in Figure 35.

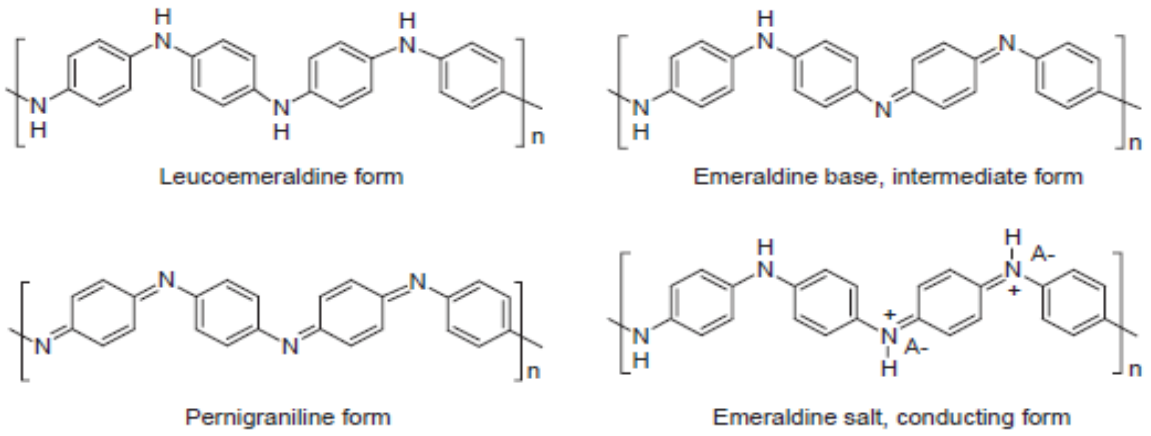

Figure 35 - Possible PANI state Leucoemeraldine (LE), Emeraldine base (EB), Pernigraniline (PG) and the salty state Emeraldine salt (ES).

The oxidation state increases from Leucoemeraldine form (LE) which is the complete reduced form to EB, and then to Pernigraniline (PG) form, the full oxidized. In the salty form, anions are necessary for balancing the charge of salts. Considering the salty and base states of Emeraldine, the equilibrium reactions of PANI includes not only redox

reactions (changing LE, EB, PG), but also proton exchange reactions, passing from EB to ES (and the opposite) as shown in Figure 36.

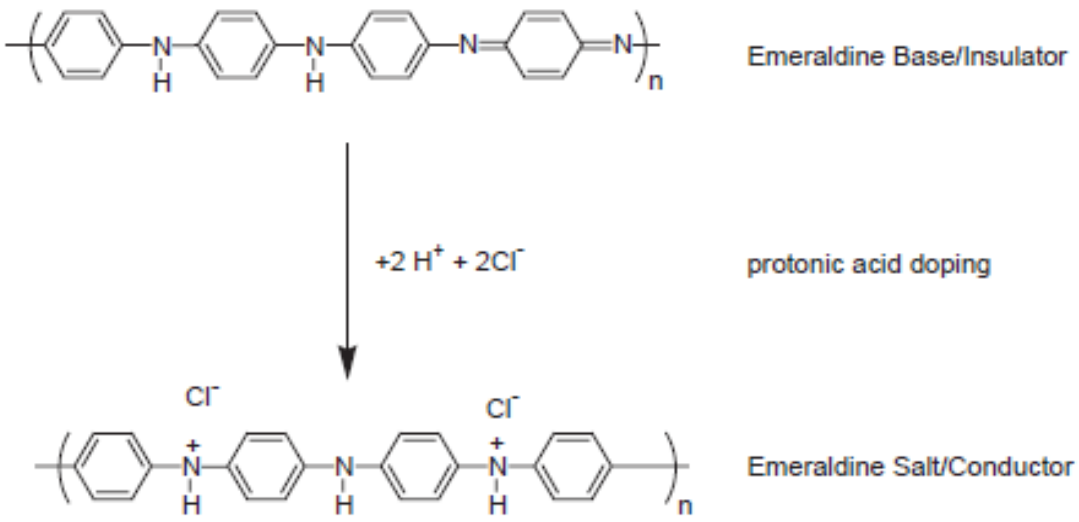

Figure 36 - Possible PANI state Leucoemeraldine (LE), Emeraldine base (EB), Pernigraniline (PG) and the salty state Emeraldine salt (ES).

Polyaniline can be obtained synthesized through electrochemical polymerization process or, via the chemical oxidative polymerization. A doping component is usually used during PAni synthesis in order to control the properties of polyaniline. Depending on the acid used, the final protonated PANI is characterized by specific solubility, electric conductivity.

Due to its unique redox properties a wide possibility of applications is attributed to PAni, such as mechanical sensors, electromagnetic shielding (EMI), pH sensors and corrosion protection.

3.2 PAni for corrosion protection purposes

The interested in Polyaniline for corrosion protection purposes begun after the works of DeBerry, who demonstrated that electrodeposited Polyaniline film, was able to reduce the corrosion rate of the 400 series stainless steel on sulfuric acid solution by forming an oxide layer between the metal and PANi [4], ICP gained attention as promising candidates for anticorrosive applications.

Several literature review about the use of ICP as corrosion protection materials are available. As an example Tallman et al. [5] reviewed a number of publications with the use of Polyaniline (PANi) for iron, steel and stainless steel corrosion protection. On the whole, there are clear evidences that ICP provide corrosion protection of steel, besides this,

several operating corrosion protection mechanisms have been proposed, such as barrier protection, corrosion inhibition, anodic protection, ennobling effect and others. However, due to the several possible configurations for an experimental analysis of corrosion, the complete understanding about the mechanisms is difficult to elucidate and thus, it has been highlighted that every single situation should to be handled separately. In this view, the role of the ICP's, in particular Polyaniline, for the corrosion protection of steel is still a controversial issue, despite the large literature available on this topic.

It was found in many studies the formation of a passive oxide layer between the steel and PANi, which reduced the corrosion rate of the metal under investigation and are in agreement with the suggestions given by DeBerry. Apart of that, these observations enhance the indication that PANi coatings act not just as a physical barrier for steel protection. Hence, from studies of corrosion protection performed with defects purposely introduced in the PANI coatings systems, it was found that diverse mechanisms are operating [1, 11-17].

The corrosion properties of iron coated with Polyaniline via dip process was evaluated by Wessling et al [12]. By using sodium chloride solution for the electrochemical analysis it was observed a significant and reproducible decrease on the corrosion rate of the coated iron. The proposed mechanism given by the author was the passivation of iron by PANi, by forming an oxide layer. Through chemical elemental analysis, the author noticed a higher content of oxygen on the passivated areas and no oxygen on pure iron, instead. Therefore he concluded that Polyaniline can lead to a reduction on the corrosion rate of the iron.

The corrosion behavior of the system made up by PANi as primer coat applied over mild steel, overcoated with epoxy resin was evaluated by Lu et al. The experiments were designed in order to compare scribed and intact samples, with and without PANi, in two different electrolytes. Concerned to the scribed/damaged systems, it was observed a reduction in the corrosion rate of samples treated with doped PANi in the HCl solution. On the other hand, neutral PANi showed greater corrosion rate reduction in the NaCl solution. It was suggested that PANi leads to the formation of a passive oxide layer. In addition, X-ray photoelectron spectroscopy (XPS) showed that the oxide layer is composed by γ-Fe2O3 and Fe3O4. From that, it was concluded by the author that corrosion protection to mild steel can be provided by Polyaniline coatings [13].

A comparative study of the electrochemical behavior between mild steel coated with undoped Polyaniline and Polyaniline doped with some organic sulfonic acids using 3.5% of NaCl and 0.1M HCl solutions as electrolytes was done by Pud et al. A reduction in the corrosion current of a potentiodynamic measurement, meaning a decreasing in the corrosion rate, was noticed from PANi doped with TSA (p-toluene sulfonic acid) and the undoped PANi, as well, in the case of NaCl solution. The system PANi/TSA showed a decrease in the corrosion current when HCl solution was environment. Authors did see the presence of the oxide layer in the case of undoped PANI, not for PANI/TSA and therefore concluded, unexpectedly, that changing the doping level of PANi did not lead to a decrease in the corrosion current [14].

A comparison in marine and urban environments between 3 thermoplastic polymer coatings and an alkyd resin loaded with 1.0 wt. % of PANI, Laco et. al. have observed better corrosion protection of carbon steel and better degradation resistance of the coating for the alkyd resin with PANI. Photo-oxidative resistance of the resin increased due to the presence of PANI as a consequence of lower amount of aggressive ions in contact with the metallic surface [15].

A contradictory idea is using Polyaniline as a physical barrier. Some studies reported the possibility to use doped PANI as a volatiles transporter, including oxygen, for novel membranes applications. Moreover, the degree of protonation plays a role in the gas transportation, by increasing the Polyaniline oxidation state the gas permeability is modified [18].

3.2.1 - Mechanisms of protection

Summarizing the above information, although there is a general agreement that PANi performs well in retarding corrosion on carbon steel, the mechanisms for this process is still under investigation. Various hypotheses have been suggested for the mechanism of corrosion protection using PANi: a) formation of an oxide layer; b) Shift of the electrochemical interface.

a) *Formation of an oxide layer*

Several studies have pointed out the surface Polyaniline in contact with steel induces the formation of an oxide layer. The passivation promoted by Polyaniline on steel, that is to say, the formation of an oxide layer is accompanied by an appreciable potential shift

towards more noble values. For instance, it was reported by Wessling et al. that PANi employed as primer coating, having a 20 µm thick, shifted the steel surface potential from about –400 mV to +250 – 400 mV, which is far into the noble region. Moreover, an Fe_2O_3 layer up to 1 µm thick was formed between the steel surface and the primer [13]. According Li et al [84], the formation of an oxide layer when Polyaniline is in contact with steel is owing to the redox characteristic of PANi, in other words, the ability of emeraldine base to be reduced into the leucoemeraldine state or oxidized into the pernigraniline state.

A scheme of the occurring reactions is given in Figure 37. Polyaniline oxidizes the iron Fe into Fe^{2+}, and in in doing so, returns itself into the reduced leucoemeraldine state form (PANi-LE). In the presence of oxygen and water, Fe^{2+} is oxidized to Fe^{3+}, the leucoemeraldine form is oxidized to the polyaniline in emeraldine base form, and oxygen is reduced to OH^-. When the sufficient amount of Fe^{3+} and OH^- are generated, they form Fe_2O_3, and the polyaniline base is transformed back to the protonated salt.

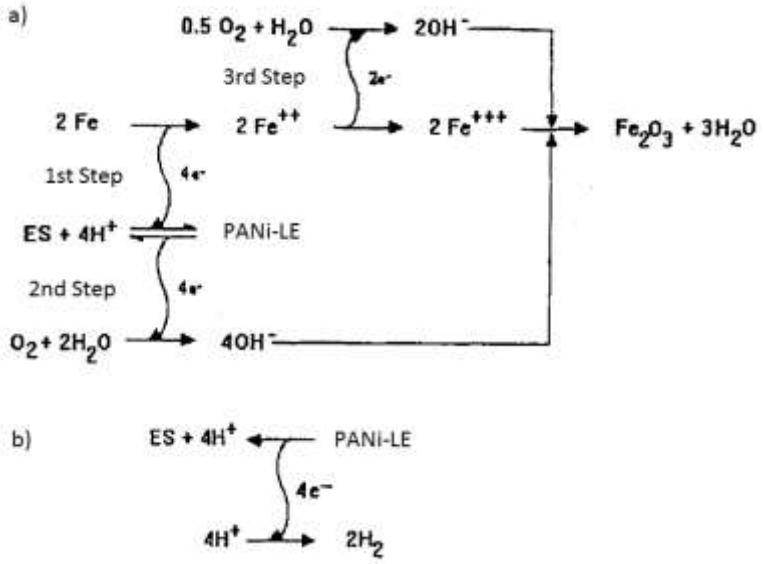

Figure 37 - Schematic diagram of mechanism of iron passivation by PANI on mild steel. Adapted from [19].

b) Shift of the electrochemical interface

One mechanism for corrosion protection was initially given by Schauer et al [8], reviewed and further upgraded [9, 85]. First of all, it was highlighted the importance of a pre-treatment at the steel surface before the application of Polyaniline over steel as a primer coat. The efficiency of PANi is attributed to an entirely oxide free state of the metal surface before PANi application. After that, ascribed to Polyaniline action initiates the formation of the oxides compounds, $FeO.Fe_2O_3$ and γ-Fe_2O_3, pioneers of the passive layer. It is well known that Polyaniline in the doped state, either *P*-Doped or *N*-Doped state, is itself a

vehicle for the electrons movement. When iron (Fe) is oxidized into Fe^{+2} in the anodic reaction, 2 electrons a generated and Polyaniline takes part in the electrochemical process, by capturing and transporting these electrons from the metal surface to the outside of the primer layer (Figure 38).

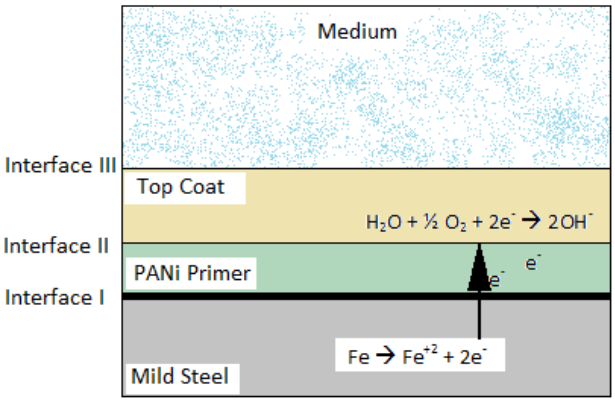

Figure 38 - Schematic representation of the protective mechanism of PANi primer coat. Adapted from [21].

In doing so, the PANi layer displaces the cathode reaction outside of the metallic substrate. By separating these electrochemical reactions, the pH at the metal surface is not increased, since the production hydroxyl occurs at interface II and by this means, the oxides previously formed, will be preserved. It is important to enhance that the previous electrochemical reaction will start, only and if only, some corrosive ions diffuse through the coating and reach the metal. Owing to the fact that, a top coat is often applied over the primer coat, the permeability of the top coat plays an important role on the coating efficiency. Thus, a top coat with good barrier properties enables Polyaniline film to successfully separate the partial electrochemical processes and the common coating defects, such as blistering or cathodic delamination, will not appear.

3.2 Methodology

The methodologies of study adopted on the investigation of PAni nanoparticles were similar to those of ceria nanoparticles described in Chapter 2 (see item 2.2.2). Taking into consideration that Polyaniline nanoparticles used in this work is available as a commercial product, much of its preparation process and properties are reserved to the supplier.

3.2.1 – Materials

Polyaniline nanoparticles were produced by Enthone Nano Science Center (Ammersbek, Germany) via the chemical oxidative polymerization of aniline in presence of sulfonic acid.

The average particle size is around 50 nm and electrical conductivity in the order of 10^{-4} S/cm^2 obtained from a spincoated film on ITO/glass substrate. Subsequently to the process of synthesis, the nanoparticles were stabilized into water-based solution at three different levels of concentration, 4.0, 6.0 and 8.0, as shown in Table 4.

Table 4 – Water based PAni Solutions: concentration and pH values after stabilization

Label	PAni content (wt. %)	pH after stabilization
W.PAni-4	4.0	2.6
W.PAni-6	6.0	2.7
W.PAni-8	8.0	2.9

One can notice from Table 4 the considerably low pH values verified for the water based solutions containing PAni after stabilization. As describe above, PAni have been synthesized in presence of sulfonic acid, doping agent of the aniline monomer. Thus, the acidic character found for the W.PAni's water based solutions is justified by the release of sulfonic acid from PAni chains into the aqueous media. In this case, the electrochemical investigation conducted for W.PAni water based solutions have been compared with the salt solution balanced with pH 3, as shown in Table 5. The Blank.S.3 water solution has been prepared as follows: 0.3 wt. % Na_2SO_4 was added into distilled water and after, pH was adjusted with 0.1 M of H_2SO_4.

Table 5 - Blank solutions: labels and pH values

Label	Na_2SO_4 content (wt. %)	pH
Blank.S.3	0.3 wt. %	3

3.2.2 – Characterization

The polyaniline containing water based solutions have been studied by means of electrochemical techniques, such as, potentiodynamic polarization curves and Electrochemical Impedance Spectroscopy. The detailed description can be found in the item 2.2.2.

Differently than ceria water based solutions, in which two process of synthesis have been investigated, the main feature of the water based solutions displayed in Table 1, are the diverse weight concentration of polyaniline obtained via the chemical oxidative polymerization of aniline and following the same parameters of synthesis.

3.3 Results and Discussion

Figures 39 and 40 show the evolution of the OCP of the water based containing Polyaniline nanoparticles solutions as well as the blank salt solution with pH 3. From Figure 39, it can be seen that, in the case of the Blank.S.3 solution the free corrosion potential was continuously reduced from -0,45 to -0,7 V, approximately, in the course of 24 hours. For the PAni containing solutions, a slight diverse evolution was observed. Higher the content of PAni into the water based solutions, higher was initial values of OCP. For instance, in the case of W.PAni.8 OCP was shifted towards more noble values, from -0,55 to -0,45 V. For the water based solutions containing 4.0 and 6.0 wt% of PAni, W.PAni.4 and W.PAni.6 respectively, similar trend of the OCP was detected, however less intense and shorter than the W.PAni.8.

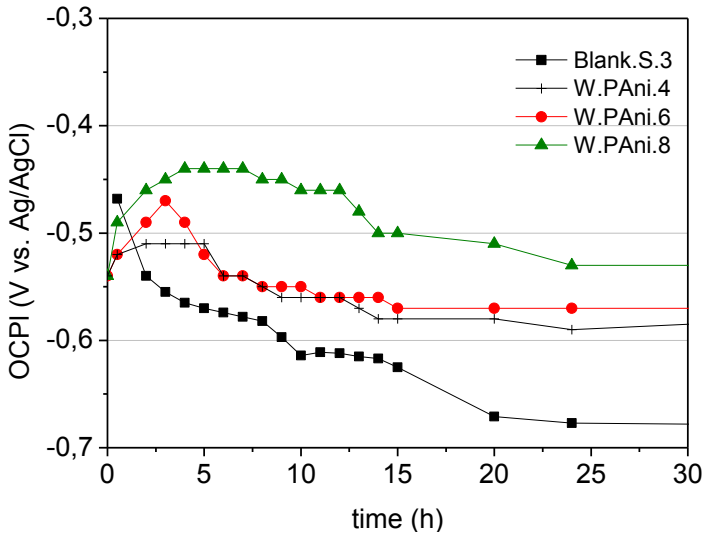

Figure 39 - Evolution of OCP of the water based containing PAni nanoparticles. From 0 to 24hours of immersion.

Later the 10th hour, for W.PAni.8 OCP evolution shifted and it has been found near -0,5 after 24 hours of immersion. The longer evolution is shown in Figure 40. The monitoring was stopped around 200 hours of immersion and the values of OCP for the all the W.PAni solutions were found near -0,60 V.

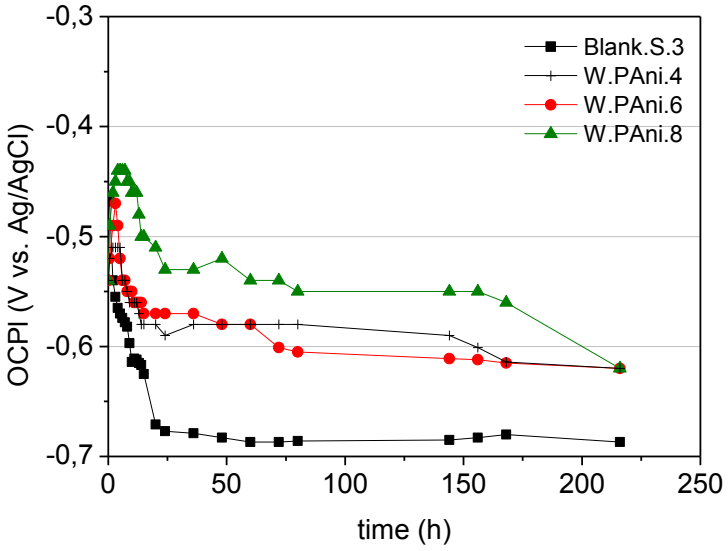

Figure 40- Evolution of OCP of the water based containing PAni nanoparticles. Longer period of immersion.

Considering Figures 39 and 40, it is likely that the 8.0 wt % of polyaniline nanoparticles into the water based solution have ennobled the surface of steel. However, one should be aware that, in the case of W.PAni.8, the level of ennoblement, ΔV near 0,1 V is considered relatively low and such effect lasted over a short period of time. Besides, the polyaniline containing water based solutions were evaluated by means of potentiodynamic polarization curves. As an example, the polarization curve of the 6.0 wt. % of PANi containing solution is shown in Figure 41.

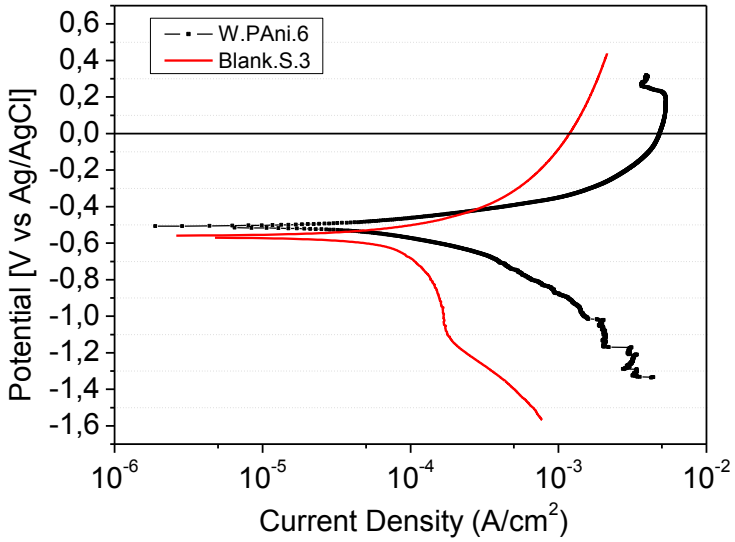

Figure 41 - Polarization curves of W.PAni.6 and the Blsnk.S.3.

The anodic and cathodic polarization curves between W.PAni.6 and Blank.S.3 are quite comparable. The OCP was found around -0,55 V for both solutions and, therefore, similar to the monitoring of the free corrosion potential depicted in Figures 39 and 40. On the

other side, for both of the curves, whenever the potential was shifted towards higher and lower values from the OCP, higher corrosion rates were seen for the W.PAni.6 than the Blank.S.3. Thus, the great acidic level of W.PAni is due to the presence of sulfonic acids along the polyaniline chains and the higher corrosion rates seen.

In order to investigate the influence of polyaniline concentration into the water based solution, the potendiodynamic polarization curves of W.Pani.4, W.Pani.6 and W.Pani.8 are shown in Figure 42.

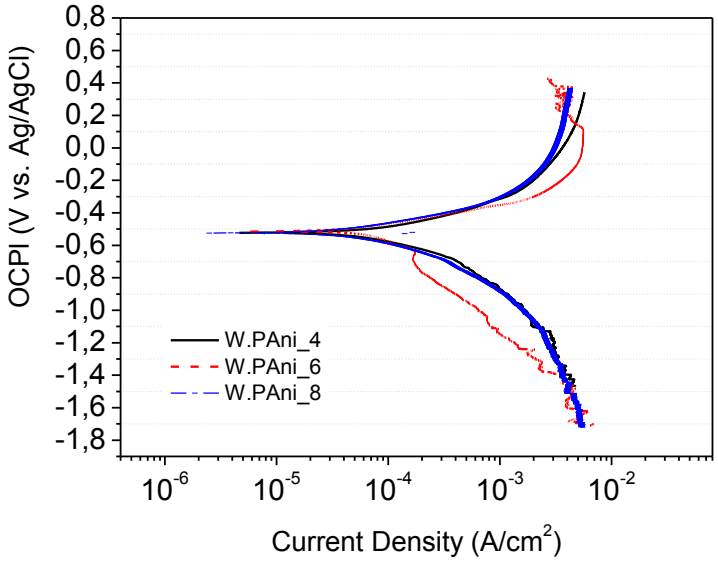

Figure 42 - Polarization curves of W.Pani.4, W.Pani.6 and 8

As far as Figure 42 is concerned, the polarization behaviour of water based solutions containing polyaniline nanoparticles is not influenced by the concentration levels of the nanoparticles. From Figure 42, both anodic and cathodic branches were found each other considerable equivalent. Recalling that potentiodynamic polarization technique scans the response of the metal specimen over potentials distant from the OCP and, therefore, such technique can be considered destructive for the working electrode, EIS has been carried out for the investigation of the polyaniline containing water based solutions.

The Bode impedance and phase angle spectra of mild steel immersed into W.PAni.8 and the Blank.S.3 solutions from initial conditions (0 h) and their evolution after 24 hours are shown in Figures 43 and 44. The first spectrum, labelled as t = 0h, was acquired when the steel specimen was put into contact with the solutions.

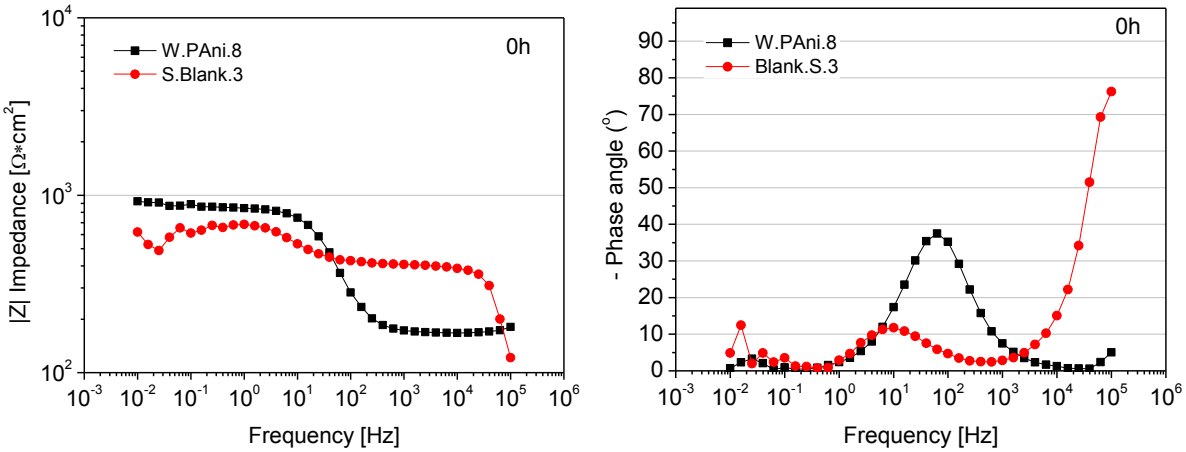

Figure 43 - Bode impedance (left) and Bode phase angle (right) spectra of W.PAni.8 and Blank.S.3 at the beginning (t=0h)

Both solutions at the beginning of the test: the values of the impedance at low frequency range were found near 10^3 Ohm.cm^2 and the phase angle spectra exhibited the presence of a second time constant from middle to low frequency range.

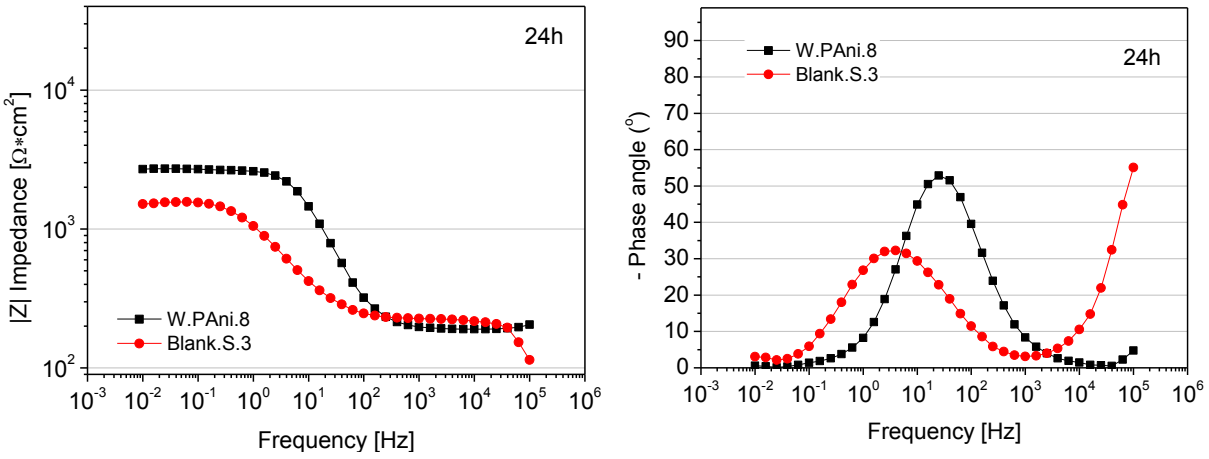

Figure 44 - Bode impedance (left) and Bode phase angle (right) spectra of W.PAni.8 and Blank.S.3 after 24h

After 24 hours, the evolutions of the EIS spectra revealed negligible influence of 8.0 wt. % of polyaniline into the water based solutions. In the case of W.PAni.4 and W.PAni.6, since no significant differences were seen, their EIS monitoring is not reported.

3.4 Conclusion on polyaniline nanoparticles

The study of polyaniline nanoparticles has been conducted on stabilized water based solutions at three diverse levels of concentration, 4.0, 6.0 and 8.0 wt. %. Likewise, the polyaniline containing solutions were delivered to the University of Trento after synthesis. Particularly, the average particle size has been found near 50 nm and electrical conductivity in the order of 10^{-4} S/cm^2. In addition, after stabilization of the polyaniline nanoparticles into the water based solutions, the pH of each have been monitored and found 3.0.

Fundamentally, the electrochemical activity of polyaniline containing nanoparticles was studied by means potentiodynamic polarization curves and electrochemical impedance spectroscopy and each time, its performances were compared with the sulphate of chloride solution with equivalent pH value.

In the case of polyaniline water based solutions no significant differences have been detected. This fact is mainly attributed to the great acidic level of the solutions, due to the release of sulphonic acids used throughout the chemical oxidation synthesis of the polymer. Corrosion of steel are to be expected at such low level of pH. Furthermore, in view of the proposed mechanisms presented in section 3.1, the conductive form of polyaniline might be able to promote anticorrosive effect onto steel whenever a physical contact between both parts is established.

4 Development of a waterborne paint system based on CeO_2 and polyaniline

Part of this chapter has been published in:

- L.G. Ecco, J. Li, M. Fedel, F. Deflorian, J. Pan - EIS and in situ AFM study of barrier property and stability of waterborne and solventborne clear coats, Progress in Organic Coatings, 77 (2014) 600-608

- L.G Ecco, M. Fedel, A. Ahniyaz, F. Deflorian - Influence of polyaniline and cerium oxide nanoparticles on the corrosion protection properties of alkyd coating - In Press Corrected Proof - Progress in Organic Coatings DOI: 10.1016/j.porgcoat.2014.04.002

The water based organic coating paint system of this project was designed with three layers: i*) the primer; ii) the intermediate coat,* and *iii) the top coat*. In view of the development of the triple layer coating system, several steps were followed in sequence. Hence, this section is mainly divided into four chronological parts:

I. Evaluation of the waterborne clear coats and selection of the binder to formulate the triple layer coating system (Section 4.1);
II. The addition of PAni nanoparticles, ceria nanoparticles and their mixture into a single layer waterborne binder (Section 4.2);
III. The optimization of the formulation of Ceria into a double layer waterborne coating system (Section 4.3);
IV. The influence of PAni and Ceria in a triple layer waterborne organic coating system (Section 4.4).

The anticorrosive pigments, Cerium Oxide and Polyaniline nanoparticles discussed in Chapter 2 and 3, respectively, have been incorporated into the primer and , owing to achieve one of the objectives of this project, large effort has been dedicated on the comprehension of their influences as anticorrosive pigments. Succeeding that, the intermediate and top coat layers have been formulated in order to enhance the corrosion protection of steel through the full organic waterborne coating system.

4.1 – Evaluation of waterborne clear coats

4.1.1 Materials

The selection of the organic coatings to formulate the paint system started with an evaluation of diverse polymeric coating resins. Therefore, four waterborne organic coatings were studied throughout the primary part of the project. Along next pages, the expression *''clear coats''* describes the steel panel coated with the waterborne polymeric binders without the presence neither of PAni nor Ceria nanoparticles. Table 6 displays the main features of clear coats.

Table 6 - General information about the clear coats coating resins.

Clear Coat's Label	Solvent	Chemical Nature	Solid Content (%)
W.ACR.1	Water	Acrylic	49-51
W.ACR.2		Styrene - Acrylic	42-44
W.ACR.3		Styrene Acrylic	49-51
W.ALK		Alkyd Emulsion	40-42

The polymeric resins as well as the coated steel panels were prepared and supplied by Arkema Coating Resins (Verneuil en Halatte, France). For that, cold rolled steel was used as substrate, supplied from Q-Panel, QD36 from Q-panel with a very smooth surface finishing. The arithmetic roughness (Ra) of the Q-Panels was controlled prior to the application of the coatings and found to be near 0.15 µm.

The coating applications were done with a Bar Coater instrument. Such technique is widely used for the application of paints, adhesives or varnishes in laboratory/development scale. In order to ensure repeatable results, it offers precise controlled speed and pressure during application of the coating as well as the possibility to work with large range of thickness, from 4 to 500 µm.

In order to have the optimal film formation, the coatings were dried with the following procedures: the coated panels were kept for at least two weeks at 23°C – 50% relatively humidity (RH) and another week inside a desiccator under dry atmosphere at room temperature. Following the film formation, the coats thicknesses were measured and all

the clear coats showed dry film thickness (DFT) around 50 µm. A scheme of the coated panels is shown in Figure 45.

Figure 45 - Scheme of the clear coating layers upon steel

4.1.2 Characterization

Thickness of the coatings

Preceding any experiment, the coating thicknesses for the all the panels have been controlled with PHYNIX equipment, model Surfix® FN, (ASTM D1186-93).

Electrochemical Impedance Spectroscopy - EIS

The protective properties of the waterborne clear coats were studied by Electrochemical Impedance Spectroscopy. The EIS measurements were obtained at the open circuit potential (OCP) using a potentiostat and frequency response analyzer (FRA) equipment (AutoLab model: PG STAT 302N), signal amplitude of 10 mV, frequency range 10^5 – 10^{-2} Hz and testing area about 10 cm^2. All the measurements have been conducted at room temperature.

A classical three electrodes arrangement was used. An Ag/AgCl (+0.205 V vs SHE) electrode and a platinum wire were used as reference and counter electrode respectively. Before the acquisition of any impedance spectra the OCP (with respect to the Ag/AgCl reference electrode) of the coated steel has been measured. Quantitative analysis, i.e., spectra fitting using an equivalent electrical circuit was made using the software ZSimpWin 3.22. Table 7 summarizes the main parameters of the EIS investigation of the clear coats.

Table 7 – Main features of the EIS investigation of the waterborne clear coats

Signal Amplitude	Electrolyte – salt concentration	Analysed area	Analysis Mode
10 mV	0.3wt. % Na_2SO_4 3.0wt. % NaCl	10 cm^2	Intact coatings

One can see from Table 7, two electrolytes were considered for the evaluation of the waterborne clear coats. The 0.3 wt. % of Na_2SO_4 was used whenever a mild solution was required whereas the more aggressive environment by the use of 3.0 wt.% of NaCl solution. The EIS investigation was conducted over intact coatings, in other words, without the presence of macroscopically induced defects.

In-situ Atomic Force Microscopy

In-situ AFM measurements were carried out in distilled water and 3.0 wt% NaCl solution. A 5500 AFM/SPM system (AC Mode 3) with a liquid cell from Agilent Technologies, was used for all the AFM measurements. The employed standard etched silicon cantilevers (spring force constant is 0.2 N/m) were purchased from Budget Sensors (Bulgaria). Contact mode operation was used for *in-situ* topography imaging in aqueous solutions. Relatively large areas, up to 80x80 μm^2, were imaged to observe the main surface features and micron-sized defects, while small areas of a few μm^2 were imaged to obtain high resolution images of the nanostructure of the coatings. The image resolution was 500 dpi. To monitor the changes taking place on the surface of the coating, the *in-situ* AFM imaging was repeated after different time intervals, up to 24 hours in the solution.

4.1.3 Results and discussion

Along next pages, the term clear coats is used to denote a single layer of the binders applied over the steel panel (see Fig 44) without the addition neither of PAni nor Ceria. The four waterborne clear coats have been primarily studied by means of Electrochemical Impedance Spectroscopy. The Bode impedance and Bode phase angle spectra of the four waterborne clear coats from initial condition (t = 0 h) and after 48 and 360 hours of exposure in 0.3 wt. % of Na_2SO_4 solution are shown in Figures 46-48.

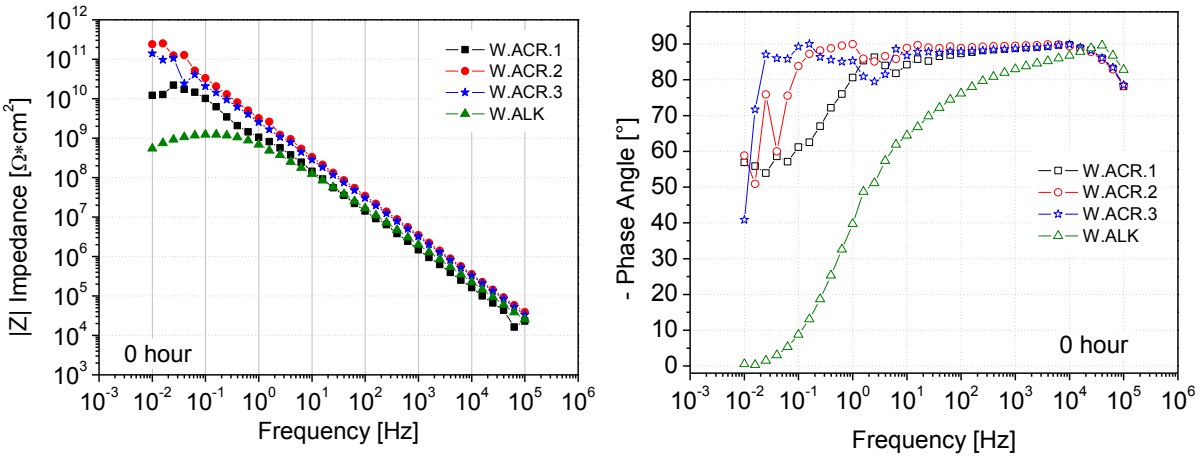

Figure 46 - Impedance (right) and phase angle spectra (left) of clear coats binders in presence of sulphate solution, time = 0h.

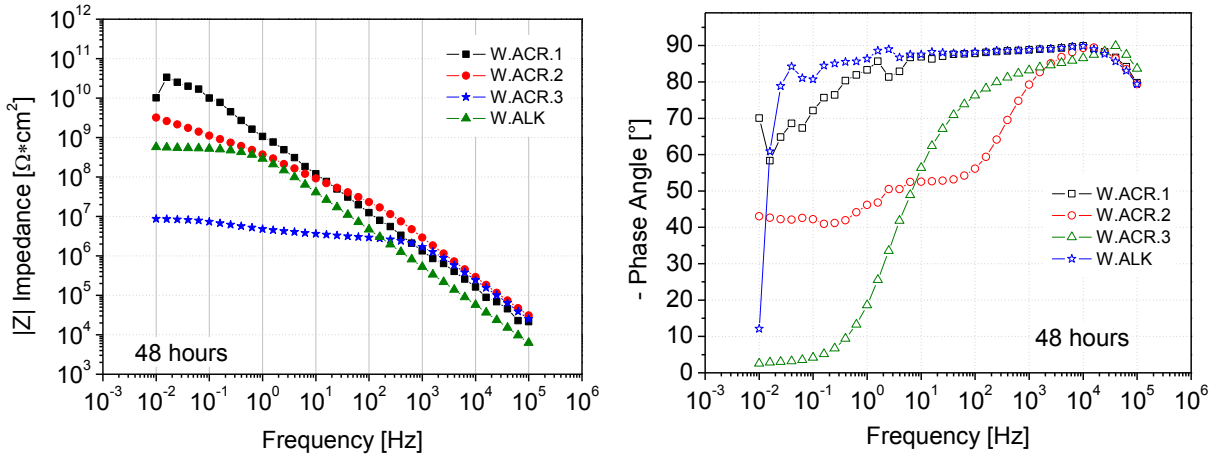

Figure 47 - Impedance (right) and phase angle spectra (left) of clear coats binders in presence of sulphate solution, time = 48 h.

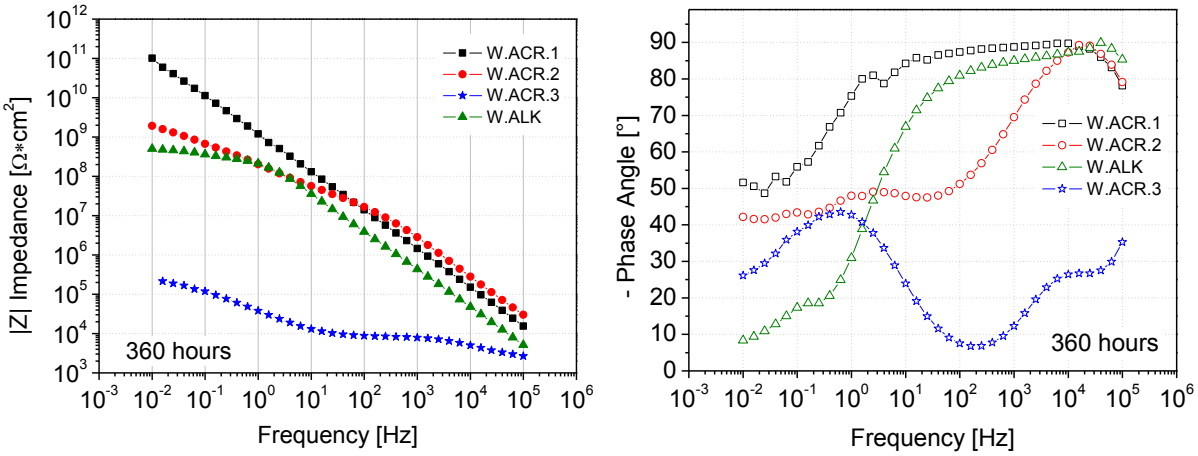

Figure 48 - Impedance (right) and phase angle spectra (left) of clear coats binders in presence of sulphate solution, time = 360h.

The four spectra shown in Figure 46 are representative of the first acquisition of each of the clear coats after the electrolyte was poured into the electrochemical cell. In other words, they are labeled as t = 0 h, however, one should be aware about the time needed

for EIS acquisition. For all the following EIS data discussed, the acquisition of each spectrum usually takes between 15 to 20 minutes.

At the beginning of the analysis, Fig 45, except the W.ALK, the clear coats showed quasi-capacitive impedance spectra associated to a single time constant accompanied by the impedance at 0.01 Hz frequency ($|Z|_{0.01Hz}$) around 10^{11} Ohm.cm^2 alongside the phase angle degree with minor fluctuations around - 90^o. Differently, the $|Z|_{0.01Hz}$ of the W.ALK clear coat was two orders of magnitude lower, near 10^9 Ohm.cm^2, with a decay of the phase spectrum towards lower angle. After certain period of exposure, differences appeared between the clear coats and an overview of their evolution is described as follows: at initial stages, W.ACR.1 showed values $|Z|_{0.01Hz}$ near 10^{11} Ohm.cm^2 with phase angle values near 90 degrees for the whole frequency range spectra. After 48 and 360 hours, there were minor changes and the values of $|Z|_{0.01Hz}$ fluctuated around 10^{11} Ohm.cm^2 for W.ACR.1. With respect to the phase angle spectra, their evolution was found with significant stability. Particularly, for quasi-capacitive EIS spectra, the values of total impedance at low frequency range, indicate the efficiency of the coating in blocking the current flow between anodic and cathodic sites, therefore, the values of $|Z|_{0.01\ Hz}$ in the order of 10^{11} Ohm.cm^2 observed over the tested period of 360 hours are attributed to elevated barrier property for W.ACR.1.

In the case of W.ACR.2, after 48 hours (Figure 47) the total $|Z|_{0.01Hz}$ was near to 10^9 Ohm.cm^2 alongside the appearance of a second time constant at the phase angle spectra in the middle to low frequency range. Later, between 48 and 360 hours the EIS behavior evolved without significant changes. The presence of the second time constant after 48 hours can be attributed to an electrochemical process which started at the interface of the coating and steel.

For W.ALK apart from the lowest $|Z|_{0.01Hz}$ value at time = 0h, the further evolution of EIS behavior did show significant stability over the period of analysis. The $|Z|_{0.01Hz}$ remained in the order of 10^9 Ohm.cm^2 during the 360 hours of exposure. Similarly, was the evolution of the phase angle spectra of W.ALK, but after 360 hours the presence of a second time constant was observed at low frequency range.

In the case of W.ACR.3, over the period of 48 hours there was a reduction of about 5 orders of magnitude of the values of $|Z|_{0.01Hz}$ from 10^{11} Ohm.cm^2 to 10^7 Ohm.cm^2, even though the phase angle spectrum did not show significant changes during equivalent period of time. After 360 hours, both the impedance and phase angle spectra indicated

degradation of the coating layer was in advanced stage and, therefore, W.ACR.3 was no longer protective.

As earlier mentioned, the evaluation of the clear coats discussed above was proposed as a selection step for the waterborne binder which would formulate the full paint system. However, two points must be stressed: i) the sulphate solution (0.3 wt. %) is considered mild solution for steel, yet has been selected for a slight degradation of the clear coats; ii) 360 hours of exposure are usually short time of exposure, but in this case has been enough to rank all the clear coats according to their performances. Furthermore, since W.ACR.3 has shown degradation within the period of 360 hours and it the clear coats were ranked, the comparison between all of the clear coats is no longer discussed. On the other hand, the longer monitoring of $|Z|_{0.01Hz}$ is shown in Figure 49.

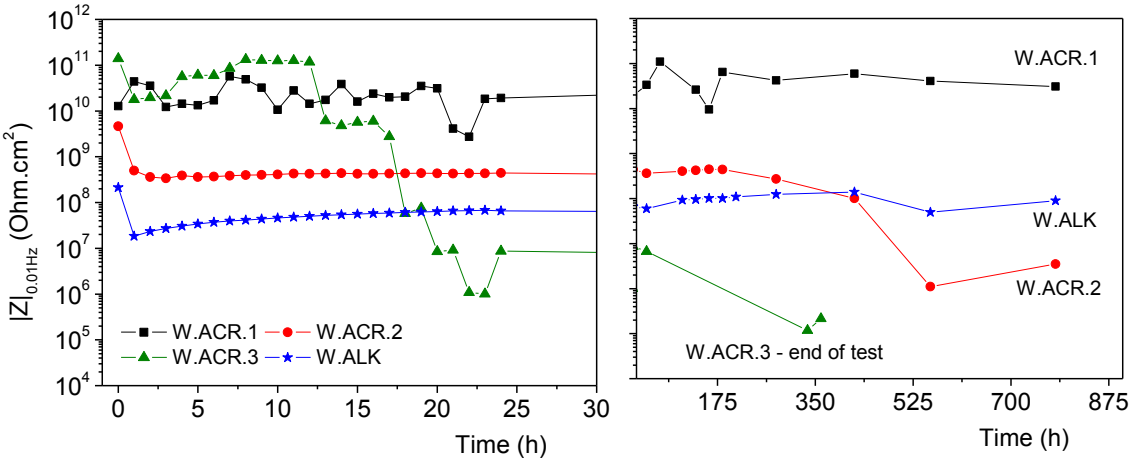

Figure 49 - Evolution of |Z| at low frequency range of clear coats. (left) over 24 hours and (right) longer exposure.

From Figure 49, one can appreciate the values $|Z|_{0.01Hz}$ of W.ACR.1 did not show any significant changes throughout the analysis, remained in the order of 10^{11} Ohm.cm^2, suggesting stability of the W.ACR during the entire 780 hours of exposure whereas the final impedance moduli of W.ALK, W.ACR.2 and W.ACR.3 were found to be near 10^8, 10^7 and 10^5 Ohm.cm^2, respectively. Considering the results discussed up to now, W.ACR.1 is ranked as the clear coat with higher intrinsic barrier property, and thus it had been selected for the formulation of the *Double Layer* and *Triple Layer* paint systems which will be described in section 4.3 and 4.4 of current chapter.

Electrical parameters of the waterborne clear coats alongside the use of in-situ Atomic Force Microscopy

The term barrier property previously discussed described the physical barrier from the coatings against the ingress of water and aggressive ions coming from the electrolyte. In other words, it defined the ability of the coating to isolate the metallic substrate from the external environment. Among the studied polymeric binders, W.ACR.1 showed relatively high barrier properties, since higher impedance magnitudes were verified to along with significant stability of these high magnitudes values versus time of exposure. Indeed, the 10^{11} Ohm.cm^2 generally is representative of a protective coating specially if one considers the relatively low thickness level of 50 micrometres without the addition of anticorrosive additives. On the other hand, similar to the W.ACR.1, such levels of impedance magnitude associated to the presence of one constant phase element it is usually attribute to water and/or aggressive ions which have not reached the metallic surface and no faradic process onto the surface of the steel were initiated. From a microstructural point of view, under the EIS investigation the coating layer itself and its microstructure are influenced from the very beginning of the immersion.

Triggered by the above, this section deals with a combination of EIS and *in-situ* AFM as an integrated electrochemical/chemo-physical approach to investigate the barrier property of the waterborne clear coats previously discussed. Mainly, attention was focused on understanding the microscopic interaction between the clear coats and the electrolyte at the very beginning period of interaction.

As an example, the waterborne acrylic binder labelled W.ACR.1 is recalled. However, for a matter of repeatability, another steel coated panel with W.ACR.1 coating sample has been treated in the following discussion. The Bode impedance and Bode phase angle spectra of W.ACR.1 from initial condition and their evolutions after 24 hours of exposure in 0.3 wt. % of Na_2SO_4 solution are shown in Figure 50.

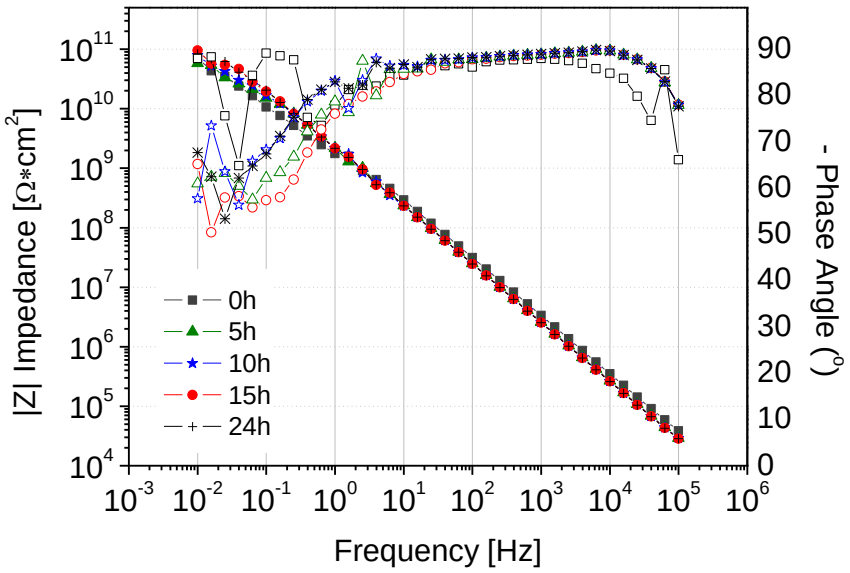

Figure 50 - Bode impedance (left axis) and Bode phase angle (right axis) of W.ACR.1 in the course of 24 hours

Yet, for this second coated panel with W.ACR.1 the EIS spectra exhibit a quasi-capacitive behaviour corresponding to only one time constant. The |Z| at low frequencies were found to be about 10^{11} Ohm.cm^2, in addition, the impedance modulus did not show any significant changes during 24 hours of exposure in the electrolyte.

The electrical parameters of W.ACR.1 have been extracted after modelling the EIS data with the electrical equivalent circuit presented in Figure 51(a). In the equivalent circuit shown in Figure 51(a), R_e stands for the electrolyte resistance, R_c for the coating resistance and Q_{Cc} for the constant phase element (CPE) of the coating, associated with the coating capacitance. For that, a CPE was used as a substitute for the pure capacitance. The use of a CPE with the exponent (*n*) gives a better fitting of the spectra using this model. In addition, *n* values ranging from 0.93 to 1.00 can be considered a reliable approximation of a pure capacitor.

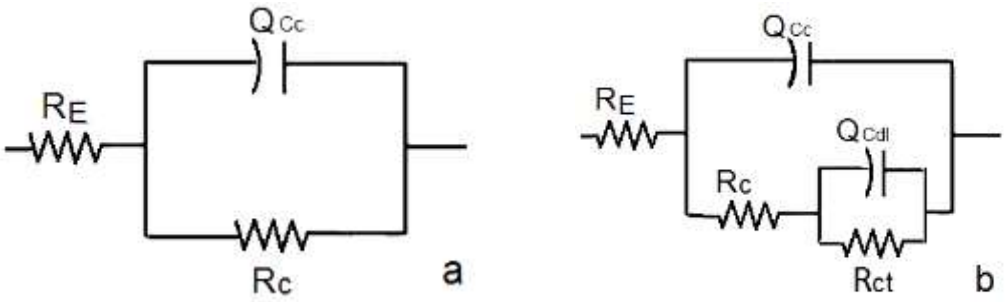

Figure 51 - Electrical circuits used for the extraction of the electrical parameters of the clear coats. (a) One-time constant Re(QcRc) and (b) two-time constants Re(Qc(Rc(QdlRct))).

Figure 52 shows the evolution of the coating capacitance as well the evolution of *n* values of W.ACR.1 during the course of 24 hours of immersion.

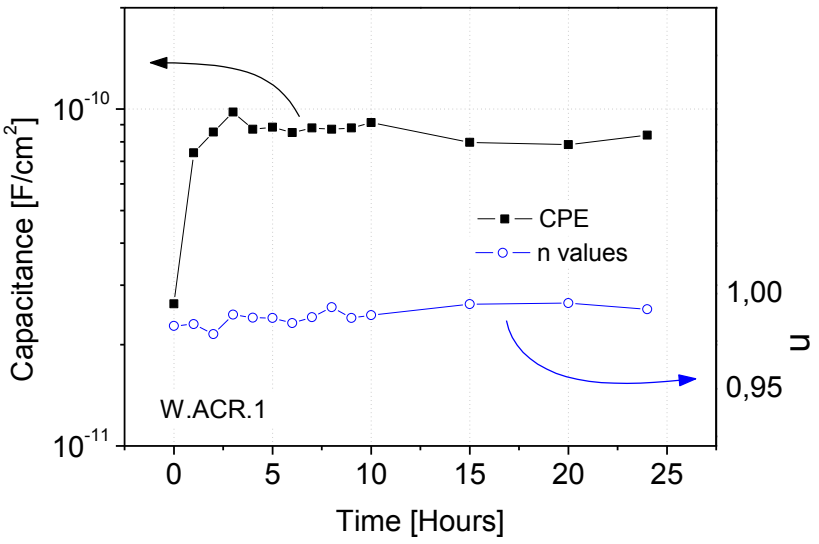

Figure 52 - Evolution of CPE (left axis) and n values of fitting (right axis) vs. time of exposure of W.ACR.1.

At first, one can notice the values of the exponent *n* ranged between 0.95 and 1.0, therefore, the evolution of the constant phase element, $Q_{Cc,}$ can be treated as the evolution of the coating capacitance of W.ACR.1 with consistency.

The evolution of the coating capacitance of the W.ACR.1 increased over the first three hours and remained considerably stable afterwards. Straightforwardly, one can observe a slight reduction of the capacitance magnitude after the 5th hour of immersion. Such observation is attributed to changes in the coating dimensions due to interaction with electrolyte.

Recalling the spectra displayed in Figure 50, as far as the shape of the impedance spectra is concerned, it can be primary assumed that not substantial amount of water or aggressive ions from the electrolyte have penetrated through the W.ACR.1 clear coat towards the metallic surface. However, from the evolution of the coating capacitance of W.ACR.1 displayed in Figure 50, at a certain level, the ingress of water into the coating layer is suggested.

It is very common the use of the Brasher-Kingsbury equation for the evaluation of water content into an organic coating from capacitance measurements. However one should be aware that such approach cannot be always consistent since water might cause swelling of the coating or with the water is not homogeneously distributed along the coating volume. In the case of W.ACR.1, the levels of absorbed water have been evaluated through the application of the Brasher-Kingsbury equation. However, none trustworthy

information was observed since the coating dimensions might have been modified while in contact with water. This supposition is better discussed ahead in the text.

Simultaneously, the topography of the W.ACR.1 has been monitored by means of *in-situ* AFM. Sequential images of the clear coat are shown in Figures 53 and 54. Prior to the contact with solution, dry condition, likewise after 0.5, 3 and 8 hours of exposure to distilled water.

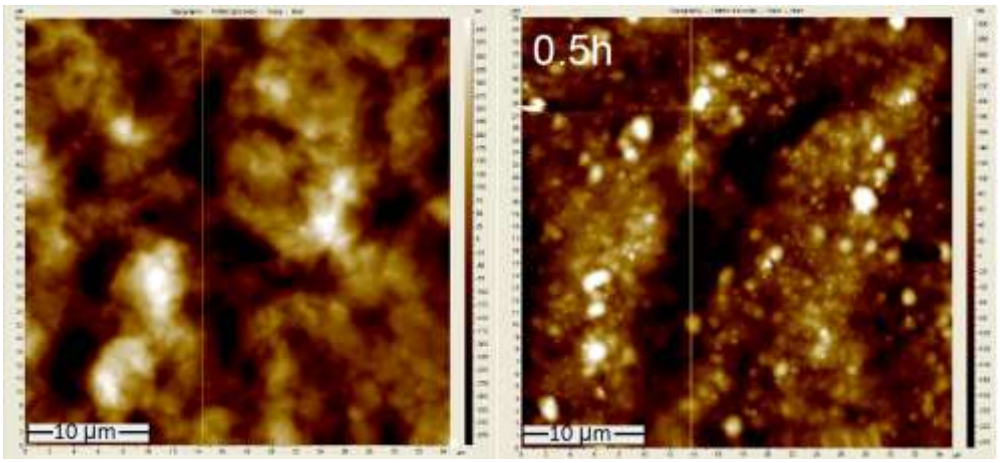

Figure 53 - AFM topography images of the W.ACR.1 clear coat: in air (left) and after 30 min of exposure in water (right).

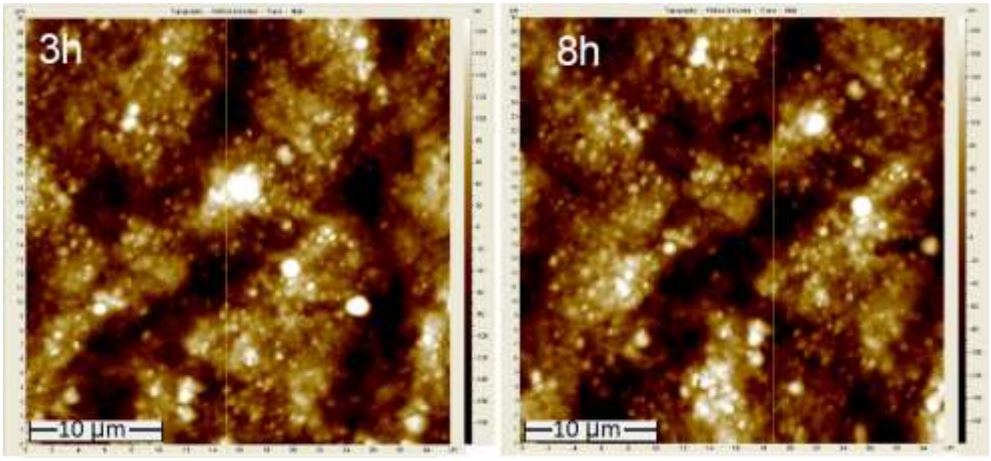

Figure 54 - AFM topography images of the W.ACR.1 sample: after 3 hours (left) and after 8 hours of exposure (right).

The initial topography in dry conditions is presented in Figure 53 (left), the colour difference is represented by the z-scale and ranged around 1.3 µm. From Figure 53 (right), even though the z-scale remained unchanged, evidences of the water upon the outermost layer appeared, the presence of spherical structure like lumps suggested a physical interaction between the solution with the clear coat. In a way, the outermost layer has been modified after 30 minutes in contact with solution.

The longer evolution of the coating topography is shown in Figure 54. *In-situ* AFM images obtained after 3 hours (Figure 54 left) and 8 hours (Figure 54 right) of exposure showed that the topography of the W.ACR.1 evolved with minor changes.

Considering the above, the *in-situ* AFM observations indicated the occurrence of interactions between the acrylic latex coating and water, which have promoted changes on the surface layer of the coating shortly after the contact with distilled water. Despite the initial variations, the topography of the W.ACR.1 coating remained considerably stable.

Similarly, an additional W.ALK coated panel has been investigated by means of *in-situ* atomic force microscopy. Again, new data with respect to W.ALK has been brought to this discussion. At first, the EIS spectra within the first 24 hours are shown in Figure 55.

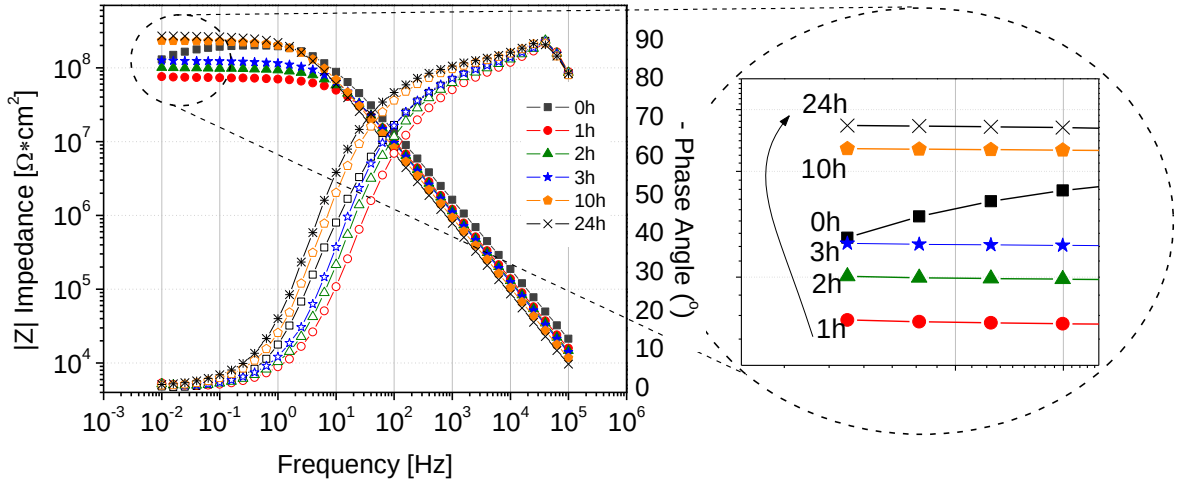

Figure 55 - Bode impedance (left axis) and Bode phase angle (right axis) of W.ALK in the course of 24 hours

At the beginning of the test, time = 0h, the impedance spectrum exhibited a quasi-capacitive behaviour related to a single time constant. The |Z| at low frequencies were found to be between 10^8 ~ 10^9 Ohm.cm^2. Besides, the total impedance modulus at 10^{-2} Hz frequency range evolved as described: From the very beginning until the first hour of analysis the $|Z|_{0.01Hz}$ decreased about one order of magnitude, from 10^8 to 10^7 Ohm.cm^2. During the following hours, there was a switch in the direction $|Z|_{0.01Hz}$, which started to move towards higher magnitudes. After 24 hours, the values of $|Z|_{0.01Hz}$ were found between 10^8 ~ 10^9 Ohm.cm^2 (see the outer picture). These changes are likewise seen in the medium frequency range of the phase angle spectra, during the first hour the spectra moved in the direction of higher frequencies, followed by a shift towards lower frequencies after the 1st hour. The electrical circuit shown in Figure 51a has been used for the extraction of the electrical parameters of W.ALK. Figure 56 shows the evolution in the

course of 24 hours of the coating capacitance and coating resistance of W.ALK coated panels.

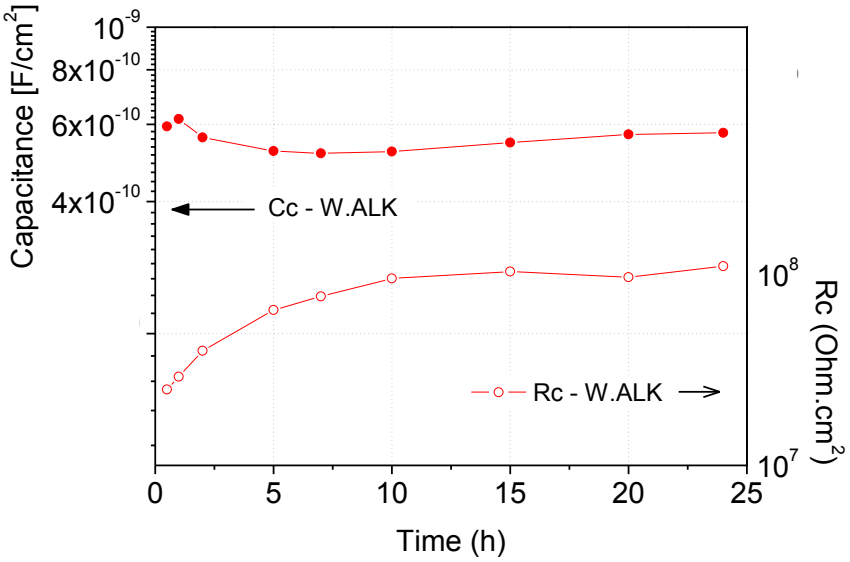

Figure 56 - Evolution of Coating Capacitance (left axis) and Coating Resistance (right axis) versus time of exposure of W.ALK.

In the case of W.ALK, electrochemical impedance spectroscopy has been conducted four times and repeatability of the data can be considered consistent.

From Figure 56, it can be seen that the evolution of the constant phase element for the W.ALK can be divided into three diverse steps (see the left axis in Figure 56): i) from the beginning until the first hour, CPE showed an initial rise; ii) between the 1st and the 5th hour, it changed direction and a reduction is noticed; iii) another rise from 5th hour onwards till the end of the analysis. Through reciprocal period of time, the Rc parameter (see right axis in Figure 56) has demonstrated continuous increase and, after 24 hours of constant exposure to the electrolyte, values of coating resistance were found to be about one order of magnitude higher than Rc at time = 0h, from 10^7 to 10^8 Ohm.cm^2.

Since W.ALK is a clear coat, therefore, the increase in $|Z|_{0.01Hz}$ after the first hour is explained by the responses of W.ALK to the electrolyte over the period of exposure. In this view, for the first hour, the increase in the coating capacitance is caused by the initial water uptake. Since water holds higher values of the dielectric constant, the presence of small quantities of water along the coating volume has led to an increase of the coating capacitance of W.ALK.

Between the first and the fifth hour of exposure, water uptake is assumed to not be interrupted, however a reduction in the CPE is noticed. Such behaviour is explained by

changes in the W.ALK coating dimension, *e.g.* swelling of the coating layer caused by its interactions with the electrolyte alongside partial closure of pores or defects across the coating volume. It is likely that the water uptake and changes in the coatings dimensions occurred simultaneously, however, the changes in the coating geometry commanded the CPE evolution between the first and the fifth hour. Afterwards, from the 5th hour until the end of this investigation, the coating capacitance is increased again due to the further ingresses of water. The evolution of Rc in Figure 56 supports the hypothesis of pores' closure along the coating volume. While water is absorbed by the coating layer, one can expect a proportional reduction of the Rc. However, for W.ALK the longer the time of exposure the higher was the coating resistance, thus, it has been assumed that after contact with electrolyte the coating layer swelled.

The AFM images of the topography of W.ALK collected in dry condition and 15 minutes after are shown in Figures 57.

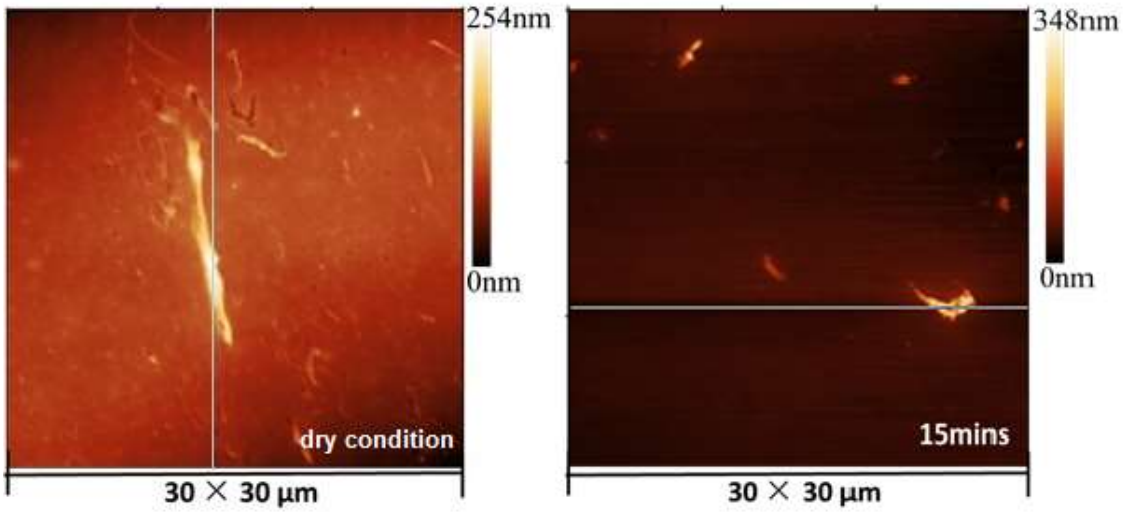

Figure 57 - AFM topography images of the W.ALK sample: in dry condition (left) and after 15 minutes of exposure (right).

The evolution of the topography of W.ALK coating before and ¼ hour after the contact with the solution suggested interactions occurred in the outermost layer W.ALK clear coat. In dry conditions (Fig 56 left) the topography of W.ALK contained certain number of micron-sized hills and cracks across the surface. The top-to-bottom distance (z-scale) was found to be 254 nm prior to the addition of the solution. When the W.ALK has been put in contact with water, the coating interacted within short time of exposure and changes were noticed on the coating topography. For instance, the z-scale after 15 minutes was found to be 146 nm higher than dry condition caused by the presences of one opened-up hole which raised z-scale dramatically. Besides, in the view of the colour aspects of Figure 57 (right), darker

aspects are seen, indicating that the whole analysed area have swelled after contact with electrolyte. In addition, the roughness has been quantified by means of line profile analysis and the evolution of the arithmetic roughness (Ra) of W.ALK is described in Table 8.

Table 8 - Ra and Rms of the W.ALK coating

Time of Exposure	Ra (nm)	z-scale (nm)
0 h (dry condition)	16	254
15 min	8	348
1.5 h	10	336
3.0 h	10	440
4.0 h	6	266

The Ra of the analysed area has been reduced from 16 to 8 nm after 15 min and later to 6 nm after 4 hours of exposure. The reduction in the arithmetic roughness is an indicative of a smoother surface after certain period of exposure. A possible swelling experimented by the coating layer due to interaction with solution explained the reduction in the Ra values. Moreover, one can expect a concomitant reduction in the values of z-scale in case of swelling and, from Table 8, z-scale values did not show regular evolution. Two reasons for that, the appearance of a micron sized defect (see Figure 57) and its further monitoring. After being put in contact with electrolyte the monitoring of a micron sized defect

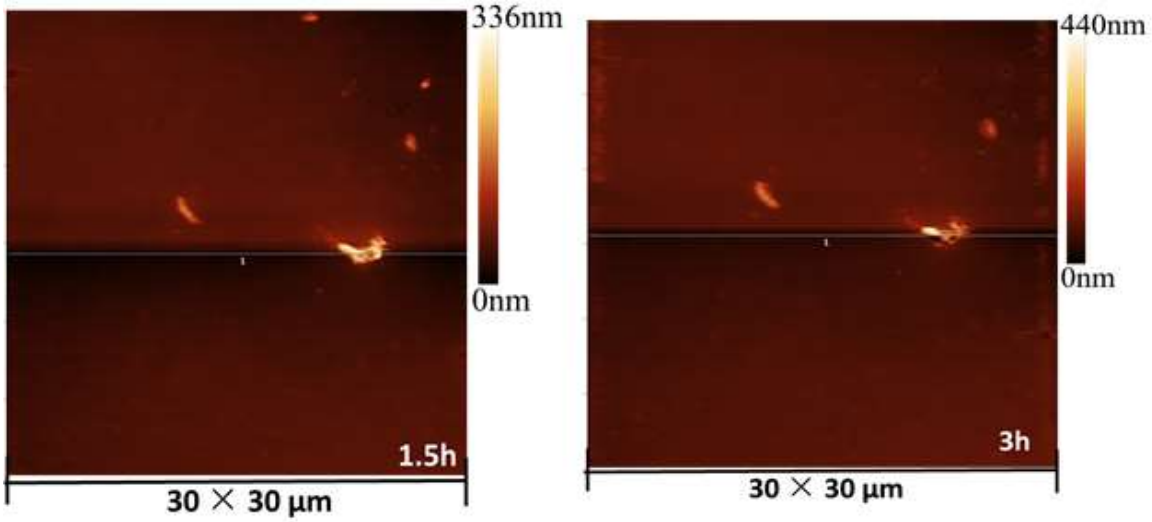

Figure 58 - AFM topography images of the W.ALK sample: after 1.5 h (left) and 3 hours (right) of exposure.

Considering above investigation, *in-situ* AFM is pointed as beneficial technique for the monitoring of coatings under exposure, variations on the coatings in the micro and nano

scale have been detected. For instance, in the case of the W.ACR, changes in the outermost layer have been noticed in the period of 10 minutes, from when the electrolyte was poured into the electrochemical cell.

On the other hand, *in-situ* AFM does not cover the bulk or the entire volume of the coating under analysis. The previously cited expression *outermost layer* can be equalized as an outermost volume, since the depth of layer in the order of tens of nanometers times the analyzed area from the electrochemical cell, thus represents a volume. Hence, *in-situ* AFM covers the outermost volume whereas EIS responses come from the entire volume.

Finally, recalling the development of the waterborne organic coating aimed by this project and prior to the discussion regarded to the addition of PAni and Ceria nanoparticles into primer layer of the waterborne organic coating, one should be aware about the choice of the binder. Considering the observations above, the **W.ACR.1** was selected on the formulation of each layer of the organic coating system. Subsequently to the selection of the binder polymer to formulate the triple layer waterborne organic coating, successive steps were devoted on the investigation of PAni and Ceria contents and further optimizations on each of the layers.

4.2 – Cerium oxide and Polyaniline containing primers

Following the investigation of the clear coats and subsequently to the selection of the polymeric binder to formulate the triple layer coating system of this project, the PAni and CeO_2 nanoparticles discussed in Chapter 2 and 3, respectively, were incorporated into the waterborne **W.ACR.1.**

Along the lines of this project, as part of the development and in order to achieve the objectives of the waterborne paint system, variables such as the thickness of the primers and the weight content of anticorrosive additives added into the primer layer have been investigated. Among all the studied combinations, it has been verified the optimal configuration given by primers layer with thickness of 10 micrometers and 1.0 wt. % of the polyaniline and cerium oxide contents.

4.2.1 Materials

Table 9 summarizes the main features of the 10 µm thick primers.

Table 9 - Main features of the primers 10 µm thick.

Primer	Ceria Nanoparticles	PAni Nanoparticles	Binder
W10_Blank	--	--	W.ACR.1
W10_Ceria	1.0 wt. %	--	
W10_PAni	--	1.0 wt. %	
W10_Mixture	1.0 wt. %	1.0 wt. %	

The above labels can be read as follows: W10 stands for the 10 micrometres thick primers; W_Blank represents the waterborne acrylic coating W.ACR.1, W_PAni stands for the W.ACR.1 loaded with 1.0 wt.% of PAni, W10_Ceria loaded with 1.0 wt.% of ceria nanoparticles (Ce.SF) and W10_Mixture when both, polyaniline and ceria nanoaparticles were added together at the concentration level of 1.0 wt. % each.

All the steel panels coated with the primer's formulations above were prepared and supplied by Arkema Coating Resins (Verneuil en Halatte, France) and the preparation of the steel coated samples is previously described (see section 4.1.1).

4.2.2 Characterization

Electrochemical Impedance Spectroscopy – EIS

The protective properties of the primers were studied by Electrochemical Impedance Spectroscopy and detailed methodology has been described in section 4.1.2. Table 10 summarizes the main parameters of the EIS investigation conducted for the primers.

Table 10 - Main features of the EIS investigation of the primers

Signal Amplitude	Electrolyte – salt concentration	Analysed area	Analysis Mode
10 mV	0.3wt. % Na_2SO_4 3.0wt. % NaCl	10 cm^2	Intact coatings

4.2.3 Results and discussion

The evolution of the open circuit potential of the W10_Blank, W10_Ceria, W10_PAni and W10_Mixture exposed to 0.3 wt. % sodium sulphate solution during the first 24 hours is shown in Figure 59.

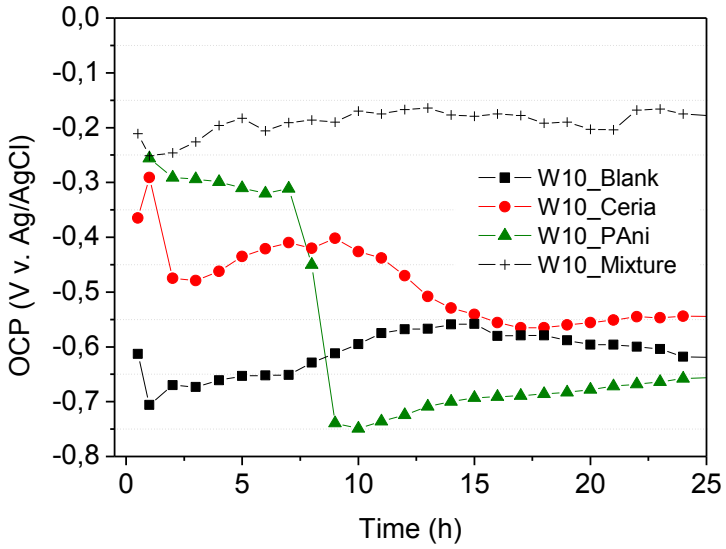

Figure 59 - OCP evolution of W10_Blank, W10_PAni, W10_Ceria and W10_Mixture over time of exposure to the sulphate electrolyte.

The OCP values of the clear acrylic waterborne, W10_Blank, fluctuated around -0.60 V during the first 24 hours of investigation. The magnitude of the OCP values of an uncoated steel panel immersed in the sulphate solution verified in Chapter 2 were in the same range, the range of OCP values observed for W10_Blank suggests the low barrier properties of the 10 micrometers thick primer layer.

In the case of the waterborne primer containing polyaniline, W10_PAni, the evolution of the potential can be divided into two parts and described as follows: OCP was first measured around -0.30 V during the first 8 hours of immersion. After, a reduction of about 0.4 V in the OCP is seen and the values fluctuated around -0.65 V from the 8th until the 24th hour. As far as the evolution of OCP of W10_PAni is concerned, it is likely that during the first stage, the potential values are attributed to a membrane potential between the coating and the electrolyte. From the time when water and ions started to ingress into the coating layer towards the working electrode, the electronic circuit is formed, thus the real open circuit potential has been measured, around -0.65 V.

Similarly, in the case of W10_Mixture, the higher starting potentials verified, OCP near -0.20 V, are explained by the relatively great physical isolation of the working electrode from the electrolyte provided by both coatings all through the investigated period. Therefore, for these coatings the values of potential did not describe the real potential between the electrolyte and the surface of the metal.

On the other side, the open circuit potential of the cerium oxide containing primer, W10_Ceria, was initially measured around -0.50 V. Later, the potential is slightly and continuously increased until the 10th hour and reached the maximum value around -0.40 V. Finally, the potential observed of W10_Ceria is reduced to – 0.60 V. In this way, it is likely that the presence of cerium oxide nanoparticles into the acrylic coating promoted an ennoblement of the metal surface.

The Bode impedance and phase angle spectra of mild steel coated with W10_Blank, W10.Ceria, W10_PAni and W10_Mixture at initial conditions and their evolutions after 10 and 48 hours are shown in Figures 60 - 62. At the beginning of the EIS monitoring, the spectra of each coating systems is described as follows: the values of $|Z|_{0.015Hz}$ of W10_Blank, W10_Pani and W10_Mixture were found near 10^5 Ohm.cm^2 whereas W10_Ceria displayed two orders of magnitude levels of $|Z|_{0.015Hz}$, 10^7 Ohm.cm^2.

The respective phase angle spectrum of W10_Mixture showed a peak attributed to a second time constant of 50° in the low frequency range of. For the others, the peak is located in the middle frequency range and is less evident for W10_Ceria and W10_PAni.

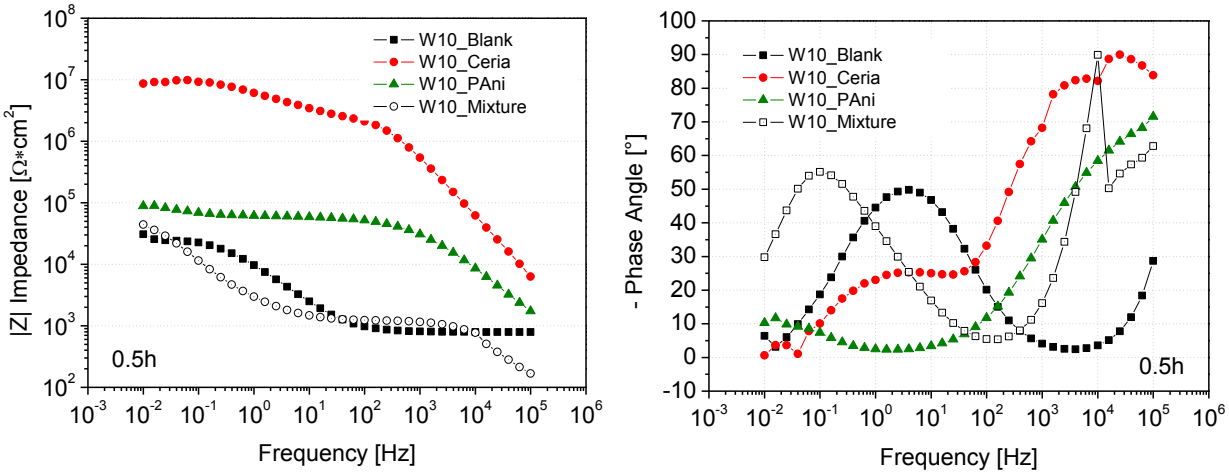

Figure 60 - EIS spectra of the W10_Blank, W10_Ceria, W10_PAni and W10_Mixure in presence of Blank.S.8 electrolyte at initial conditions.

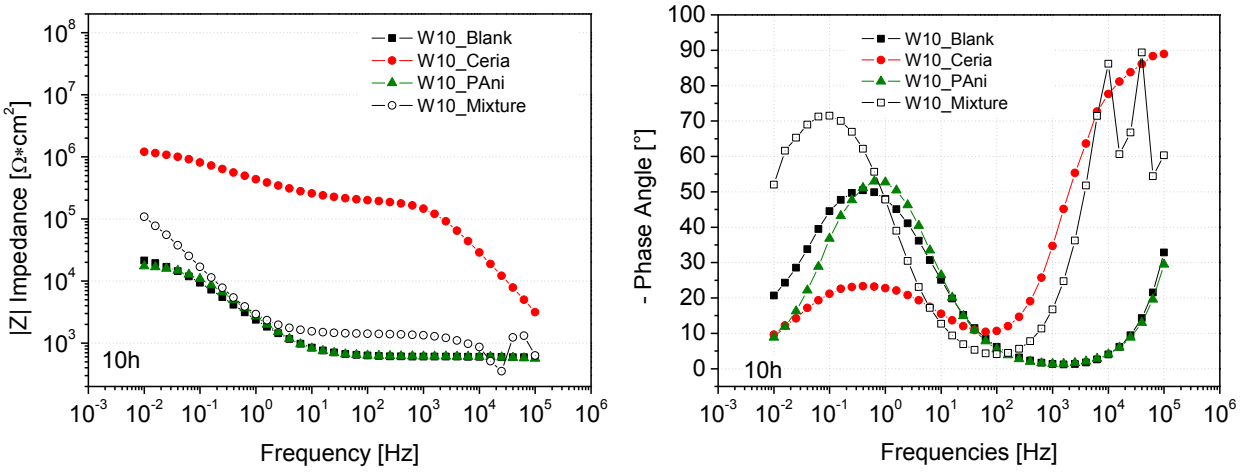

Figure 61 - EIS spectra of the W10_Blank, W10_Ceria, W10_PAni and W10_Mixure in presence of Blank.S.8 electrolyte after 10 hours

After 10 hours of immersion the three spectra of W10_Blank and W10_PAni were found very similar. The values of impedance at low frequency range were near 10^4 Ohm.cm^2 alongside the presence of a second time constant in the middle to low frequencies range on the phase angle spectra. These observations are typical of an organic coating undergoing degradation.

The electrochemical evolution after 10 hours of W10_Ceria suggested beneficial effect on the presence of ceria nanoparticles into the waterborne acrylic coating. For instance, the two orders of magnitude higher levels on the $|Z|_{0.015Hz}$, 10^7 Ohm.cm^2 against 10^5 Ohm.cm^2 verified by the others. In the case of W10_Mixture, after 10 hours of the values of $|Z|_{0.015Hz}$ were slightly increased near 10^5 Ohm.cm^2. Moreover, the presence of a second time constant, earlier observed around 50°, was shifted towards higher phase angles and it was found near 70°. From the 10th hour onwards, the spectra were found to have evolved with significant stability. At the end of the test, the same 10^5 Ohm.cm^2 is verified and the phase angle spectra showed the presence of a second time constant near 70°.

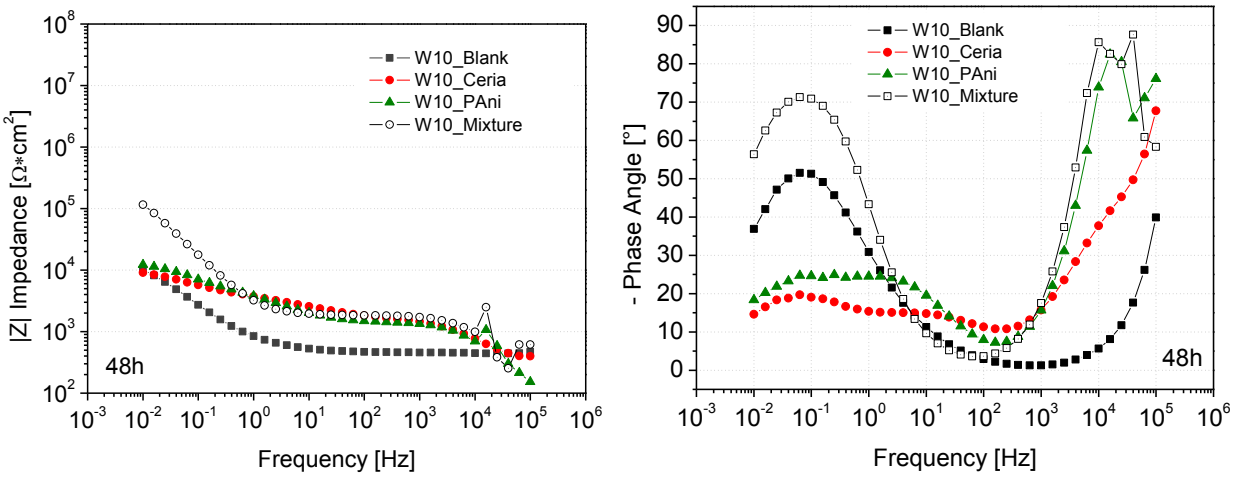

Figure 62 - EIS spectra of the W10_Blank, W10_Ceria, W10_PAni and W10_Mixure in presence of Blank.S.8 electrolyte after 48 hours.

From the evolution of OCP combined with the EIS spectra of the waterborne primers, at first, one can notice the relatively short period of investigation. The electrochemical investigation was not longer than 48 hours conducted due to low barrier property given by the waterborne primers at 10 micrometres thick. Nevertheless, in the case of W10_Ceria, the observed ennoblement in the evolution of OCP alongside the higher impedance magnitudes, are suggestive of reinforcement on the anticorrosive properties of the acrylic waterborne coating due to the presence of 1.0 wt. % of cerium oxide nanoparticles.

It is important to highlight the missing information from the fitting data of the spectra. Again, because of low thicknesses levels and, consequently, elevated permeability of the coating, the extraction of the electrical data of these coatings systems had been restricted.

Furthermore, one can find in literature similar investigation on the influence of PAni and ceria nanoparticles on the anticorrosive properties of a solvent borne alkyd coating instead. Investigated by means of EIS and sustained by accelerated salt spray test, the blank alkyd coating has been loaded with PAni, ceria nanoparticles and the combination of both with 1.0 wt.% content. Through the monitoring of open circuit potential, an ennoblement effect was detected for the solventborne alkyd coatings systems containing Pani and cerium oxide nanoparticles. Moreover, EIS evolution of the alkyd containing polyaniline revealed a stable performance of the system in presence of sulphate solution for over 500 hours of exposure, whereas for those containing ceria nanoparticles a considerable raise in the |Z|0.015Hz, from 10^7 to 10^8 Ohm.cm^2 in the course of 24 hours of immersion, an increasing trend of the charge transfer resistance during the equivalent period of exposure was observed. Also, the anticorrosive contribution given by the ceria

nanoparticles is supported by the accelerated salt spray test which revealed lower delamination rates.

4.3 The Influence of ceria nanoparticles on waterborne double-layer organic paint system.

From the electrochemical results of ceria nanoparticles verified in Chapter 2 and the anticorrosive contribution given by the presence of ceria in a single layer coating (section 4.2.3) and, at the same time, as a step for the formulation of the full paint system, diverse concentrations of ceria nanoparticles were added into a double layer paint system. Therefore, the anticorrosive influence of 0.5, 1.0, 2.0 and 0.5 wt. % of cerium oxide nanoparticles was investigated by means of EIS alongside to the accelerated salt spray test.

Over the primer's, another thicker layer loaded with bentonite was applied to offer superior resistance for water and ions, thus, the influence of diverse wt.% of ceria had been investigated in an environment which simulated a full paint system. In view of that, the goal of this section is attributed to the investigation of diverse concentrations of cerium oxide nanoparticles dispersed along the primer's layer of double layer system.

4.3.1 Materials

Succeeding, diverse concentration of ceria nanoparticles were added into the primer layer of the double layer coating system. The primer layer itself was formulated with the water borne acrylic W.ACR.1described in section 4.1.1. On the top of the primer's layer, the same waterborne W.ACR.1 binder loaded with 3.0 wt. % of bentonite was applied (Laviothix P100 from Laviosa Chimica Minerairia S.p.A. - Italy). It is worth highlight the thicknesses of each layer, 10 and 25 µm for the primer and the top layers, respectively. Figure 63 schematizes the DL's organic coating paint systems.

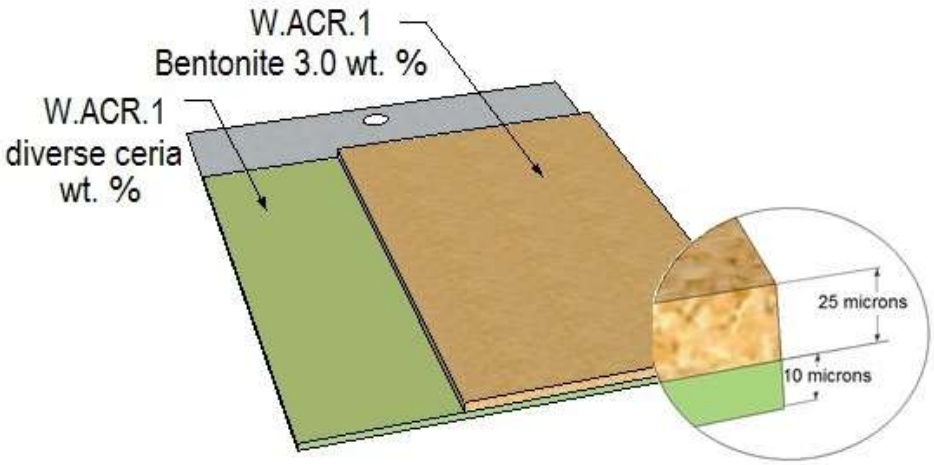

Figure 63 - Scheme of the Double Layer paint systems

The contents of 0.5, 1.0, 2.0 and 3.0 wt. % were added into the W.ACR.1. Therefore, the characteristics which distinguish the DL's coatings species are exclusively attributed to the wt. concentration of ceria nanoparticles at the primer's layer. Table 11 refers to the main features of the DL's coated panels.

Table 11 - Main features of the double layer paint systems.

Label	Primer Layer		Top Layer		Total Thickness
	Binder	**CeO_2 (wt.%)**	Binder	Bentonite	(µm)
DL-0		**0.0**			34.1 ± 2.6
DL-0.5		**0.5**			38.6 ± 2.4
DL-1	**W.ACR.1**	**1.0**	W.ACR.1	3.0 wt. %	33.8 ± 3.1
DL-2		**2.0**			32.9 ± 2.8
DL-3		**3.0**			33.9 ± 2.4

The labels presented in Table 11 can be read as follows:

- DL – double layer system;
- 0.5, 1, 2 and 3 – concentration (wt. %) of ceria nanoparticles.

4.3.2 Characterization

Electrochemical Impedance Spectroscopy – EIS

The protective properties of the double layer coated panels were studied by Electrochemical Impedance Spectroscopy and detailed methodology has been described in section 4.1.2. Table 12 reports the EIS parameters selected during the investigation of the DL's.

Table 12 - Main features of the EIS investigation of the waterborne DL's coated panels

Signal Amplitude	Electrolyte – salt concentration	Analysed area	Analysis Mode
20 mV	0.1 M NaCl	10 cm^2	Intact coatings
5 mV	0.3 wt. % Na_2SO_4	10 cm^2	Scratched coatings

Accelerated Salt Spray

The accelerated salt spray tests have been performed following the standard ISO 9227. According to the standard, temperature inside the chamber: 35 ^oC and the saline chloride concentration: 5.0 wt.%. The exposure into the chamber was done in both situations: intact coatings and with the presence of a 2 cm long scratch.

4.3.3 Results and discussion

EIS conducted on intact coatings

At first, the investigation of the double layer (DL) coated panels started with EIS on the intact coatings. For that, a chloride electrolyte (NaCl) at the molar concentration of 0.1 has been used and Figures 64 - 66 display the evolution of the EIS spectra of the double layer systems after 0, 24 and 192 hours, respectively. Recalling the labels displayed on Table 11, DL-0 stands for the double layer system without the addition of ceria into the primer. DL-0.5 loaded with 0.5 wt. %, DL-1 when 1.0 wt. % were added and likewise for 2.0 and 3.0 wt. %.

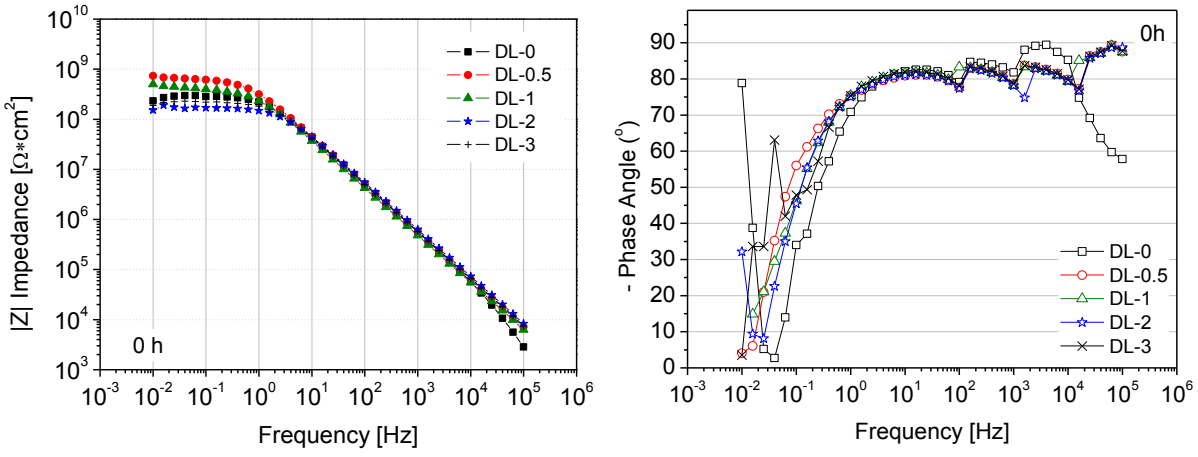

Figure 64 – Impedance (left) and phase angle (right) spectra of double layer systems in presence of 0.1 NaCl, time = 0h.

At the moment the chloride electrolyte was poured into the electrochemical all EIS acquisition of the double layer systems have given similar outline. Basically there was a single time constant and values of the total impedance at 10^{-2} Hz fluctuating between 10^{8} and 10^{9} Ohm.cm^2. Few non-linear and dispersed points are seen in the phase angle spectra, they are attributed to measurements matters. Apart from these scattered data, from phase angle spectra of all the double layer systems, it can be seen the presence of two time constants. After 24 hours, few differences are noticed between the DL samples. For DL-0.5 and DL-1 there was a left shift in the phase angle spectra alongside a slight increase in the values of $|Z|_{0.01Hz.}$ Also, after 24h the values of $|Z|_{0.01Hz}$ were found to be around one order of magnitude higher than DL-0. In the case of DL.2 and DL-3, after 24 hours the bode impedance spectra are comparable to the DL-0, however from the phase angle spectra, the appearance of a second time constant is noticed in the low frequency range.

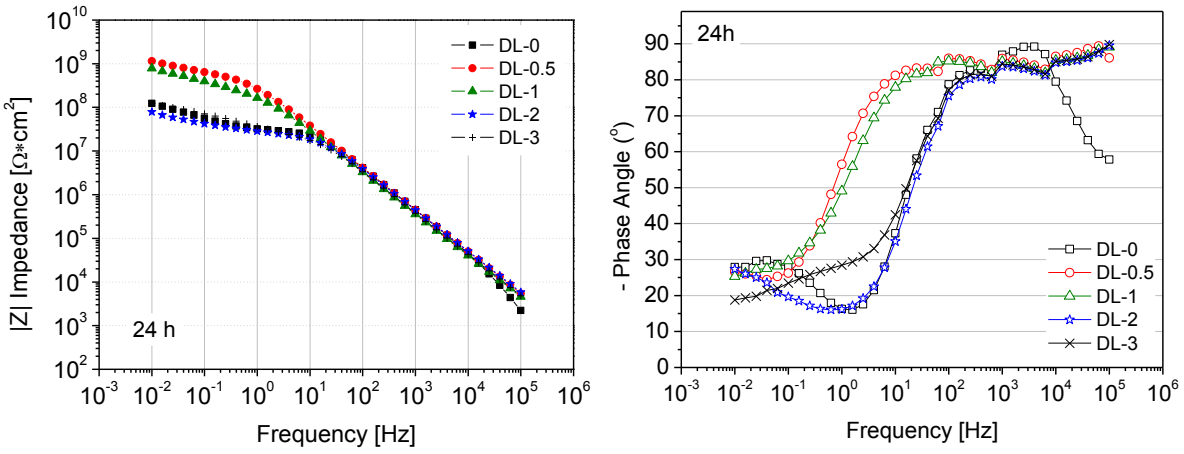

Figure 65 - Impedance (left) and phase angle (right) spectra of double layer systems in presence of 0.1 NaCl, time = 24h.

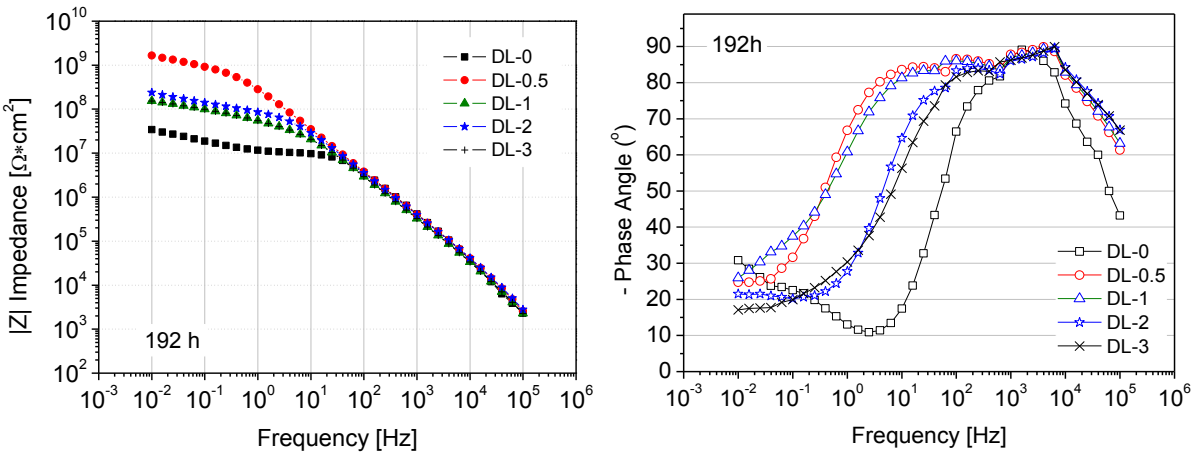

Figure 66 - Impedance (left) and phase angle (right) spectra of double layer systems in presence of 0.1 NaCl, time = 192h.

The EIS evolution after 192 hours indicated that degradation of DL-0 did initiate. On the other side, DL-0.5 showed stability for this equivalent period of time, as it can be seen from phase angle spectrum and the value of total impedance at low frequency range ~ 10^9 Ohm.cm^2.

The longer performances of the double layer systems can be appreciate from the evolution of the impedance at low frequency range in the course of 2450 hours, approximately 100 days of exposure to the chloride solution. Figure 67 (left) highlights the evolution of $|Z|_{0.01Hz}$ in the first 72 hours whereas the longer is seen on Figure 67 (right). The $|Z|_{0.01Hz}$ values of DL-0 over the first 24 hours were found have fluctuated with stability near 10^8 Ohm.cm^2. The DL's containing 0.5 and 1.0 wt. % of ceria nanoparticles, showed an order of magnitude higher values within equivalent period of analysis, around 10^9 Ohm.cm^2.

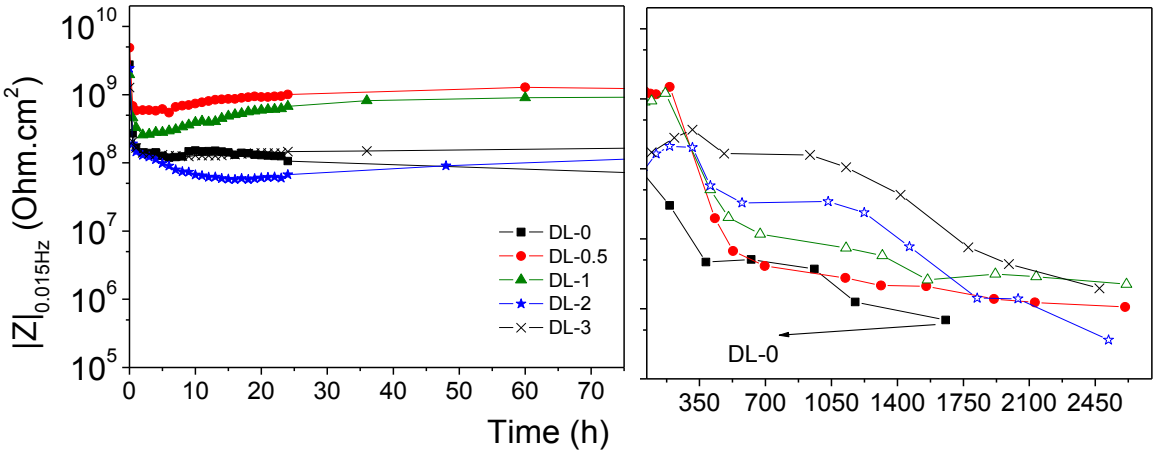

Figure 67 - |Z|0.015 Hz evolution of the DL's systems in presence of 0.1 M of NaCl over approximately 2450 hours of analysis

The higher initial values observed by the DL-0.5 and DL-1 when compared to DL-0 are suggestive about higher protection efficacy given. In other words, the contents of 0.5 and 1.0 wt. % of ceria nanoparticles were able to promote an increase of the low frequency impedance – and the $|Z|_{0.01Hz}$ are attributed to comprehend both, the impedance of the coating layer itself, as well as the impedance associated to the faradic process occurring at the metal/coating interface. Since a certain active effect of the ceria particles has been demonstrated these observations indicate that the weight amount of 0,5 – 1% of CeO_2 particles is able to promote an considerable protection of the metal substrate in the very first hours of immersion.

EIS data were modelled with the electrical equivalent circuits shown in Figures 51a and 51b. Figure 68 shows the evolution of the electrical parameter, coating resistance. From

that, apart from DL-1 the trend followed by Rc's values indicated the presence of water. There was a reduction of about one order of magnitude, from 10^8 to 10^7 Ohm.cm^2.

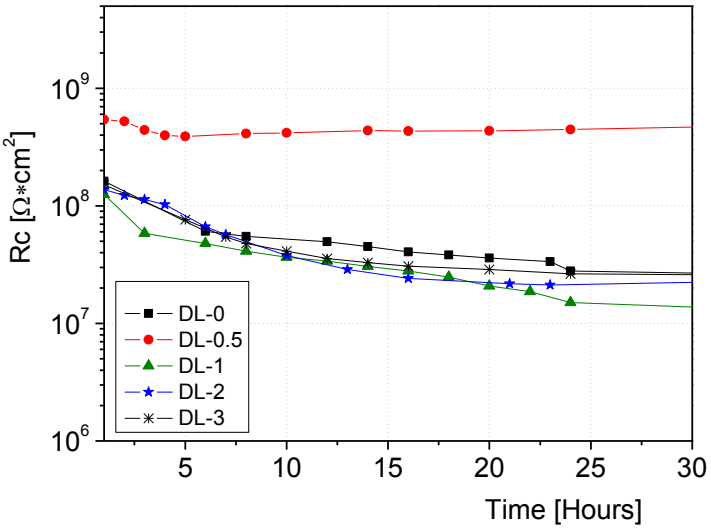

Figure 68 - Evolution of the coating resistance of DL's systems over the first 24 hours of exposure in 0.1 M NaCl.

Hence, even though the DL-1 absorbed certain quantity of water in the course of 24 hours the coating resistance remained considerably stable, approximately near 10^9 Ohm.cm^2. As a result, it is likely that the presence of 1.0 wt. % on the primer promoted extended anticorrosive protection of steel. The efficiency has been verified by increase in the impedance at low frequency range of DL-01 together with constant values of the coating resistance while water has being absorbed.

From Figure 67, the initial values for the total impedance at low frequency range of DL-2 and DL-3 were found close to 10^8 Ohm.cm^2, close to the DL-0. As a general assumption, the ingress of the electrolyte through the coating layer and later contact with the metallic substrate initiates the processes of coating degradation and one can expect a reduction of impedance values. Therefore, from the EIS spectra of DL-3 after 192 hours (see Figure 27) where the presence of a second time constant is attributed to corrosion process taken underneath the paint, the higher the amount of ceria, the later was the decay observed for the values of $|Z|_{0.01Hz}$.

EIS conducted on coatings with macroscopic defect

Following, owing to a complete investigation regarded to the influence of the ceria nanoparticles, the EIS has been carried out after the application of a macroscopic defect over the surface of DL's coated panels. The evolution of the $|Z|_{0.01Hz}$ over 72 hours of exposure is shown in Figure 69.

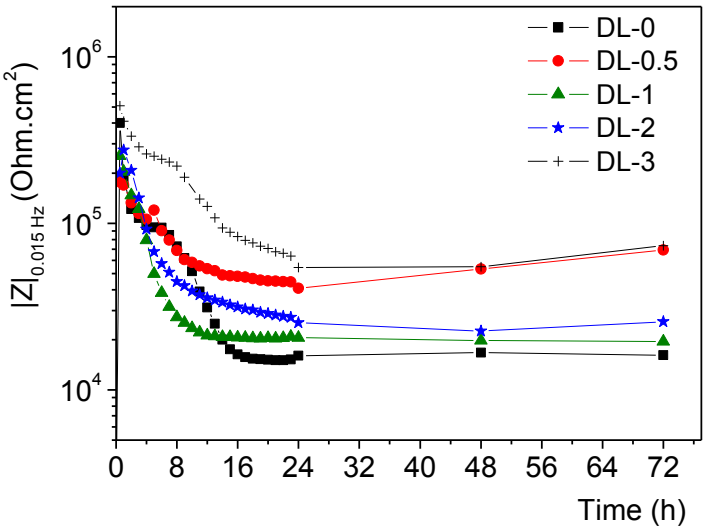

Figure 69 - Evolution of $|Z|_{0.01Hz}$ of scratched DL's coated panels

In the case of scratched coatings, as the active corrosion area increases near the defect, diffusion is no longer the predominant phenomenon and the processes of charge-transfer at the interface coating layer steel are dominating. In Figure 69, there was common tendency for the $|Z|_{0.01Hz}$ for the undercoat systems. All of them reduced of about one order of magnitude, from near 10^5 ~ 10^4 Ohm.cm^2, which indicated that corrosion reactions begun, preferentially around the defect and form the very beginning of the test.

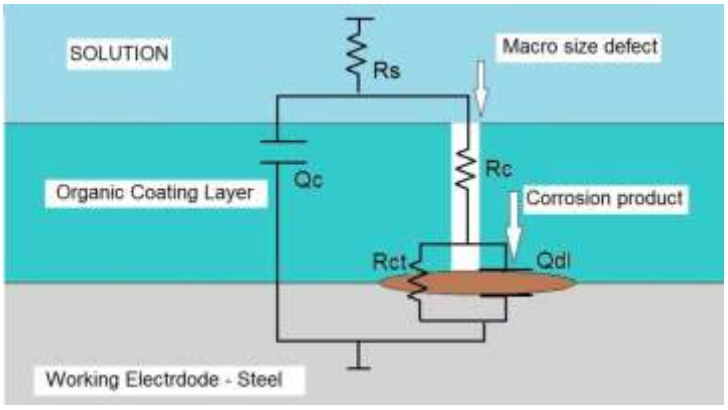

Figure 70 - Scheme of macro sized defect on the DL's coating and electrical circuit.

For that reason, the influence of diverse concentrations of cerium oxide has been estimated from the evolution of the double layer capacitance (Qdl), as shown in Figure 70. Qdl is an indicative about the wet area underneath the paint and the ration of between the Qdl as function of time and the Qdl at the very beginning of the exposure ($Qdl_{t=t^*}$ / $Qdl_{t=0}$) suggests about the delamination rate of the coating. Figure 71 shows the evolution in the course of 24 hours for the $Qdl_{t=t^*}$ / $Qdl_{t=0}$ of the DL's systems.

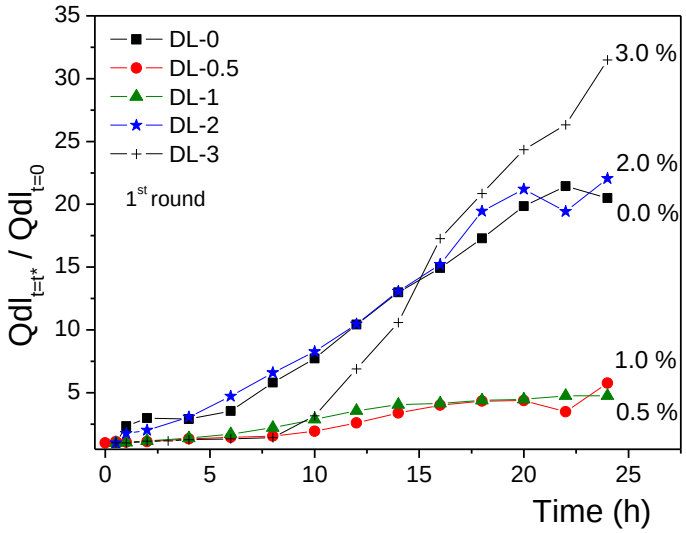

Figure 71 - Normalized double layer capacitance evolution for the scratched undercoat systems coatings -1st round of measurements.

For DL-0, a quasi-linear increase of the ratio $Qdl_{t=t^*}$ / $Qdl_{t=0}$ from the beginning of the test until the 24th hour is seen. By adding ceria nanoparticles at the levels of 0.5 and 1.0 wt. %, a remarkable decline of the delamination rate is promoted. The evolution of $Qdl_{t=t^*}$ / $Qdl_{t=0}$ ratio over time and its final value of DL-0.5 and DL-1 after 24 hours are approximately 4 times lower than those of the DL-0. On the other hand, for DL-2 and DL-3, opposite contribution is given. The DL-2 showed comparable evolution to the DL-0 whereas the highest increase in rate and final value of $Qdl_{t=t^*}$ / $Qdl_{t=0}$ was verified by DL-3.

In the case of DL-2 and DL-3 the higher rates and final values might be justified by the presence of aggregates at the primer's layer. For the application of the paint onto substrate, the higher the amount of ceria nanoparticle at the primer's, the lower is the probability of obtaining homogeneous dispersion of the nanoparticles. The aggregates themselves may have induced the formation of micron-size defects zones upon the primer layer. Consequently, the delamination rate became higher than a possible inhibition protection provided by 2.0 or 3.0 wt. % of ceria.

The results presented in Figure 71 are considered consistent. The repeatability of these results has been verified and considered reasonable. Thus, from the ratio $Qdl_{t=t^*}$ / $Qdl_{t=0}$ as a parameter for assess the delamination rate that occurred underneath the coatings, the drop of about 4 times given by the addition of 0.5 and 1.0 wt. % of ceria nanoparticles suggested, at a certain level, enhanced inhibition protection.

Accelerated Salt Spray test

Completing the EIS investigation, the influence of diverse concentrations of cerium oxide nanoparticles into a double layer system has been investigated by the accelerated salt spray test. Figure 72 shows the DL-0, reference undercoat systems and those containing 0.5 and 1.0 wt. % of ceria nanoparticles after 24 hours inside the salt spray chamber. The non-transparent visual aspect of the DL's coatings limited the evaluation of the delamination level after the salt spray tests. Thus, the main information provided by Figures 72 and 73 remains restricted to the diverse amount of blister present upon each panel. From Figure 72, the DL-0 sample showed many blisters distributed not only around the scratched zone, but across the whole coating area whereas the presence of few quantities of blisters were seen for the DL-0.5 sample mainly localized at the scratched area. In the case of DL-1, the amount of blisters was even lower than DL-0.5, however the presence of blisters is detected across the coating. Following, Figure 73 shows the DL-0 panel matched with those containing 2.0 and 3.0 wt. % after equivalent period of testing at the salt spray chamber.

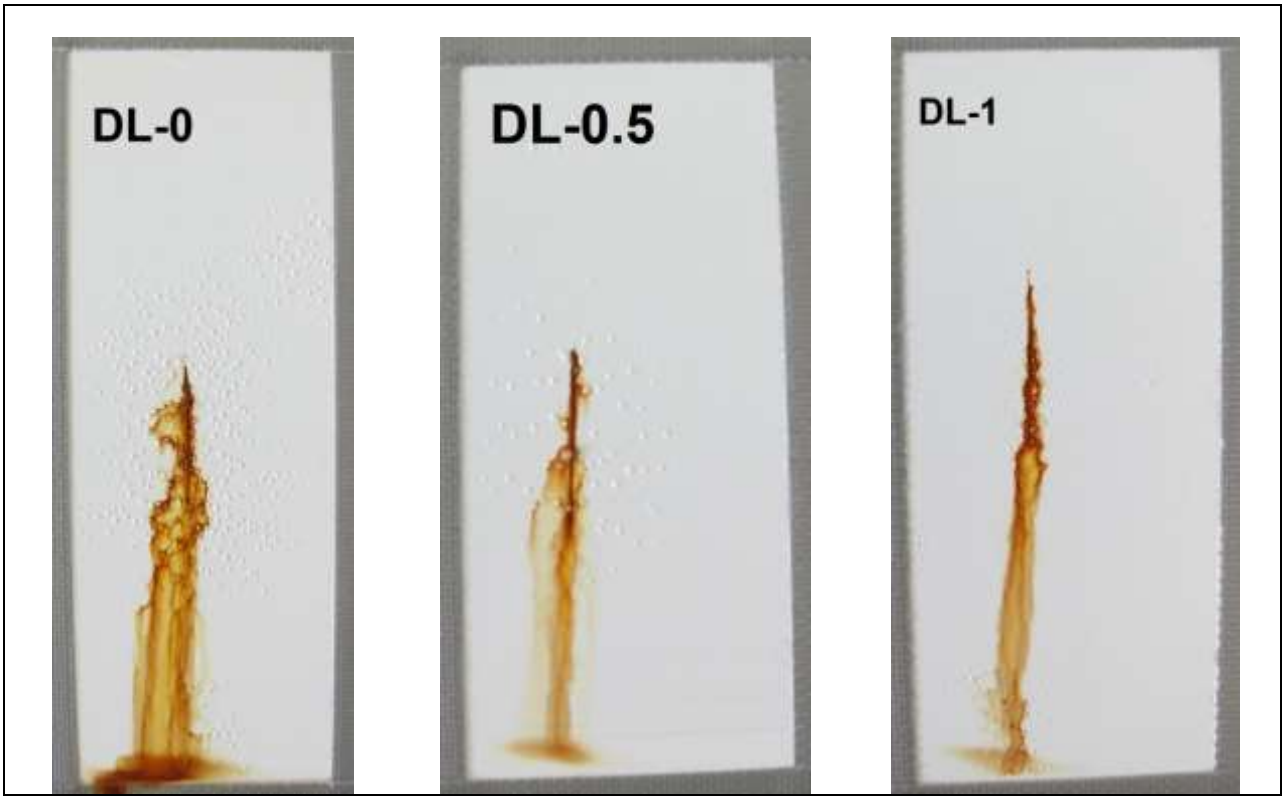

Figure 72 – DL-0, DL-0.5 and DL-0.5 after 24 hours of exposure inside salt spray chamber

The DL-2 undercoat showed a very few quantity of blisters which are exclusively surrounding the macroscopic defect. Differently, the DL-3 showed larger extent of blisters than the reference systems and DL-2.

In a whole, looking to the Figures 72 and 73 it is likely that the presence of 0.5, 1.0 and 2.0 t. % % of ceria reduced the presence of blisters when compared to the DL-0 sample. By adding 3.0 wt. % of ceria nanoparticles, it is possible to see that the protective effect is not linear, a quantity of blisters as equivalent as the DL-0 is seen. The observations from salt spray tests can be partially matched with the evaluation of delamination rate displayed on Figure 71. Apart from the differences in the solutions as well as the area under analysis, the delamination rate and the quantity of blisters have been reduced by the addition of 0.5 and 1.0 w/w % of ceria.

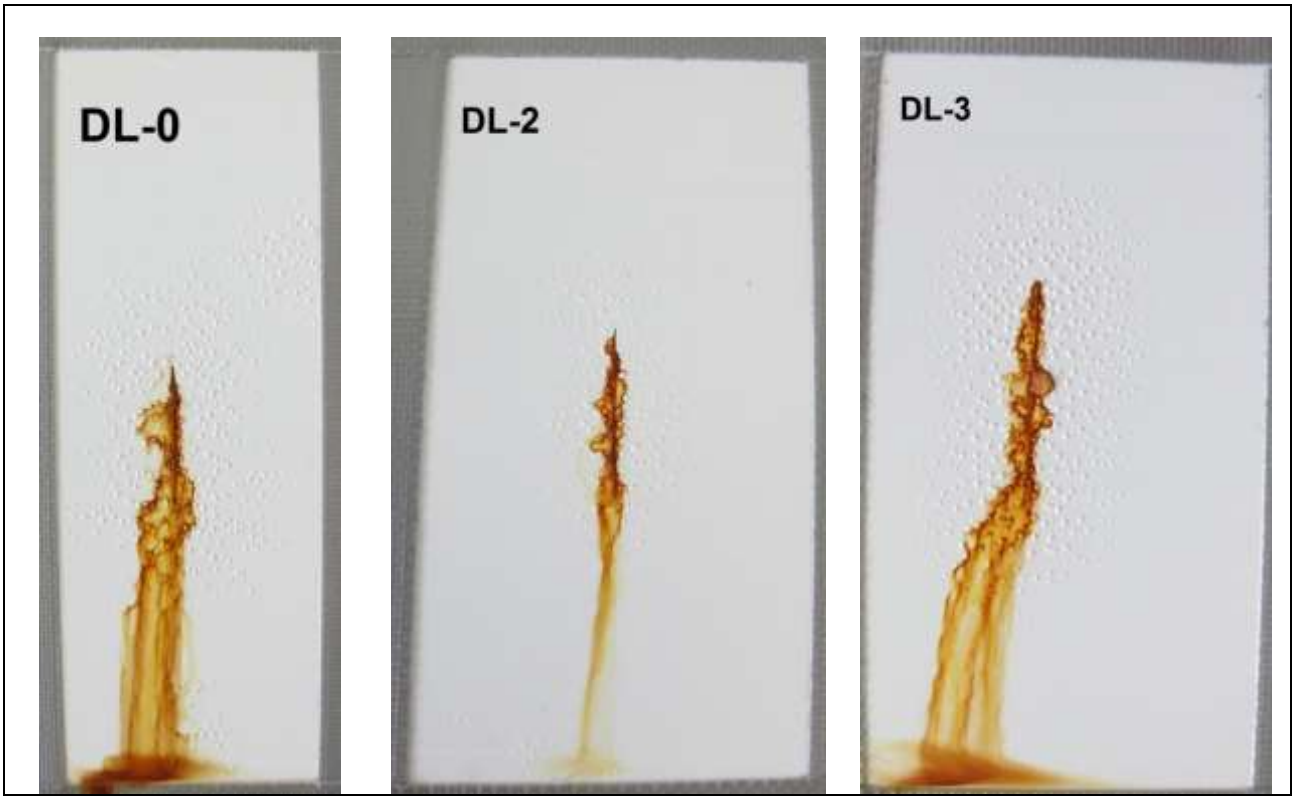

Figure 73 – DL-0, DL-2 and DL-3 after 24 hours of exposure inside salt spray chamber

Along the lines of this project, from an optimization point of view, the electrochemical measurements conducted for the waterborne double layer organic coatings alongside the salt spray chamber evaluation, but likewise to the experimental data reported on, two parameters have been chosen to design the full system waterborne coating system aimed by this project: the weight content of 1.0 wt. % as well as the thickness level of 10 micrometres were decided.

4.4 The influence of PAni and Ceria into a triple layer waterborne paint system

4.4.1 Materials

The last step of this project aimed the development of a triple layer paint system. Particularly, all of the three layers – the primer, the intermediate and the top coat layer – were formulated with the W.ACR.1 binder. The characteristics which discriminate the TL's coatings species are exclusively attributed to the diverse combination of PAni and CeO_2 nanoparticles added into the primers layer. Table 13 summarizes the main features of the TL's coated panels.

Table 13 - Main features of the triple layer paint systems

Label	Primer binder	PANi (1.0 wt%)	CeO_2 (1.0 wt%)	Total Thickness (µm)
TL-PAni-Ce.SF	W.ACR.1	W.PAni	Ce.SF	185.1 ± 12.1
TL-PAni-Ce.HP		W.PAni	Ce.HP	181.0 ± 12.4
TL-Blank		--	--	171.6 ± 11.8

In Table 13, the TL-Blank represents the triple layer specimen which has the primer layer formulated with W.ACR.1 waterborne clear coat without the presence of polyaniline neither ceria nanoparticles. The respective labels TL-PAni-Ce.SF and TL-PAni-Ce.HP, are with respect to the triple layer systems which the primer is loaded simultaneously with polyaniline and ceria nanoparticles obtained via supercritical flow and homogenous precipitation methods, respectively. Figure 74 depicts a scheme of the triple layer paint system.

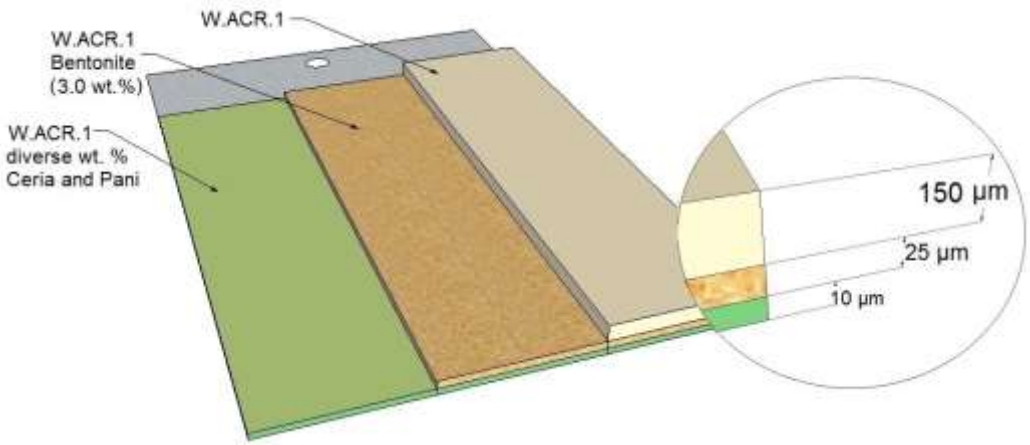

Figure 74 - Scheme of the triple layer paint systems

As concerned to the intermediate layer of the TL's species, it was formulated with the W.ACR.1 containing 3.0 wt. % of bentonite at a thickness level of 25 micrometers. On the top of the intermediate's layer the top coat was assembled. The W.ACR.1 clear coat has been chosen as the binder at a thickness level of 150 micrometers.

4.4.2 Characterization

Electrochemical Impedance Spectroscopy - EIS

The protective properties of the double layer coated panels were studied by Electrochemical Impedance Spectroscopy and detailed methodology has been described in section 4.1.2. Table 14 reports the EIS parameters selected during the investigation of the DL's.

Table 14 - Main features of the EIS investigation of the waterborne TL's coated panels

Signal Amplitude	Electrolyte – salt concentration	Analysed area	Analysis Mode
20 mV	0.5 M NaCl	10 cm^2	Intact coatings
5 mV	0.3 wt. % Na_2SO_4	10 cm^2	Scratched coatings

4.4.3 Results and discussion

The values of the thickness of all the TL's system coatings systems ranged between 170 – 190 µm and the 0.5 M NaCl electrolyte has been selected to conduct the EIS measurements of TL's coatings. Figure 75 shows the impedance and phase angle spectra

of all the TL's coatings systems at time equal to 0 h, it is important to highlight the electrolyte used for the investigation of the TL's coatings was 0.5 M of NaCl.

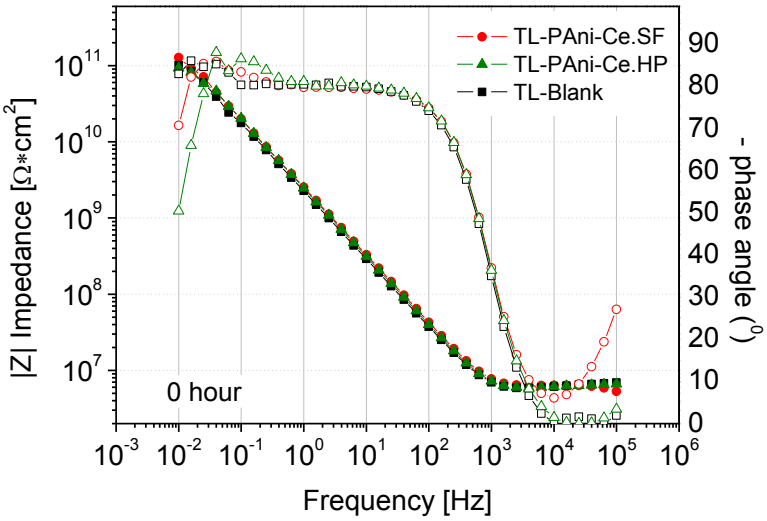

Figure 75 - Impedance (left axis) and phase angle (right axis) spectra of the TL's coatings at t = 0 hour of exposure to the chloride solution

At the very beginning, both impedance and phase angle spectra all the EIS spectra exhibited a quasi-capacitive behavior attributed to only one time constant response and values the total impedance modulus at 10^{-2} Hz frequency fluctuated near 10^{11} Ohm.cm^2. Much comparable were EIS spectra acquired after 24 hours, Figure 76, the impedance spectra and the phase angle response evolved with certain stability and yet, are attributed to only one time constant response.

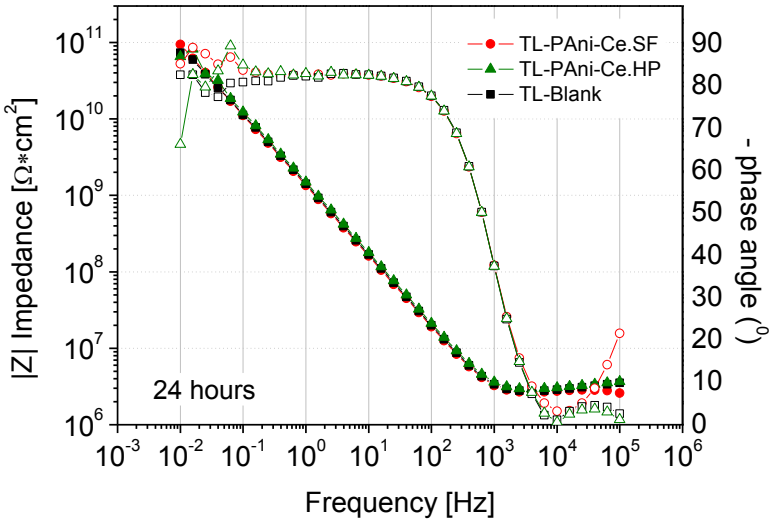

Figure 76 - Impedance and phase angle spectra of the TL's coatings after 24 hours of exposure to the chloride solution

Although the impedance levels of TL's, (10^{11} Ohm.cm^2) are considered relatively high, nevertheless, considering that the clear coati W.ACR.1 formulated the top layer of the TL's systems one can expect the ingress of certain amount of water moving into the bulk of the TL's coatings. Thus, the electrical parameters of the TL's samples were obtained by modelling the EIS spectra with the single time constant electrical circuit showed in Figure 77.

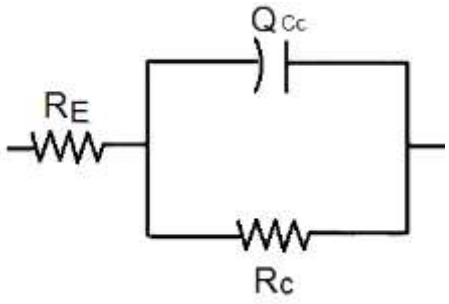

Figure 77 - Electrical circuit used for modeling the EIS spectra; Re(QCcRc)

Figure 78 shows the evolution of the capacitance of the Y_0 value related to the CPE ($|Z|_{CPE} = 1/(Y_0 \cdot (j\omega)^n)$) and the values of the exponent *n.*

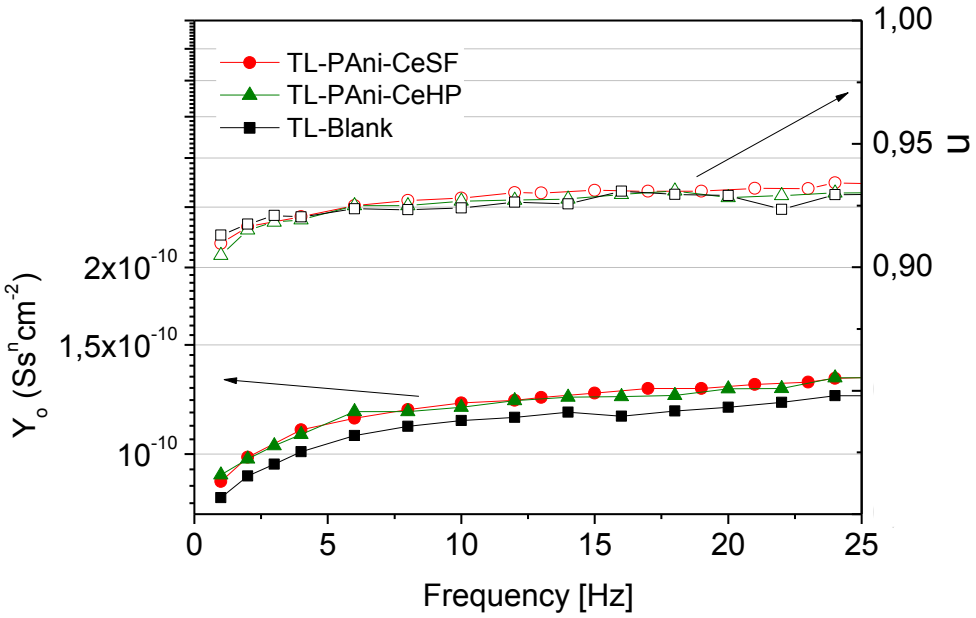

Figure 78 - Water uptake assessment according to the evolution of coating capacitance

From Figure 78, there was an increasing trend on the values of Y_o, justified by the ingress of water into the coating layer [ref] and the *n* values of the exponent fluctuated between 0.90 and 0.95.

Few differences on the EIS spectra of the triple layer systems started to appear after 160 days of exposure to 0.5 M NaCl solution, as it can be seen in Figure 79.

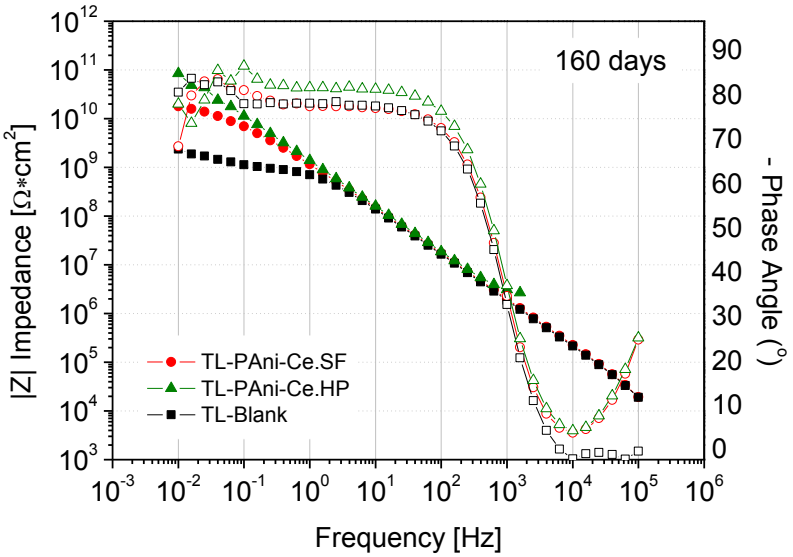

Figure 79 - Bode impedance spectra (left) and Bode phase angle spectra (right) of the TL's coating after 160 days of exposure into chloride solution

For instance, the values of $|Z|_{0.01Hz}$ of TL-Blank were slightly lowered after 160 days of exposure. On the other hand, the phase angle spectra did not evidence the presence of a second time constant, thus, it can be concluded that any process undergoing at the metal surface had been initiated. After 160 days, no significant changes were seen for the TL-PAni.CeSF and TL-PAni.CeHP. Their magnitudes of $|Z|_{0.01Hz}$ remained in the order of 10^{11} Ohm.cm^2 and the phase angle indicates the quasi-capacitive level of these two TL's specimens. An overview about the TL's performances over 160 days is given through the evolution of the total impedance at 10^{-2}Hz, as depicted in Figure 80.

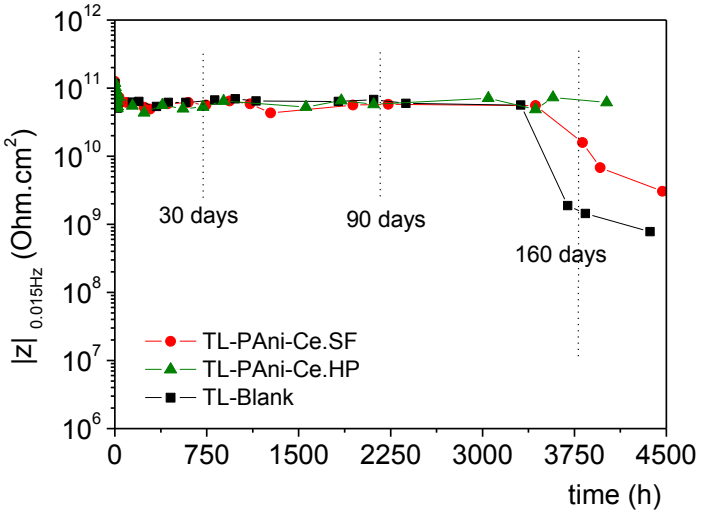

Figure 80 - $|Z|_{0.01\ Hz}$ over time of exposure to 0.5M NaCl for all the complete systems

Remembering the values of the total impedance at 10^{-2} Hz provide information on the overall protection properties for organic coatings, in other words, it is an estimation of both impedance contributions: i) the impedance of the organic coating layer itself and ii) the impedance influence related to the interface of the metal and the electrolyte, the faradic process taking place underneath the coating.

Thus, from the evolution of $|Z|_{0.01Hz}$ of the TL's systems, the two specimens which contained polyaniline and ceria into the primer layer, TL-PAni.CeSF and TL-PAni.CeHP, showed higher values of $|Z|_{0.01Hz}$ after 160 days of exposure.

EIS conducted on coatings with macroscopic defect

From the evolution of $|Z|_{0.01Hz}$ of the TL's systems displayed in Figure 80, it has been observed about one order of magnitude higher values for the specimens containing polyaniline and ceria when compared to the TL-Blank. Indeed, all of the specimens maintained high impedance levels, around 10^{10} Ohm.cm^2 for the duration of 160 days of exposure. Thus, one can assume that after 5 months of exposure to the aggressive 0.5 M NaCl solution, the protective properties of all the three TL's specimens have been preserved. However, it should be carefully analysed the influence of polyaniline and ceria into the primers layer of the TL's specimens. The evolution of the $|Z|_{0.01Hz}$ are suggestive the after 160 days, water and ions coming from the electrolyte might have reached the steel surface and initiated corrosion reaction which led to the reduction of $|Z|_{0.01Hz}$ magnitude of TL-Blank whereas the TL-PAni.CeSF and TL-PAni.CeHP showed higher values of $|Z|_{0.01Hz}$. Such assumption is not enough in order to drawn conclusion, therefore, EIS investigation has been carried out with the steel surface directly exposed to the electrolyte, after the application a macroscopic defect 1.0 centimetre long on TL's coatings. The electrical parameters from the EIS results of the scratched coatings were obtained with the electrical circuit showed in Figure 81.

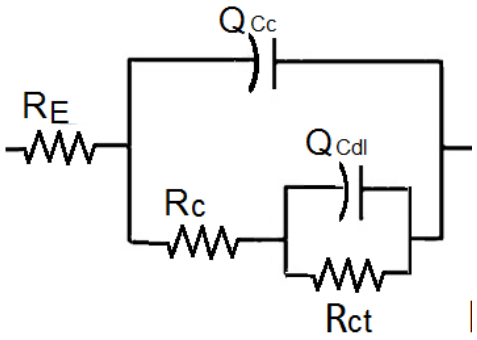

Figure 81 - Examples of equivalent Electrical circuit used for modeling the EIS spectra; Re(QCc(Rc(QdlRct)))

The electrical circuit depicted in Figure 81 considers the phenomena occurring at the interface of the metal and the coating, second time constant. Recalling the terms, R_{CT} stands for the charge transfer resistance while the Q_{dl} for the CPE associated to the double layer capacitance. The evolution of the parameter from the second time constant Q_{dl} as function of time, normalized by the Q_{dl} value at the beginning of the investigation (time = 0h) is shown in Figure 82.

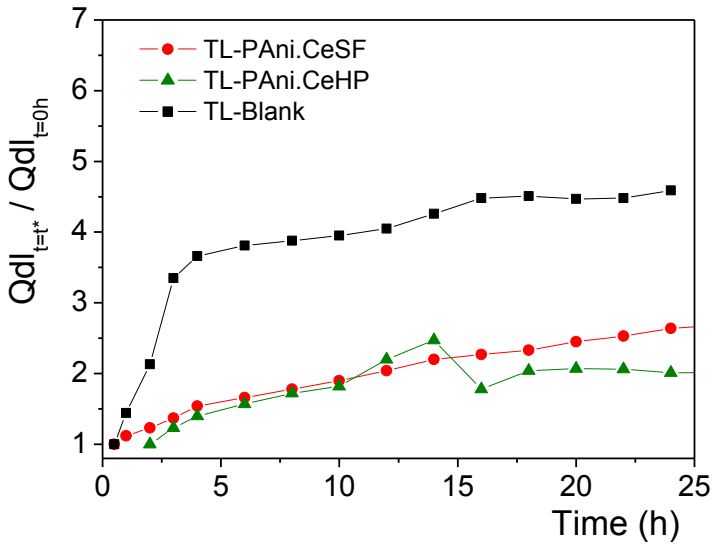

Figure 82 – Normalized double layer capacitance evolution of the scratched complete systems coatings

For the sample TL-Blank, it is possible to see a rapid increase of the normalized Q_{dl} in the first 10 hours of analysis and after 24 hours the final rate was found near to 4.5.

For the TL's coating formulated with PAni and Ceria, TL-PAni.CeSF and TL-PAni.CeHP, the evolution of the normalized Q_{dl} was slower than the TL-Blank with final value verified to be near to 2. Slower rates of delamination than the reference have been demonstrated by TL-PAni.CeSF and TL-PAni.CeHP. These have been formulated with polyaniline

nanoparticles alongside the two species of cerium oxide nanoparticles at their primer's layer, CeSF and CeHP, respectively.

As far as the Figure 82 is concerned, the ratio between the Qdl at certain time and the Qdl at time = 0h suggests about the delamination process taking place near around the defect. Considering this, it can be mentioned that the presence of ceria nanoparticles alongside polyaniline nanoparticles promoted a reduction of the delamination rate of the complete coatings. Furthermore, the steel panels tested in this work were given no surface/adhesion treatment before being coated. Since the coating efficiency, as a consequence, the steel protection can be improved by surface treatment, observations from Figure 82 are suggesting efficacy as anticorrosive additives for ceria nanoparticles.

4.5 Conclusion on the development of waterborne paint system based on CeO_2 and polyaniline

A first approach on the anticorrosive properties of four waterborne polymer dispersion has been done by means of Electrochemical Impedance Spectroscopy. Going deeper into the waterborne paints investigation the use of *in-situ* Atomic Force Microscopy has supported electrochemical information of the clear waterborne coatings.

Through the use of Electrochemical Impedance Spectroscopy it was possible to evaluate, to rank and, specially, to select the proper waterborne polymer dispersion for the formulation and development of the full paint systems aimed by the project.

It has been verified microscopic changes on the coatings features when the waterborne polymer dispersions were in contact with electrolyte, mainly, the ingress of water into the coating. The interactions or the changes in the topography as well as the stability of the coating were found to be dependent on the chemical nature of the polymer. As a consequence, the microstructure and properties of the paints were affected. For instance, the sequential *in-situ* AFM images revealed that changes on the order of hundreds of nanometres at the coating surface have occurred shortly, less than 24 hours, after the exposure to the electrolytes. EIS observations for the clear waterborne alkyd coating revealed a rise in the $|Z|_{0.01Hz}$ and a decrease in the coating capacitance after a few hours of exposure. It has been evidenced by means of *in-situ* AFM the phenomenon swelling of the coating layer caused by water uptake and led to the closure/blockage of pores along the coating volume.

However, the information given by *in.situ*-AFM should be handled with care. Generally speaking, a full connection between the two techniques was not possible and depended on the system under investigation. Finally, as far as the investigation was concerned, the main limit consisted in the possibility to extrapolate to all the coating the information obtained by means of AFM, which are referred to a very thin volume close to the surface of the organic coating.

The anticorrosive properties of a waterborne acrylic polymer dispersion loaded with polyaniline and cerium oxide (CeO_2) nanoparticles has been investigated by means of Electrochemical Impedance Spectroscopy. The blank acrylic coating at the level of 10 micrometres thick had been loaded with PAni, ceria nanoparticles and the combination of both at 1.0 wt. % content. Regardless the lower barrier property due to the relatively thin layer of the systems, through the monitoring of open circuit potential, and the EIS evolution in the course of 48 hours, ennoblement effect OCP alongside the higher impedance magnitudes were detected for the systems in presence of ceria nanoparticles. Thus, a suggestive reinforcement on the anticorrosive properties of the acrylic waterborne coating due to the presence of 1.0 wt. % of cerium oxide nanoparticles was observed. Due to low thicknesses levels and, consequently, elevated permeability of the coating, the extraction of the electrical data of these coatings systems had been restricted

The anticorrosive properties of the waterborne acrylic polymer dispersion designed for Double paint coating systems were investigated by means of Electrochemical Impedance Spectroscopy and accelerated salt spray tests. From the salt spray chamber, it has been observed the optimal concentration of the ceria nanoparticles into the primer layer of th e double layer waterborne coating at 1.0 wt%. Higher amount of ceria did not to provide any beneficial effect in decreasing delamination creep. On the other side, EIS measurements carried out on the double layer intact coatings revealed that also higher amount of ceria nanoparticles (2.0 – 3.0 wt%) have a beneficial effect on the protection system.

Finally in the case of the triple layer waterborne acrylic latex, the observations from Electrochemical Impedance Spectroscopy showed that the full paint system designed afforded corrosion protection for about 6 months upon exposure to the 0.5M NaCl solution. Furthermore, the combination of polyaniline nanoparticles and ceria were able to reduce the delamination of the acrylic waterborne coating from the steel substrate.

5 Conclusion

All over the last three years, this project focused the development of an environmentally friendly anticorrosion organic coating with long durability for corrosion protection of steel. Basically, a water based paint system based on cerium oxide and polyaniline nanoparticles was settled.

On the whole, the thesis reported an investigation on the electrochemical activity of water based dispersions containing ceria nanoparticles and polyaniline nanoparticles. Later in the project, these, have been stabilized into a waterborne polymeric binder which has been applied onto low carbon steel specimens for enhanced anticorrosive properties. The organic coating paint systems containing the nanoparticles were likewise investigated with special emphasis on the influence of the presence of ceria and polyaniline upon the anticorrosive properties. The methodology of study of both, water dispersions and paint systems, was chiefly conducted by the use of electrochemical techniques, such as, potentiodynamic polarization curves and electrochemical impedance spectroscopy.

At first, water based dispersions containing the cerium oxide nanoparticles studied were synthesized via two different routes of synthesis, homogeneous precipitation method and the supercritical flow method. The influence of pH and ceria contents into the water based dispersions was covered. Regardless the route of synthesis, remarkable electrochemical activity of the ceria nanoparticles was observed, for example the reduction of three orders of magnitude of anodic current - a current density of 10^{-6} A/cm^2 for the anodic branch was verified - consequently the reduction of the overall corrosion reactions, of steel specimen immersed into the 10 wt. % of water based dispersion containing ceria nanoparticle.

Frequently, from the polarization curves of steel immersed into the ceria dispersions, the reduction of cathodic or anodic currents was accompanied by an ennoblement effect. For instance, the OCP value of ceria dispersion at concentration level of 10 wt. % was found approximately 0.5 V more noble than steel immersed into the sulphate solution. Moreover, the monitoring of the open circuit potential of steel immersed into ceria dispersions, has demonstrated the ennoblement lasted for about 72 hours.

Likewise, less concentrated contents of ceria into the salt solutions were studied. For instance, an investigation performed in chloride solutions revealed 3.0 wt. % of these particles inside the solution was needed to guarantee a long term stability of the steel

electrodes surface in such a way that the corrosion processes are delayed. In addition, the electrochemical impedance evolution of the steel electrodes immersed in the 0.1M NaCl solutions containing 1.0, 3.0, and 5.0 of CeO_2 nanoparticles have shown the presence of 5 wt. % of ceria into the chloride solution kept the values of total impedance at low frequency range near 10^6 Ohm.cm^2 for over 400 hours of immersion. For that, it was attributed that the steel electrodes immersed in the cerium oxides containing solutions showed a switch from an “active electrode” behavior to a “blocking electrode” behavior. Few statements on that were proposed, however, it has also been stressed that a further and deeper investigations in order to clarify and prove the statements are yet necessary.

Differently, the electrochemical investigation of water based dispersion containing polyaniline did not demonstrate beneficial effects. Due to the great acid values of the water based solutions containing PAni, pH near 3, steel is expected to go under corrosion at fast rates.

Thus, at certain point in the project the motivations were turned into the use of ceria nanoparticles as anticorrosive additives and the influence of ceria contents were studied. It has been found the optimal concentration of the ceria nanoparticles in the polymeric matrix between 0.5 – 1.0 wt. % range. Higher amount of ceria seemed not to provide any beneficial effect in decreasing delamination creep. Besides, EIS measurements carried out on intact coatings revealed that also higher amount of ceria nanoparticles (2.0 – 3.0 wt%) have a beneficial effect on the protection system.

As concerning to the complete paint systems developed, so-called Triple Layer, from EIS investigation it is suggested relatively elevated barrier properties of the systems. The 10^{11} Ohm.cm^2 values of impedance at the low frequency range associated to the quasi-capacitive level of the triple layers specimens were maintained for approximately 6 months of exposure into the aggressive solution. It has been put forward the elevated barrier properties of the sum of the top and intermediate layers. Later on the examination, when the beneficial influence of polyaniline and ceria was verified on the lower rates of reduction on the values of impedance at the low frequency range when compared to the triple layer system without the combination of these nanoparticles. Furthermore, from the EIS evaluation of the scratched coatings, lower delamination rates were seen for the systems containing the combination of polyaniline and ceria nanoparticles on the primer layer. Therefore concentration level of 1.0 wt. % of each, ceria and polyaniline nanoparticles

added together, seemed to be effective for enhance the anticorrosive properties of the waterborne acrylic coating.

As a general overview, by means of the electrochemical studies, most especially EIS, the step-by-step on the development of the organic coating was favored. The selection of the proper waterborne polymeric binder to formulate the organic coating paint system, the influence of ceria contents into the primer's stratum of a Double Layer paint system and the optimization of the formulation of the primers layer, have been verified throughout EIS data and their fitting with proper electrical circuit. Besides, the electrochemical information was confirmed by means of the accelerated salt spray test.

Lastly, the scientific production given by the project evolved simultaneously with its aims. The research group of the Anticorrosion Laboratory from the University of Trento communicated the obtained results necessary to the step-by-step of the project alongside the dissemination of the scientific activity. The comprehension about the anticorrosive mechanisms of protection of the ceria nanoparticles for steel were attempted, however, deeper elucidations still need to be achieved. Explicitly, great is the literature available on the use of PAni for anticorrosive protection of steel, however, the clear influence given by these nanoparticles remained unclear, intrinsically justified by the routes of synthesis. On the other hands, the most interesting observations were seen the use of ceria nanoparticles and, in particular their effective potential as corrosion inhibitors. Despite only very few literatures regarding this topic are available, the present work contributes to better clarify the effect of cerium oxides nanoparticles on the electrochemical activity of steel.

6 Suggestion for future works

Considering the above, one can find suggestive as succeeding works:

- Optimization of the route of syntheses of Polyaniline, in order to obtain enhanced electrochemical activity of these nanoparticles onto steel;
- Full comprehension about the mechanisms of protection involved in the anticorrosive protection of nanoceria given to steel.

Acknowledgments

The author shows his gratitude to Professor Flavio Deflorian, who tutored the work with competence. The author is particularly thankful to Dr. Michele Fedel, glad to have worked and learned with him and also for the shared moments.

Author is grateful to Prof. Stefano Rossi, to Dr. Caterina Zanella and to Mr Luca Benedetti for the technical support and the shared moments together.

This work was part of and supported by the SteelCoat Project (NMP-1910.1.2-2 Substitution of materials or components utilizing Green Nanotechnology. Project Number: 263262) funded by FP7 program of European Commission. Therefore, author would like to thank Prof. Jinshan Pan and Ms Jing Li from KTH Royal Institute of Technology. D. Sci. Anwar Ahniyaz, Dr Karin Persson, Dr Anders Larsson, Dr Diego Peñaloza from SP Technical Research Institute of Sweden Chemistry. Dr. Jacob Becker from Aarhus University. Ms Isabelle Betremieux and Mr Grégory Delmas from Arkema Coating Resins. Dr Nigel Whitehouse and Dr Peter Collins from PRA Coatings Techology Centre. Dr Carsten Schellbach and Dr Monika Schwarzenberg form Enthone Nano Science Center. Dr. Kenneth Möller from. Dr Valentina Ermini from Laviosa Chimica Spa.

References

1. Ahmad, Z., Principles of Corrosion Engineering and Corrosion Control. 2006, Oxford, UK: Elsevier Ltd.

2. Cohen, S.M., Replacements for Chromium Pretreatments on Aluminum. Corrosion Science, 1995. 51(1): p. 71- 80.

3. The Environmental Protection (Prescribed Processes and Substances) Regulations ISBN 0-11-752999-0. 1991.

4. Costa, M., and C.B. Klein, Toxicity and Carcinogenicity of Chromium Compounds in Humans. Critical Review in Toxicology, 2006. 36(2): p. 155- 163.

5. Adhikari, A., et al., Electrochemical behavior and anticorrosion properties of modified polyaniline dispersed in polyvinylacetate coating on carbon steel. Electrochimica Acta, 2008. 53(12): p. 4239-4247.

6. Stoyanova, E., and D. Stoychev, Corrosion behavior of stainless steels modified by cerium oxides layers, in Corrosion Resistance, H. Dhih, Editor 2012, inTech Puplishing. p. 240- 270.

7. DeBerry, D.W., Modification of the Electrochemical and Corrosion Behaviour of Stainless Steel with and Electroactive Coatings. Electrochemical Society, 1985. 132(5): p. 1022- 1026.

8. Schauer, T., A. Joos, L. Dulog, and C.D Eisenbach, Protection of iron against corrosion with polyaniline primers. Progress in Organic Coatings, 1998. 33(1): p. 20- 27.

9. Spinks, G.M., A.J. Dominis, G.G. Wallace, and D.E. Tallman, Electroactive conducting polymers for corrosion control. Part 2 Ferrous Metals. Solid State Electrochemistry, 2002. 6: p. 85- 100.

10. Pud, A.A., G.S. Shapoval, P. Kamarchik, N.A. Ogurtsov, V.F. Gromovaya, I.E. Myronyuk, and Yu.V. Kontsur, Electrochemical behavior of mild steel coated by polyaniline doped with organic sulfonic acids. Syntetic Metals, 1999. 107(2): p. 111-115.

11. Kalendová, A., D. Veselý, and J. Stejskal, Organic coatings containing polyaniline and inorganic pigments as corrosion inhibitors. Progress in Organic Coatings, 2008. 62(1): p. 105-116.

12. Wessling, B., and J. Posdorfer, Corrosion prevention with an organic metal polyaniline corrosion test results. Electrochimica Acta, 1999. 44(12) p. 2139- 2147.

13. Wessling, B., Corrosion prevention with an organic metal (polyaniline): surface ennobling, passivation, corrosion test results. Materials and Corrosion, 1996. 47(8): p. 439- 445.

14. Sathyanarayanan, S., V. Karpakam, K. Karmraj, S. Muthukrishnan, and G. Venkatachari, Sulphonate doped polyaniline containing coatings for corrosion protection of iron. Surface and Coatings Technology, 2010. 204(9-10): p. 1426-1431.

15. Sathiyanarayanan, S., S. Muthkrishnan, and G. Venkatachari, Corrosion protection of steel by polyaniline blended coating. Electrochimica Acta, 2006. 51(28): p. 6313-6319.

16. Sun, C., H. Li, and L. Chen, Nanostructured ceria-based materials: synthesis, properties, and applications. Energy and Environmental Science, 2012. 5: p. 8475-8505.

17. Carabineiro, S. A. C., S.S.T. Bastos, J.J.M. Orfao, M.F.R. Pereira, J.J. Delgado, and J.L Figueiredo, Exotemplated ceria catalysts with gold for CO oxidation. Applied Catalysis A-General, 2010. 381(1-2): p. 150- 160.

18. Trovarelli, A., Catalytic properties of ceria and CeO2-containing materials. Catalysis Reviews - Science and Engineering, 1996. 38(4): p. 439-520.

19. Nagarale, R. K., U. Hoss, and A. Heller, Mixed-Valence Metal Oxide Nanoparticles as Electrochemical Half-Cells: Substituting the Ag/AgCl of Reference Electrodes by CeO2–x Nanoparticles. Journal of the American Chemical Society, 2012. 134(51), p. 20783- 20787.

20. Evans, A., A. Bieberle-Hutter, J.L.M. Rupp, and L.J. Gauckler, Review on microfabricated micro-solid oxide fuel cell membranes. Journal of Power Sources, 2009. 194(1): p. 119-129.

21. Shcherbakov, A.B., V.K. Ivanov, N.M. Zholobak, O.S. Ivanova, E.Y. Krysanov, A.E. Baranchikov, N.Y. Spivak, and Y.D. Tretyakov, Nanocrystalline Ceria Based Materials – Perpectives for Biomedical Application. Biophysisc, 2011. 56(6): p. 987-1004.

22. Saadat-Monfared, A., M. Mohseni, and M.H. Tabatabaei, Polyurethane nanocomposite films containing nano-cerium oxide as UV absorber. Part 1. Static and dynamic light scattering, small angle neutron scattering and optical studies. Colloids and Surfaces, 2012. 408: p.64- 70.

23. Faure B., G. Salazar-Alvarez, A. Ahniyaz, I. Villaluenga, G. Berriozabal, Y.R. De Miguel, and L. Bergstrom, Dispersion and surface functionalization of oxide nanoparticles for transparent photocatalytic and UV-protecting coatings and sunscreens. Science and Technology of Advanced Materials, 2013. 14(2).

24. Llusar, M., L. Vitaskova, P. Sulcová, M.A. Tena, J.A. Badenes, and G. Monrós, Red ceramic pigments of terbium-doped ceria prepared through classical and non-conventional coprecipitation routes. Journal of European Ceramic Society, 2010. 30(1): p. 37- 52.

25. Patil, S., S.C. Kuiry, and S. Seal, Nanocrystalline ceria imparts better high–temperature protection. Proceedings of the Royal Society of London, Series A: Mathematical, Physical and Engineering Sciences, 2004. 460(2052): p. 3569- 3587.

26. Durán, A., Y.Castro, M. Aparicio, A. Conde, and J.J. de Damborenea, Protection and surface modification of metals with sol–gel coatings. International Materials Reviews, 2007. 52(3): p. 175- 192.

27. Sharmila, R., N. Selvakumar, and K. Jeyasubramanian, Evaluation of corrosion inhibition in mild steel using cerium oxide nanoparticles. Materials Letters, 2013. 91: p. 78-80.

28. Montemor, M.F., and M.G.S. Ferreira, Cerium salt activated nanoparticles as fillers for silane films: Evaluation of the corrosion inhibition performance on galvanised steel substrates. Electrochimica Acta, 2007. 52(24): p. 6976-6987.

29. Fedel M., F. Deflorian., S. Rossi, and P. Kamarchik, Study of the effect of mechanically treated CeO2 and SiO2 pigments on the corrosion protection of painted galvanized steel. Progress in Organic Coatings, 2012. 74(1): p. 36-42.

30. Deflorian, F., S. Rossi, and M. Fedel, Organic coatings degradation: Comparison between natural and artificial weathering. Corrosion Science, 2008. 50(8): p. 2360-2366.

31. Amirudin, A., and D. Thieny, Application of electrochemical impedance specstroscopy to study the degradation of polymer coated metals. Progress in Organic Coatings, 1995. 26 (1): p. 1- 28.

32. Malucelli, G., A. Di Gianni, F. Deflorian, M. Fedel, and R. Bongiovanni, Preparation of ultraviolet-cured nanocomposite coatings for protecting against corrosion of metal substrates. Corrosion Science, 2009. 51(8): p. 1762-1771.

33. Donkers, P.A.J., H.P. Huinink, S.J.F. Erich, N.J.W. Reuvers, and O.C.G. Adan, Water permeability of pigmented waterborne coatings. Progress in Organic Coatings, 2013. 76(1): p. 60-69.

34. Bonnel, K., C Le Pen, and N Pébère, E.I.S. characterization of protective coatings on aluminium alloys. Electrochimica Acta, 1999. 44 (24) p. 4259 - 4267.

35. Galliano F., and D. Landolt, Evaluation of corrosion protection properties of additives for waterborne epoxy coatings on steel. Progress in Organic Coatings, 2002. 44(3) p. 217- 225.

36. Collong W., A. Göbel, B. Kleuser, W. Lenhard, and M. Sonntag, 2K waterborne clearcoat—a competition between crosslinking and side reactions. Progress in Organic Coatings, 2002. 45(2) p. 205 - 209.

37. Wegmann, A., Chemical resistance of waterborne epoxy.amine coatings. Progress in Organic Coatings, 1997. 32: p. 231- 239.

38. Bai, C.Y., X.Y. Zhang, J.B. Dai, and W.H.Li, A new UV curable waterborne polyurethane: Effect of CC content on the film properties. Progress in Organic Coatings, 2006. 55(3): p. 291-295.

39. Liu, X., K. Xu, H. Liu, H. Cai, J. Su, Z. Fu, Y. Guo, and M. Chen, Preparation and properties of waterborne polyurethanes with natural dimer fatty acids based polyester polyol as soft segment. Progress in Organic Coatings, 2011. 72(4): p. 612-620.

40. Bonora, P.L., F. Deflorian, and L. Fedrizzi, Electrochemical Impedance spectroscopy as a tool for investigating underpaint corrosion. Electrochimica Acta, 1996. 41(7-8): p. 1073- 1082.

41. Bierwagen, G., D. Tallman, J. Li, L. He, and C. Jeffcoate, EIS studies of coated metals in accelerated exposure. Progress in Organic Coatings, 2003. 46(2): p. 149-158.

42. Touzain, S., Some comments on the use of the EIS phase angle to evaluate organic coating degradation. Electrochimica Acta, 2010. 55(21): p. 6190- 6194.

43. Bastos, A.C., and A.M.P. Simões, Effect of uniaxial strain on the protective properties of coil-coatings. Progress in Organic Coatings, 2003. 46(3): p. 220-227.

44. Hinderliter, B.R., S.G. Croll, D.E. Tallman, Q. Su, and G.P. Bierwagen, Interpretation of EIS data from accelerated exposure of coated metals based on modeling of coating physical properties. Electrochimica Acta, 2006. 51(21): p. 4505-4515.

45. Schiller, C.A., W. Strunz, The evaluation of experimental dielectric data of barrier coatings by means of different models. Electrochimica Acta, 2001. 46(24-25): p. 3619- 3625.

46. Jorcin, J.B., M.E. Orazem, N. Pebere, and B. Tribollet, CPE analysis by local electrochemical impedance spectroscopy. Electrochimica Acta, 2006. 51(8-9): p. 1473-1479.

47. Deflorian, F., L. Fedrizzi, S. Rossi, and P.L. Bonora, Organic Coating Capacitance Measurements by EIS ideal and actual trends. Electrochimica Acta, 1999. 44(24): p. 4243- 4249.

48. Sykes J. M., A variant of the Brasher–Kingsbury equation. Corrosion Science, 2004. 46(3): p. 515-517.

49. Castela A.S., and A.M. Simoes, Assessment of water uptake in coil coatings by capacitance measurements. Prog. Organic Coating, 2003. 46 (1) p. 55-61.

50. Anupriya, K., E. Vivek, and B. Subramanian, Facile synthesis of ceria nanoparticles by precipitation route for UV blockers. Journal of Alloys and Compounds, 2014. 590: p. 406-410.

51. Yin, L., Y. Wang, G. Pang, Y. Koltypin, and A. Gendanken, Sonochemical Synthesis of Cerium Oxide Nanoparticles—Effect of Additives and Quantum Size Effect. Journal of Colloid and Interface Science, 2002. 246(1): p. 78-84.

52. Sathyamurthy, S., K.J. Leonard, R.T. Debestani, and M.P. Paranthaman, Reverse micellar synthesis of cerium oxide nanoparticles. Nanotechnology, 2005. 16(9): p. 1960-1964.

53. Sun, C., H. Li, H. Zhang, Z. Wang, and L. Chen, Controlled synthesis of CeO2 nanorods by a solvothermal method. Nanotechnology, 2005. 16(9).

54. Korsvik, C., S. Patil, S. Seal, and W.T. Self, Superoxide dismutase mimetic properties exhibited by vacancy engineered ceria nanoparticles. Chemical Communications, 2007. 14(10): p. 1056- 1058.

55. Masui, T., H. Hirai, N. Imanaka, and G. Adachi, Synthesis of cerium oxide nanoparticles by hydrothermal crystalization with citric acid. Journal of Materials Science and Letters, 2002. 21: p. 489- 491.

56. Khalipova, O.S., V. Lair, and A. Ringuedé, Electrochemical synthesis and characterization of Gadolinia-Doped Ceria thin films. Electrochimica Acta, 2014. 116: p. 183-187.

57. Kai, L., W. Xuezhong, Z. Zexing, W. Xiaodong, and W. Duan, Oxygen Storage Capacity of Pt-, Pd-, Rh/CeO2-Based Oxide Catalyst. Journal of Rare Earths, 2007. 25(1): p. 6-10.

58. Ivanov, V.K., A.B. Shcherbakov, I.G. Ryabokon, A.V. Usatenko, N.M. Zholobak, and D. Yu.D. Tretyakov, Inactivation of the Nitroxyl Radical by Ceria Nanoparticles. Chemistry, 2010. 430(2): p. 43-46.

59. Skorodumova, N., S.I. Simak, B.I. Lundqvist, A. Abrikosov, and B. Johansson, Quantum Origin of the Oxygen Storage Capability of Ceria. Physical Review Letters, 2002. 89(16): p. 166601-166605.

60. Bethencourt, M., F.J. Botana, J.J. Calvino, M. Marcos, and M.A. Rodriguez-Chacon, *Lanthanide compounds as environmentally friendly corrosion inhibitors of aluminium alloys: a review.* Corrosion Science, 1998. 40(11): p. 1830-1819.

61. Hinton, B.R.W., D.R. Arnott, and N.E. Ryan, The Inhibition of Aluminum Alloy Corrosion by Cerous Cations. Metals Forum, 1985. 7(4): p. 211- 217.

62. Hinton, B.R.W., D.R. Arnott, and N.E. Ryan. Mater Forum, 1986. 9(3): p. 162- 169

63. Aballe, A., M. Bethencourt, F.J. Botana, M.A. Cauqui, M. Marcos, and M.A. Rodriguez, Proceedings Eurocorr, 1997. **2**. p. 339-344. Trondheim Norway.

64. Aldykiewicz, A.J., A.J. Davenport, and H.S. Isaacs, Studies of the Formation of Cerium-Rich Protective Films using X-Ray Absorption Near-Edge Spectroscopy and Rotating Disk Electrodes Methods. Electrochemical Society, 1996. 143(1): p. 147-154.

65. Li, X., S. Deng, H. Fu, and G. Mu, Synergistic inhibition effect of rare earth cerium(IV) ion and sodium oleate on the corrosion of cold rolled steel in phosphoric acid solution. Corrosion Science, 2010. 52(4): p. 1167-1178.

66. Zheludkevich, M., R. Serra, M.F. Montemor, M.G.S. Ferreira, Oxide nanoparticle reservoirs for storage and prolonged release of the corrosion inhibitors. Electrochemistry Communications, 2005. 7(8): p. 836-840.

67. Miao, W., I.S. Cole, A.K. Neufeld, and S. Furman, Pitting Corrosion of Zn and Zn-Al Coated Steels in pH 2 to 12 NaCl Solutions. Journal of The Electrochemical Society, 2007. 154(1): p. C7-C15.

68. Amaraki, K., Self-healing protective films prepared on zinc by treatments with cerium (III) nitrate and sodium phosphate. Corrosion Science, 2002. 44(11): p. 2621- 2634.

69. Hayes, S.A., P. Yu, T.J. O'Keefe, M.J. O'Keefe, and J.O. Stoffer, The Phase Stability of Cerium Species in Aqueous Systems. Journal of The Electrochemical Society, 2002. 149(12): p. C623-C630.

70. Rosenkranz P, M.L. Fernandez-Cruz, E. Conde, M.B. Ramírez-Fernández, J.C. Flores, M. Fernández, and J.M. Navas, Effects of cerium oxide nanoparticles to fish and mammalian cell lines: An assessment of cytotoxicity and methodology. Toxicology in Vitro, 2012. 26(6): p. 888- 896.

71. Ma J.Y., R.R. Mercer, M. Barger, D. Schwegler-Berry, J. Scabilloni, J.K. Ma, and V. Castranova, Induction of pulmonary fibrosis by cerium oxide nanoparticles. Toxicology and Applied Pharmacology, 2012. 262(3): p. 255- 264.

72. Tseng, M.T., X. Lu, X. Duan, S.S. Hardas, R. Sultana, P. Wu, J.M. Unrine, U. Graham, D.A. Butterfield, and E.A. Grulke, , Alteration of hepatic structure and oxidative stress induced by intravenous nanoceria. Toxicology and Applied Pharmacology, 2012. 260(2): p. 173- 182.

73. Lopez-Moreno M., G. de la Rosa, J.A. Hernández-Viezcas, J.R. Peralta-Videa, and J.L. Gardea-Torresdey, XAS Corroboration of the Uptake and Storage of CeO2 Nanoparticles and Assessment of their Differential Toxicity in Four Edible Plant Species. Journal of Agriculture and Food Chemistry 2010. 58(6): p. 3689- 3693.

74. Ma, Y., L. Kuang, X. He, W. Bai, Y. Ding, Z. Zhang, Y. Zhao, and Z. Chai, Effects of rare earth oxide nanoparticles on root elongation of plants. Chemosphere, 2010. 78(3): p. 273- 279.

75. Gaiser, B.K., T.F. Fernandes, M. Lepson, J.R. Lead, C.R. Tyler, and V. Stoneal., Assessing exposure, uptake and toxicity of silver and cerium dioxide nanoparticles from contaminated environments. Environmental Health, 2009. 21(suppl1), S2.

76. Auffan, M., J. Rose, T. Orsiere, M. De Meo, A. Thill, O. Zeyons, O. Proux, A. Masion, P. Chaurand, O. Spalla, A. Botta, M.R. Wiesner, and J.Y. Bottero, CeO2 nanoparticles induce DNA damage towards human dermal fibroblasts in vitro. Nanotoxicology, 2009. 3(2): p.161- 171.

77. Schubert, D., R. Dargusch, J. Raitano, and S.W. Chan, Cerium and yttrium oxide nanoparticles are neuroprotective. Biochemical and Biophysical Research Communications, 2006. 342(1): p. 86- 91.

78. Nguyen, T.-D., C.-T. Dinh, D. Mrabet, M.-N. Tran-Thi, and T.-O. Do, Controlled synthesis of ceria nanoparticles for the design of nanohybrids. Journal of Colloid and Interface Science, 2013. 394: p. 100-107.

79. Yang, H., C. Huang, A. Tang, X. Zhang, and W. Yang, Microwave-assisted synthesis of ceria nanoparticles. Materials Research Bulletin, 2005. 40(10): p. 1690-1695.

80. Zawadzki, M., Preparation and characterization of ceria nanoparticles by microwave-assisted solvothermal process. Journal of Alloys and Compounds, 2008. 454(1-2): p. 347-351.

81. Ozawa, M., and Y. Nishio, Thermal stabilization of γ-alumina with modification of lanthanum through homogeneous precipitation. Journal of Alloys and Compounds, 2004. 374(1-2): p. 397-400.

82. Kim, S.-J., S.-D.Park, Y.H. Jeong, and S. Park, Homogeneous Precipitation of TiO2 Ultrafine Powders from Aqueous ToOCl2 Solution. Journal of American Ceramic Society, 1999. 82(4): p. 927- 932.

83. Chen, H.-I., and H.-Y. Chang, Homogeneous precipitation of cerium dioxide nanoparticles in alcohol/water mixed solvents. Colloids and Surfaces A: Physicochemical and Engineering Aspects, 2004. 242(1-3): p. 61-69.

84. Li, P., T.C. Tan, and J.Y. Lee, Corrosion protection of mild steel by electroactive polyaniline coatings. Syntetic Metals, 1997. 88(3): p. 237- 242.

85. Lacroix, J.-C., J.-L. Camalet, S. Aeiyach, K.I. Chane-Ching, J. Petitjean, E. Chauveau, and P.-C. Lacaze, Aniline electropolymerization on mild steel and zinc in a two-step process. Electroanalytical Chemestry, 2000. 481(1): p. 78-81.

86. Philippe, L.V.S., G.W. Walter, and S.B. Lyon, Investigating Localized Degradation of Organic Coatings. Journal of The Electrochemical Society, 2003. 150(4): p. B111-B119.

87. Zawadzki, M., Preparation and characterization of ceria nanoparticles by microwave-assisted solvothermal process, Journal of Alloys and Compounds, 2008. 454: p. 347– 351

88. Yang, H., et. al. Microwave-assisted synthesis of ceria nanoparticles, Materials research bulletin, 2005. 40(10): p. 1690-1695

89. Fedel, M, A. Ahniyaz, L.G. Ecco, F. Deflorian - Electrochemical investigation of the inhibition effect of CeO2 nanoparticles on the corrosion of mild steel – Electrochimica Acta, 131 (2014) 71-78.